Evaluating Network Technologies for Industrial Intelligent Transportation Systems

Samuel Pell

A thesis submitted in partial fulfilment
of the requirements for the degree of
Master of Science
in
Computer Science
at the
University of Canterbury,
Christchurch, New Zealand.

30 April 2021

ABSTRACT

An Intelligent Transportation System (ITS) is a network of connected vehicles, pedestrians, and infrastructure sharing information to improve safety and efficiency. To enable an ITS, so called vehicle-to-everything (V2X) technologies are used. V2X technologies are *ad hoc* wireless communication technologies which target the 5.9 GHz radio band and can handle the highly mobile vehicular environment whilst supporting the often strict service requirements of vehicular safety applications. The majority of prior research into ITS and V2X technologies has focused on traditional roads, however vehicles are also extensively used in industrial environments, which could also benefit from the safety and efficiency gains an ITS offers. This thesis investigates applying V2X technologies to safety applications in one possible industrial environment: the logistics warehouse.

In particular, two different V2X technologies (C-V2X and IEEE 802.11p) are compared, evaluated based on the error rate of an aisle-end collision warning application in warehouses, to determine which is more suited to the warehouse environment. To quantitatively evaluate the technologies an aisle-end collision scenario and collision warning application simulator was developed to simulate each technology. The simulator includes a custom warehouse aisle-end channel model which was parameterised using measurements conducted in a real-world warehouse.

Using the collision warning application simulator the application error rate was observed for each technology for different average spacing between forklifts, modulation and coding schemes (MCS), and transmit powers. It was found that the average spacing between forklifts had the most effect on the failure rate of the application. As the average spacing between forklifts decreased, the false negative rate increased relative to the baseline for C-V2X but stayed roughly constant for IEEE 802.11p. The differing behaviour of the two technologies is attributed to the different channel access procedures used by the two technologies. The effect of MCS and transmit power was negligible for IEEE 802.11p. For C-V2X however, the false negative error rate increased with MCS index and there appears to be a minimum transmit power, below which, C-V2X performs significantly worse. This behaviour is hypothesised to also be caused by C-V2X's channel access algorithm. Based on the quantitative evaluation of the technologies, at least for the warehouse environment, IEEE 802.11p is superior to C-V2X.

In addition to the quantitative evaluation of the current generation of V2X tech-

nologies, this thesis also presents a qualitative discussion of what possible change in performance the next generation V2X technologies (NR-V2X and IEEE 802.11bd) may bring. The next generation of V2X technologies focus on improving the physical layer performance of the current generation (C-V2X and IEEE 802.11p). However, all the problems with the technologies identified in this thesis are in the channel access procedures. Thus, next generation V2X technologies are not expected to significantly improve performance in this scenario. This thesis also discusses the regulatory support for each technology in different regions. In the United States of America, C-V2X is the only V2X technology allowed to use the 5.9 GHz ITS band, making it more suitable for deployment in a warehouse ITS in that region.

CONTENTS

ACKNOWLEDGEMENTS

Firstly, I would like to thank my supervisors Dr Graeme Woodward and Professor Andreas Willig, without their patience, guidance, and feedback this thesis would not be half as well written or complete.

Thank you to Dr Lisa Wong, Sian Phillips, and Dr Avi Kumar, your feedback and insight into the warehouse environment and use case was invaluable.

In this thesis I performed measurements at two different warehouse locations. I would like to thank Stuart Park, Ryan Estep, and the rest of the team at Location 1, without your help and feedback, completing the measurements would not have been possible. Thank you to the team at Location 2 for allowing me access to their site. Thank you to Kelvin Barnsdale, your advice on RF propagation and measurement was incredibly helpful.

Thank you to François Bissey, Peter Glassenbury, the University of Canterbury Research Computing Cluster, without your support the simulations, which make up the core of this thesis, could not have been completed.

Thank you to Robert Rankin for proofreading this thesis and listening to me complain about my code not working over many, many flat dinners.

Thank you to my colleagues in the Wireless Research Centre: Amy Inwood, Aston Taylor, Hamish Shaw, Jackson Godfrey, Matthew Pike, Will Sloane, and Zubia Ishrat. Our discussions were welcome distractions from the drudgery of writing, coding, and debugging.

GLOSSARY

3GPP	Third generation partnership project — the standards body responsible for developing cellular standards
5G	The fifth generation of cellular standards released by the 3GPP
802.11bd	IEEE 802.11bd — the next generation evolution of IEEE 802.11p
802.11p	IEEE 802.11p — a vehicle-to-everything communication technology based on WiFi
AIP	Average introduction period
AWGN	Additive white Gaussian noise
BER	Bit error rate
BLER	Block error rate
BPSK	Binary phase shift keying
CBR	Channel busy ratio — the ratio that channel is considered occupied or 'busy'
CSR	Candidate sub-frame resource — one possible resource block in a single sub-frame which could be reserved
C-V2X	Cellular-vehicle-to-everything — an LTE based vehicle to everything technology developed as part of 3GPP release 14
DMRS	Demodulation reference symbol
DSRC	Dedicated short range communication — A V2X standard which uses IEEE 1609 and IEEE 802.11p as its base
eNodeB	An LTE cellular network base station
EU	European Union
FCC	Federal Communications Commission — the regulatory body responsible for licensing and allocation of radio frequency spectrum in the United States of America
FEC	Forward error correction
Forklift	An umbrella term for a number of specialist industrial vehicles which have forks and are used to move, organise, and store pallets in a warehouse environment
gNodeB	A 5G cellular network base station

IBC	Intermediate bulk container — a container used to store and transport liquids, pastes, and powders in an industrial and warehouse environment
IEEE	Institute of Electrical and Electronics Engineers
ITS	Intelligent transportation system — a network of connected vehicles, roadside infrastructure, and other road users, sharing information to increase safety and efficiency
LOS	Line of sight
LTE	Long term evolution — the fourth generation of 3GPP standard for cellular communication
MAC	Medium access control layer — the layer of a transceiver responsible for determining and scheduling access to the shared channel
MCS	Modulation and coding scheme
NIST	National Institute of Standards and Technologies
NLOS	Non line of sight
NR-V2X	New radio-vehicle-to-everything — the next generation of C-V2X developed as part of 3GPP release 16
NZ	New Zealand
OBU	On board unit
OFDM	Orthogonal frequency division multiplexing
OLOS	Obstructed line of sight
PC5	The device-to-device communication sidelink defined for use in LTE based hand-held radios, C-V2X, and NR-V2X
PER	Packet error rate
PRR	Packet reception rate
PSCCH	Physical sidelink control channel
PSFCH	Physical sidelink feedback channel
PSSCH	Physical sidelink shared channel
QAM	Quadrature amplitude modulation
QPSK	Quadrature phase shift keying
RB	Resource block
RBW	Resolution bandwidth
RF	Radio frequency
RSM	Radio Spectrum Management — the branch of the Ministry of Business, Innovation, and Employment responsible for licensing and allocating RF spectrum in NZ
SC-FDMA	Single-carrier frequency division multiple access
SINR	Signal-to-interference-plus-noise ratio
SNR	Signal-to-noise ratio

UE	User equipment — the term used to describe end user terminal in cellular communication standards
UHT	Ultra high temperature
USA	United States of America
V2I	Vehicle-to-infrastructure
V2N	Vehicle-to-network
V2P	Vehicle-to-pedestrian
V2V	Vehicle-to-vehicle
V2X	Vehicle-to-everything
WINNER II	A set of wireless channel models commonly used for V2X simulation

NOTATION

All symbols with a wide-hat (e.g. $\widehat{PL\,(d_0)}$ or $\widehat{G_{\mathrm{rx}}}$) are in the logarithmic (dB) domain. Those without are in the linear domain. Similarly, all symbols with an over-arrow (e.g. $\overrightarrow{s}$ or $\overrightarrow{p}$) are vectors.

α	Path loss exponent
BER	Bit error rate
$BLER$	Block error rate
d	Distance, typically in metres
d_0	Reference distance
f	Frequency, typically in hertz
G_{rx}, $\widehat{G_{\mathrm{rx}}}$	Receive antenna gain
G_{tx}, $\widehat{G_{\mathrm{tx}}}$	Transmit antenna gain
N_0, $\widehat{N_0}$	Background noise power
N_{rx}, $\widehat{N_{\mathrm{rx}}}$	Noise figure
$\widehat{P_{\mathrm{rx}}}$	Received power
P_{tx}, $\widehat{P_{\mathrm{tx}}}$	Transmit power
PL, $\widehat{PL}$	Path loss
$\widehat{PL\,(d_0)}$	Reference path loss. The path loss at the reference distance (d_0)
PRR	Packet reception ratio
$SINR$, $\widehat{SINR}$	Signal-to-interference-plus-noise ratio
SNR, $\widehat{SNR}$	Signal-to-noise ratio
t	Time, typically in seconds
v	Speed, typically in metres per second

Chapter 1

INTRODUCTION

An Intelligent Transportation System (ITS) is a network of connected vehicles sharing information to provide enhanced safety and efficiency. However, vehicles are not the only participants of an ITS, which can include other road users, such as pedestrians and cyclists, and road infrastructure. With all these parties sharing information, ITS have many interesting potential applications like collision avoidance systems [1], congestion-aware route planning [2, 3], smart traffic lights [4], and autonomous vehicle collaboration [5].

So far, the majority of ITS research has been focused on traditional roads. However, this is not the only environment where vehicles operate; they are used extensively in industrial environments like warehouses. In fact, warehouses are prime candidates for the deployment of an ITS, as an ITS may offer many benefits logistics businesses are interested in: increasing efficiency, automation, and safety. This last factor is the most pressing as in 2020 the New Zealand Government pledged to reduce workplace vehicular accidents, specifically addressing the warehousing and logistics sector [6]. One area of warehouse safety an ITS could improve is preventing collisions between forklifts, the vehicles used to move and store contents in warehouses. Collisions between forklifts are dangerous, potentially fatal to operators, and are the most common form of accident for stand-up forklift operators [7]. As in traditional roads, many collisions in warehouses happen at intersections.

To realise an ITS, wireless communications technologies support data transfer between ITS members. However, not all communication technologies are appropriate for use in an ITS. This is as many technologies cannot reliably support the highly mobile nature of an ITS and the often safety-critical application requirements. In particular, many ITS applications must operate in a decentralised manner, with or without co-ordinating infrastructure. Thus, specialised *ad hoc* communication technologies have been developed to support an ITS. These technologies are responsible for enabling all participants of the ITS to communicate and share information and as such have been dubbed vehicle-to-everything (V2X) technologies. It is these V2X technologies which are the focus of this thesis.

There are two main families of V2X communication technologies: standards based on cellular communication technologies and standards based on Wireless Local Area Network (WLAN or WiFi) technologies. For cellular-based standards there is Cellular-V2X (C-V2X) [8], and for WiFi-based technologies there is IEEE 802.11p [9]. Both types of technologies have been thoroughly investigated in the literature for normal roads [10–12], and the WiFi-based standards have seen real world, long-term deployments [13, 14]. However, neither standard has been considered for deployment in warehouses. In addition to IEEE 802.11p and C-V2X, next-generation V2X technologies are under development or have been recently released. These include IEEE 802.11bd and New Radio-V2X (NR-V2X) which are WiFi- and cellular-based standards, respectively [10]. Each build upon their pre-existing versions, evolving them to improve performance and support more advanced applications.

This thesis investigates the use of V2X technologies in a warehouse environment, considering their application to an intersection collision warning system. This application has been selected as a suitable test case to evaluate the technologies more generally as, due to the clear risk to forklift operators, it is a likely day-one application for a warehouse ITS. The performance of each technology is quantified using the failure rate of a dummy collision warning application under otherwise ideal circumstances. The remainder of this chapter: defines the research questions that focus the investigation into V2X technologies; defines the contributions resulting from these questions; and outlines the structure of this document.

1.1 RESEARCH QUESTIONS

This thesis seeks to answer the following overarching research question: Is there a difference in performance between V2X technologies for safety applications in a warehouse environment? If so, which is better?

To help answer this question, this thesis will simulate a safety application to prevent aisle-end collisions in the warehouse traffic scenario presented in Figure 1.1. In this context, the following high-level sub-questions will be answered:

Q1 What are the key differences between the V2X technologies?

Q2 For two streams of forklifts arriving at the end of an aisle, what is the effect of average spacing between forklifts on the technologies' error rate of a collision warning application?

Q3 What is the effect of transmit power and modulation scheme on the error rate of a collision warning application?

Q4 What improvements do the evolved forms of the V2X standards offer that potentially mitigate any flaws in the current generation?

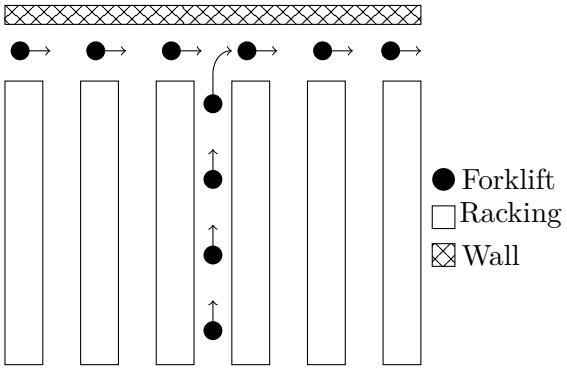

Figure 1.1 The aisle-end collision scenario showing two independent streams of forklifts arriving at a T-junction.

For clarity each of these sub questions will be referenced throughout this thesis by their identifier, rather than restating the question each time. The sub-questions will also be refined throughout the thesis.

Whilst the research questions stated above are broad, the aim of this thesis is not to develop a complete model of how each of the V2X technologies performs in a warehouse environment. Rather, the purpose of this thesis is to develop an understanding of *some* of the limitations of each technology in the cluttered warehouse environment. As such, not all features of the V2X technologies (introduced in more detail in Section 2.4) will be investigated, only their below 6 GHz *ad hoc* and unsupervised operating mode will be considered. This limited consideration is based on the decentralised, infrastructure free, and broadcast operating requirements safety applications often have.

1.2 CONTRIBUTIONS

To answer the overarching research question and sub-questions, the following contributions are made:

- An up-to-date summary of the WiFi- and cellular-based V2X communication technologies. This includes a description of the regulatory support for each technology in the United States of America, the European Union, and New Zealand.
- Development of an intersection collision scenario and test collision warning application. As part of this development, suitable performance measures were identified for the technologies.
- A warehouse intersection collision warning computer-based simulator including WiFi and Cellular V2X technology stacks.
- A custom warehouse intersection wireless channel model, parameterised based on a measurement campaign conducted at two different locations.

To the best of the author's knowledge, this is the first work exploring the use of C-V2X in a warehouse environment and the first work to characterise the warehouse wireless channel for V2X technologies.

1.3 STRUCTURE

The remainder of the thesis is structured as follows:

Chapter 2 provides an introduction to the topics covered in this thesis and partially answers research question Q1. This background includes defining V2X communications, providing some examples of potential applications of V2X in warehouses, discussing techniques for indoor localisation, describing the currently available V2X technologies, and introducing wireless channel modelling.

Chapter 3 discusses the previous comparisons between the V2X technologies, helping further answer research question Q1. It also explores prior work using V2X systems in industrial environments, the current state-of-the-art of warehouse wireless channel modelling at V2X frequencies, and discusses some collision prediction and avoidance algorithms.

Chapter 4 describes the scenario and dummy collision warning application used to answer research questions Q2 and Q3. Then, Chapter 5 discusses the design and implementation of the simulator to simulate the evaluation scenario described in Chapter 4. It also verifies the simulator is correct, ensuring the results it produces are representative of the model and can be trusted.

Chapter 6 documents the warehouse channel model design, a measurement campaign to parameterise the model at two different locations, and validation of the implementation for the simulator discussed in Chapter 5.

Chapter 7 details the simulation campaign to answer research questions Q2 and Q3. It determines: the baseline failure rate of the collision warning application, the relative strength of the effect of average vehicles spacing, modulation scheme, and transmit power on the performance of the application, and then looks at each of these factors in more depth.

Chapter 8 looks towards the future of V2X technologies, considering the potential impact the next generation of V2X technologies will have on the results presented in Chapter 7, answering Q4. It also considers the regulatory support for V2X technologies in the United States of America, the European Union, and New Zealand, as part of answering Q1.

Finally, Chapter 9 summarises the work completed in Chapters 2–8, addressing the overarching question posed in Section 1.1, and describes some avenues for future research.

Chapter 2

BACKGROUND

This chapter provides an introduction to the topics discussed in this thesis. First, Section 2.1 defines the concept of vehicle-to-everything (V2X) communication and provides some example applications for traditional roads. This is followed by Section 2.2, which highlights possible applications of V2X technologies in warehouses, motivating this investigation. Section 2.3 then deals with techniques for localisation in warehouses, where the Global Positioning System (GPS) is unreliable, providing support for an assumption made in collision warning application in Section 4.3. Then, Section 2.4 explores the currently available technologies designed to support V2X communications, partially answering research question Q1. Finally, Section 2.5 gives a brief introduction to wireless channel modelling as a foundation to the simulators used throughout the remainder of the thesis and warehouse channel model developed in Chapter 6.

2.1 VEHICLE-TO-EVERYTHING (V2X) COMMUNICATIONS

V2X communication is an overarching term which covers all communication between vehicles and other parties, including:

- Vehicle-to-Vehicle (V2V) communication — communication directly between two or more vehicles. An example application of V2V communication is the congestion aware routing system developed in [3].

- Vehicle-to-Infrastructure (V2I) communication — communication between a vehicle and a road side unit, base station, or other road infrastructure. Some example applications of V2I communications are the electronic toll collection system in [15] and the smart traffic light system developed in [16].

- Vehicle-to-Pedestrian (V2P) communication — communication between a vehicle and pedestrian or other vulnerable road users such as cyclists. This is typically used for collision avoidance applications such as the one developed in [17].

- Vehicle-to-Network (V2N) communication — communication between a vehicle and the wider internet. This service is typically provided by connecting to a traditional cell tower or an internet enabled road side unit.

These forms of communication are summarised in Figure 2.1. The term V2X is useful as most applications require a combination of above communication types to provide their functionality.

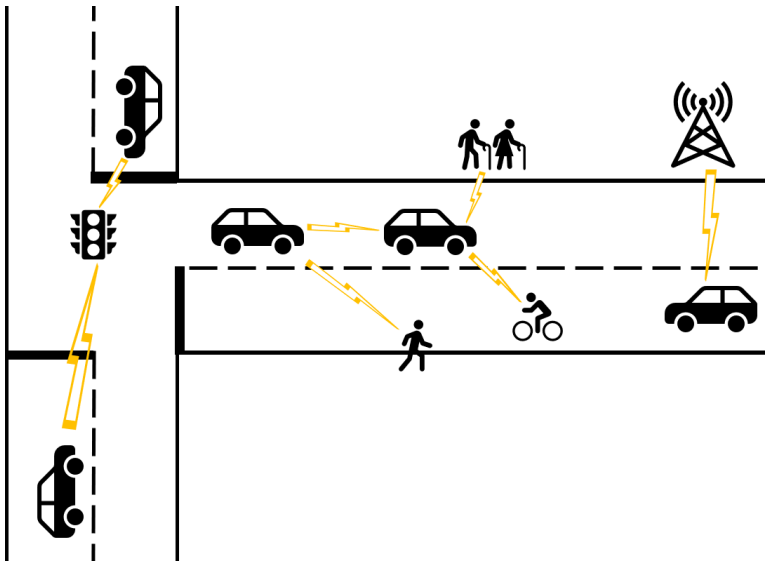

Figure 2.1 An example of an intelligent transportation system, illustrating V2X communications.

2.2 APPLICATIONS OF V2X TECHNOLOGIES IN WAREHOUSE ENVIRONMENTS

V2X communication can enable many different applications focused around increasing safety and efficiency. Current investigations of V2X communications focus on the traditional road environment [3, 16, 17] or the industrial mining environment [18].

Some possible applications of V2X in warehouse environments are:

- Collision warning and avoidance systems, similar to those discussed in [19] for traditional roads, but at lower speeds and in the absence of GPS.
- Real-time forklift position tracking. This could allow picking requests to be ordered to reduce contention for limited resources like narrow warehouse aisles, where for safety reasons there are limits on the number of forklifts allowed. This possibly reduces operator waiting time, increasing efficiency.
- Teleoperation of forklifts. Allowing remote operation of forklifts removes forklift operators from the possibly dangerous warehouse environment, increasing worker safety and comfort. Additionally, this could increase efficiency by allowing large

logistics companies to centralise their staff and allocate them to warehouses as needed.

- Distributed sensor-data fusion. Allowing vehicles to share sensor information to provide vehicles participating in the network a wider view of the world is expected to help improve the autonomy of vehicles on traditional road systems [5]. This may also be useful for developing fully autonomous forklift systems.

2.3 LOCALISATION IN WAREHOUSES

Localisation is the process of determining the position of an object in some coordinate system. One common localisation system is GPS, which primarily relies on radio signals from orbiting satellites to allow the receiver to determine its location [20]. Outdoors, GPS can provide a highly accurate position within 5–10 m of the real location using satellites alone [21], but can be augmented to achieve positioning accuracy below 0.01 m [22]. However indoors, GPS is often unavailable and cannot be relied on for localisation [23, 24].

Despite being unable to use GPS, there are many other localisation techniques possible within warehouses. This section will discuss two different major techniques for localisation: radiolocalisation and computer vision. Radiolocalisation technologies use wireless signals to locate a vehicle, working in similar ways to GPS. One possible radiolocalisation technology possible for warehouse localisation is ultra-wideband (UWB) explored in [25]. In [25], an UWB based pedestrian localisation system was developed and tested in a real-world warehouse environment, and managed to achieve an average localisation error of 1.4 m, with a maximum error of 4.0 m at 95% confidence intervals. A similar system for forklifts, rather than pedestrians, was developed in [26] and achieved localisation accuracy to 0.1–0.2 m in simulations. However the system in [26] is only simulated, not tested in a real warehouse.

Computer-vision-based systems use cameras to determine location of forklifts in a warehouse. Many of these systems use cameras to match unique fiducial markers, placed at known locations in the warehouse, to determine the location of the forklift. Often, this data is combined with other inputs, like accelerometers, to refine the localisation accuracy and handle the case where there are no markers in view. Fiducial markers can be placed on the ceiling, floor, or attached to the warehouses racking [27–29]. Localisation systems using purely fiducial markers claim to be able to achieve at least metre-level accuracy [30]. Another technique within computer vision, is to use laser scanning or Light Detection and Ranging (LIDAR) systems to determine the position of the forklift. An example of a system which uses laser scanners, combined with odometry data from the wheels, is presented in [31]. The system described in [31] was tested in an automated forklift test warehouse and can achieve sub-centimetre localisation accuracy.

2.4 TECHNOLOGIES TO SUPPORT V2X COMMUNICATIONS

There are currently two different wireless technologies which support V2X communication: cellular and WiFi. Cellular V2X is the application of cellular technology to enable V2X communication via the PC5 sidelink, achieving device-to-device communication. Cellular communication standards are defined by the Third Generation Partnership Project (3GPP) which is a group of seven communication standard organisations and 18 market representation partners [32]. Each of the standards and studies performed by the 3GPP are proposed and driven by member companies through the market representation partners [33]. There are currently two generations of cellular support for V2X communications: one based on the Long Term Evolution (LTE) standards and the other on the Fifth Generation (5G) standards. These technologies are discussed in Sections 2.4.1 and 2.4.2, respectively.

The WiFi-based technology is called Wireless Access in Vehicular Environments (WAVE) and consists of the IEEE 1609 family of standards and Dedicated Short Range Communication (DSRC) standard, also known as IEEE 802.11p[1] [35]. The structure of the WAVE protocol stack is shown in Figure 2.2. In November 2018, the 802.11 Working Group — the group responsible for developing the IEEE 802.11 family of standards — authorised the development of IEEE 802.11bd to replace IEEE 802.11p in the WAVE protocol stack [36]. The details of IEEE 802.11p and IEEE 802.11bd will be discussed in Sections 2.4.3 and 2.4.4, respectively.

2.4.1 Cellular-V2X (C-V2X)

Cellular V2X (C-V2X) is the initial cellular-based V2X technology, first specified in 3GPP release 14 as part of the Long Term Evolution (LTE) standard [38]. C-V2X builds upon the LTE standard, using a lot of the same physical layer (PHY) components. The LTE standard specifies many different interfaces which allow communication between

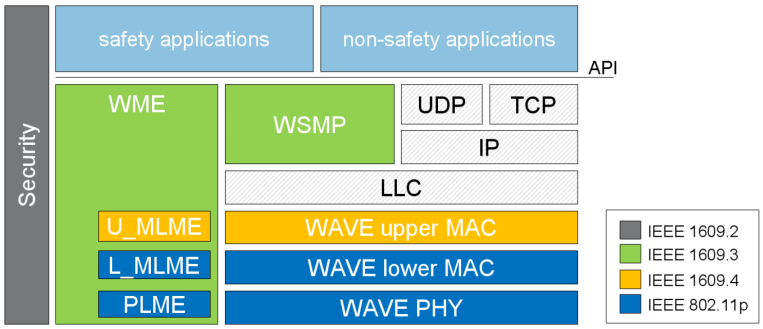

Figure 2.2 The WAVE protocol stack. Source: [35] © 2008 IEEE. Note that IP here refers to IPv6 and the WAVE standard does not support IPv4 operation [37].

[1]IEEE 802.11p was an amendment to the IEEE 802.11 standard which was folded into the main standard in 2012 [34]. The most recent version of the IEEE 802.11 standard was published in 2020.

different elements of the cellular network. As the C-V2X radio builds upon LTE, it can use the standard LTE-Uu interface to interact with an eNodeB — a traditional cellular network base station. C-V2X also uses the PC5 sidelink interface to communicate directly between two vehicles, without involving the eNodeB.

Like the LTE-Uu interface, the PC5 interface uses single-carrier frequency-division multiple access (sc-FDMA) in 10 or 20 MHz channels [39]. Each channel is divided into sub-frames, Resource Blocks (RBs), and sub-channels. A sub-frame is 1 ms long and consists of 14 symbols [10]. An RB is the smallest unit of resource allocated to one C-V2X user for a single sub-frame and consists of 12 15 kHz sub-carriers [40]. A sub-channel consists of one or more RBs in the same sub-frame. How individual RBs are allocated to C-V2X devices is discussed below in Section 2.4.1.1.

sc-FDMA is a type of linear precoded orthogonal FDMA scheme, where instead of each data symbol being transmitted on one sub-carrier, all M carriers carry the data symbol for $\frac{1}{M}$th of the sc-FDMA symbol period [41]. This technique is contrasted against Orthogonal Frequency Division Multiplexing (OFDM), where each sub-carrier holds a single data symbol for the entire OFDM symbol period, c.f. Figure 2.3. Converting the data symbols from being transmitted in parallel to being transmitted in series, reduces the peak-to-average power ratio compared to OFDM, increasing the battery life of LTE devices [41].

Data is modulated onto each of the sub-carriers in an RB using either Quadrature Phase Shift Keying (QPSK) or 16-Quadrature Amplitude Modulation (16-QAM). In addition to the data symbols, special control and reference symbols are inserted into each sub-frame [43]. To provide error correction for transmissions, C-V2X uses blind Hybrid Automatic Repeat reQuests (HARQ). Automatic repeat request systems allow for retransmissions of data if errors are detected. However, retransmissions can be disruptive for the efficient flow of data from transmitter to receiver, so it is often combined with Forward Error Correction (FEC) mechanisms to form a HARQ system. Using FEC allows the receiver to correct some of the received errors in the data, reducing the number of retransmissions. In the case of C-V2X, the FEC scheme is Turbo Coding [44]. C-V2X specifically uses blind HARQ, where data is retransmitted automatically, regardless of whether any errors were detected.

The PC5 sidelink is divided into two logical channels: the Physical Sidelink Control Channel (PSCCH) and the Physical Sidelink Shared Channel (PSSCH). The PSCCH contains the control data needed to demodulate and decode the information in the PSSCH. The PSSCH contains the payload data of the transmission. These logical channels are on transmitted on separate sub-channels (Figure 2.4).

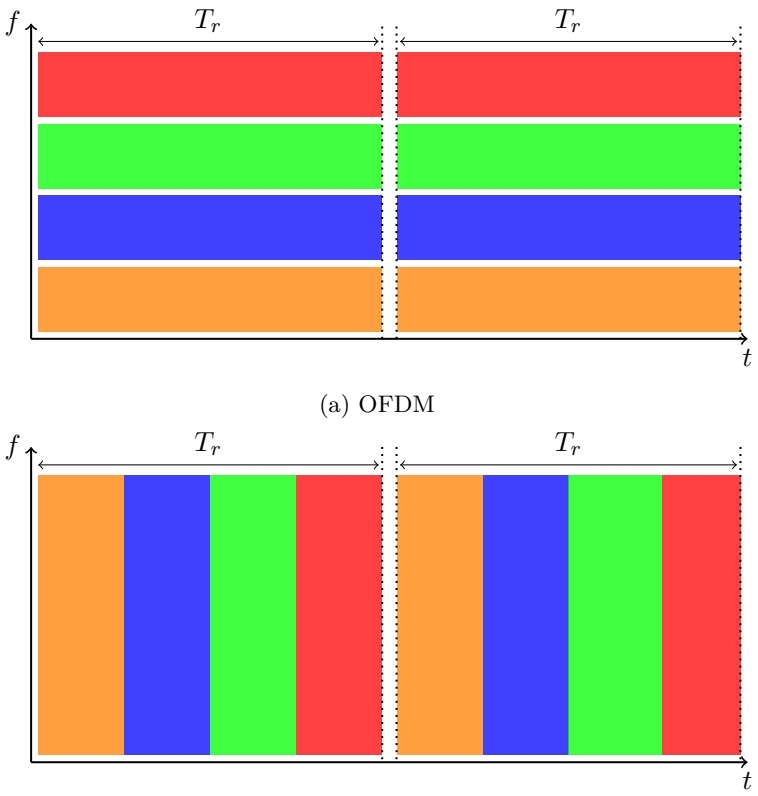

(a) OFDM

(b) sc-FDMA

Figure 2.3 Comparing the use of frequency (f) and time (t) resources to transmit data with four resource elements, for OFDM and sc-FDMA. Each colour represents a different data symbol and the overall resource element period is indicated by T_r. The resource element is the atomic unit of frequency and time in LTE and consists of a single 15 kHz sub-carrier for a single sc-FDMA or OFDM symbol period [42].

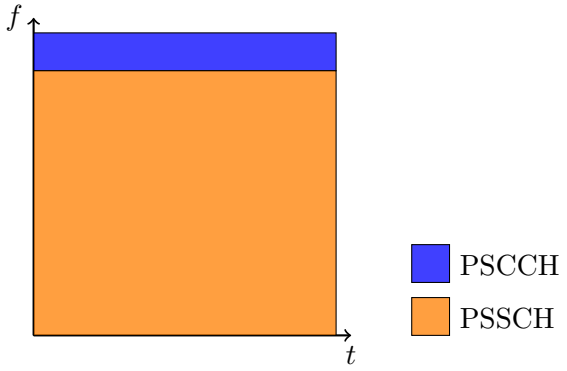

Figure 2.4 Multiplexing of the PC5 sub-channels in time (t) and frequency (f) for C-V2X over a single sub-frame. The PSSCH can contain a variable number of RBs, whereas the PSCCH always contains two RBs. Note that the PSSCH and PSCCH are shown as adjacent blocks of RBs here, however, this is not required.

2.4.1.1 Resource Allocation in C-V2X

Each of the different interfaces in C-V2X have different resource allocation methods. For the LTE-Uu interface, the normal LTE resource allocation algorithm is used. In this method, User Equipment (UE) requests transmission slots from the controlling eNodeB on a one-off or semi-persistent basis. The exact details of this algorithm are beyond the scope of this thesis, and the reader is referred to [45] for more details. Using the traditional LTE-Uu interface allows V2X applications to communicate with centralised servers, providing a wider view of the current network state than is achievable via device-to-device communication.

The PC5 sidelink has four different resource allocation methods for device-to-device communication: two designed for handheld radios and two for V2X communication. The original PC5 specification in release 12 introduced support for mode 1 and mode 2, for use in handheld radios. These modes prioritise battery life at the expense of increased latency [40]. Since V2X communications demand low latency, neither of these modes were suitable. 3GPP release 14 added mode 3 and mode 4 to support low latency V2X communication [46].

Mode 3 of the PC5 interface is device-to-device communication controlled by the eNodeB. In this mode, the eNodeB is responsible for managing and allocating resources to prevent collision and ensure fair channel access. In mode 3, user devices request resources from the eNodeB using the LTE-Uu interface, but there is no standard specified algorithm for resource allocation [10]. Using this mode means that resources can be allocated with a wider view of traffic demands, leading to globally optimal resource allocation. However, as there is no standard resource allocation algorithm, the overall performance of mode 3 will be vendor dependent.

PC5 sidelink mode 4 is used for V2X communications outside of complete eNodeB coverage. In this mode, a UE reserves resources autonomously using a sensing-based semi-persistent scheduling mechanism. The resource allocation algorithm has three stages: sensing, reservation, and transmission [42, 47]. The sensing process is as such: the Medium Access Control layer (MAC) requests a sensing report from the PHY at sub-frame n. The PHY, which has been listening to all the previous transmissions and recording them, creates a sensing window containing all possible resources that could be reserved by the MAC layer. These resources are called the candidate single sub-frame resources (CSRs). The sensing window is generated for the sub-frames $[n-1,\ n-10P_{\text{step}}]$. P_{step} is a parameter proposed to avoid synchronisation conflicts and the 3GPP suggests setting it to 100 ms [42]. With $P_{\text{step}} =$ 100 ms, the sensing window contains all records from the past one second.

The PHY then generates the report window containing all CSRs which will meet the latency requirements of the application. The lower bound of the latency requirement in sub-frames (τ_1) is set by the higher layers of the protocol stack based on the

processing time the device requires and the upper bound (τ_2) is set by the application. τ_1 is required to be less than or equal to four sub-frames and τ_2 is typically set to 100 sub-frames for safety applications, however it can be set to any value such that $20 \leq \tau_2 \leq 100$ [42]. Thus, the report window contains all CSRs from the sensing window between $[n + \tau_1,\ n + \tau_2]$. After generating the report window, the PHY then shrinks it to create the set S_A by excluding any candidate CSRs which meet either of the following criteria:

- there is some sub-frame in the sensing window that was not monitored and one of the possible reservations of the candidate CSR in the reservation horizon overlaps with that sub-frame.

- there is some sub-frame in the sensing window that received more energy than a preset threshold and one possible reservation of the candidate CSR in the reservation horizon overlaps with that sub-frame.

These criteria are based on measured channel energy and do not require successful reception of data in the sub-frames in question. The reservation horizon covers the time period between the last reserved resource and the initial reservation of the resource and is further defined below. If after this exemption procedure, there are fewer than 20% of the original resources left, the exemption procedure starts again with a 3 dB increase in the threshold. This process repeats until at least 20% of the CSRs remain in S_A.

The CSRs remaining in S_A are then ranked based on the average received power over the sensing window period, calculated as:

$$E_{x,y} = \frac{1}{10} \sum_{i=1}^{10} \left[\sum_{j=x}^{x+L-1} RSSI_{(y-iP_{\text{step}}),j} \right], \tag{2.1}$$

where x is the first of L sub-channels that make up the CSR at time y, and $RSSI_{t,j}$ is the measured signal strength of channel j during sub-frame t. The 20% of CSRs in S_A with the lowest $E_{x,y}$ are then placed in another set S_B, which is then passed up to the MAC.

Once the MAC receives S_B, the reservation procedure begins. The MAC randomly selects a CSR from S_B. The MAC layer then locally reserves that CSR, C_{resel} times, once every P_{rsvp} milliseconds. Each of these reserved CSRs is considered a transmit opportunity. P_{rsvp} is the reservation period which is specified by the higher layers, and can take one of the following values $\{20, 50, 100, 200, \ldots, 1000\}$. When a new resource selection occurs, the sidelink resource reselection counter (SLRRC) is set to a value

drawn from the following uniform distribution:

$$U \sim \begin{cases} U(5,15), & \text{for } P_{\text{rsvp}} \geq 100 \\ U(10,30), & \text{for } P_{\text{rsvp}} = 50 \\ U(25,75), & \text{for } P_{\text{rsvp}} = 20. \end{cases} \tag{2.2}$$

Each time the PHY layer transmits the SLRRC is decremented. When the SLRRC reaches zero, the MAC can reselect new resources with a probability P_{reselect} which can be set to one of the following values: $\{1, 0.8, 0.6, 0.4, 0.2\}$. If the MAC does not reselect resources, it reserves the same resources for another C_{resel} periods, where $C_{\text{resel}} = 10SLRRC$. Thus, the reservation horizon becomes $P_{\text{rsvp}}(C_{\text{resel}} - 1)$.

However, the SLRRC expiring is not the only trigger for resource reselection. The reselection process can begin if any of the following conditions are met:

- The device has not used any of its slots for a transmission or retransmission in the past second.
- The device has missed more opportunities to transmit than the higher layers allow.
- The currently reserved resources cannot meet the latency requirement for the latest incoming data packet.
- There are not enough reserved resources to transmit the incoming data packet in one go.

When a device has data to transmit, the PHY waits until one of the reserved slots becomes available and then broadcasts the data in that slot. Since C-V2X uses blind HARQ, the retransmissions must also be scheduled and are scheduled randomly in the 15 sub-frames before and after the reserved transmission window [47].

2.4.2 New Radio-V2X (NR-V2X)

New Radio-V2X (NR-V2X) is the next generation of V2X communication from the 3GPP and takes advantage of the advances developed as part of the 5G standardisation work. The 3GPP have developed this new generation of cellular V2X to support advanced applications such as vehicle platooning, automated driving, and coordinated manoeuvring [48]. All of these applications have strict quality of service requirements, more stringent than C-V2X can support, requiring highly reliable, high throughput, low latency communication over long distances at high relative speeds [48]. NR-V2X was designed to meet the requirements of advanced applications, not to replace the services offered by C-V2X [49]. As such, NR-V2X and C-V2X are not interoperable, however, this does not mean NR-V2X cannot provide the same services C-V2X does [10].

For NR-V2X to meet these requirements several changes to C-V2X were made to the PHY and resource allocation algorithms. Additionally, NR-V2X introduces support for addressing transmissions to a single receiver (unicast) and to a group of receivers (groupcast). NR-V2X now supports [10]:

- Flexible sub-carrier spacing — NR-V2X can now have 30 and 60 kHz wide sub-carriers, increasing the possible symbol rate.

- Orthogonal Frequency Division Multiplexing (OFDM) — Instead of using sc-FDMA, the NR-V2X transmitter uses OFDM. OFDM uses individual sub-carriers which hold a symbol for the whole symbol period, allowing 12 symbols to be transmitted in parallel. OFDM is compared to sc-FDMA in Figure 2.3.

- Variable length transmission slots — Using C-V2X the smallest amount of time a transmission could take was one sub-frame of 1 ms. In NR-V2X, users with less data can transmit in smaller slots, reducing latency for small messages.

- Time multiplexing of PSCCH and PSSCH sub-channels — In an effort to reduce processing delays, NR-V2X now multiplexes PSCCH and PSSCH in time, where the PSCCH data is transmitted first then the PSSCH is sent (Figure 2.5). In C-V2X, the PSCCH and PSSCH sub-channels are multiplexed in frequency, meaning the control data transmission finishes at the same time as the data transmission. Multiplexing the data in time allows the control data transmission to finish before the data transmission begins. Meaning the receiver can begin immediately decoding the data in the PSSCH, rather than waiting for the whole transmission to complete, reducing processing delays.

- A sidelink feedback channel — C-V2X automatically retransmits its packets as part of a blind HARQ scheme, even if the first transmission was successful. This is resource inefficient. NR-V2X introduces a sidelink feedback channel (PSFCH) to overcome this, allowing the recipients to indicate if a transmission was received successfully. However, this is only for the unicast and groupcast transmissions modes and does not cover the broadcast mode typically used for disseminating safety information. The reader is referred to [50] for more information on the PSFCH and feedback mechanisms in NR-V2X.

- Higher order modulation schemes — NR-V2X now supports QPSK, 16-QAM, and 64-QAM. This allows more data to be encoded per symbol, increasing overall data throughput.

- Low Density Parity Check (LDPC) coding — The HARQ scheme now uses LDPC as its FEC scheme.

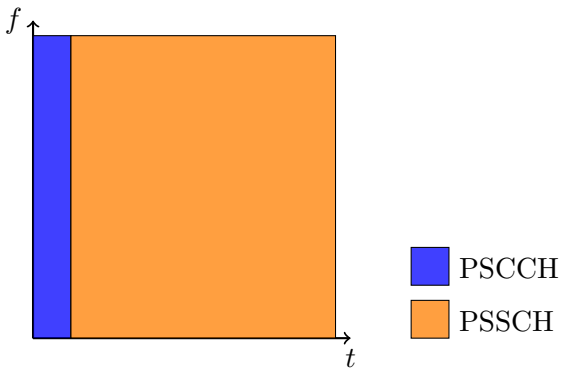

Figure 2.5 Multiplexing of the PC5 sub-channels in time (t) and frequency (f) for NR-V2X over a single sub-frame.

5G, and thus NR-V2X, also supports millimetre-wave (mmWave) operation [51]. mmWave operation refers to using the frequencies from 30 to 300 GHz [52]. mmWave support is added to 5G and NR-V2X to increase data throughput, as the higher frequency bands are less crowded and wider channel bandwidths, needed to support high data rates, are available. However, mmWave signals are easily attenuated and coverage can be easily and completely blocked by humans and obstacles [52]. To overcome this limitation beamforming — directing a signal's propagation path — and other PHY techniques are used. The mmWave operating modes of NR-V2X will not be discussed further as this thesis focuses on the sub 6 GHz frequency range of V2X communication. Additionally, it is not known how well these techniques will perform in the highly mobile, cluttered, and broadcast focused environment discussed in the remainder of the thesis.

2.4.2.1 Resource Allocation in NR-V2X

For NR-V2X, the 3GPP have redesigned the resource allocation scheme for the PC5 interface. They have created two new modes, creatively named mode 1 and mode 2. Mode 1 is where resource allocation is performed by the gNodeB (the 5G version of an eNodeB), similar to C-V2X mode 3. Mode 2 is similar to C-V2X's mode 4, where devices autonomously select their own resources. Unlike C-V2X, NR-V2X mode 2 allows mode 2 resources to be selected for one-off transmissions, rather than always being selected on a semi-persistent basis. The selection procedure for one-off transmissions is the same as for semi-persistent reservation, however resources are only reserved once.

For a detailed description of mode 1 and mode 2 resource allocation algorithms in NR-V2X, the reader is directed to [50].

2.4.3 IEEE 802.11p

IEEE 802.11p (henceforth referred to as 802.11p) is an amendment to the IEEE 802.11 family of protocols, designed to introduce support for V2X communication [9]. The

changes from the base IEEE 802.11 standard for 802.11p can be split into two distinct categories: PHY changes and MAC changes.

The PHY of 802.11p is based on the IEEE 802.11a amendment which introduced OFDM support to WiFi and moved the operating frequency from 2.4 GHz to the 5 GHz frequency band [53]. IEEE 802.11a uses a 20 MHz wide OFDM channel with 64 sub-carriers: 48 data, 4 pilots, and 12 guard sub-carriers. However, 802.11p only uses 10 MHz wide channels with the same number of sub-carriers. This means the time-domain OFDM parameters (such as symbol time) have to double, halving the overall data rates [54]. The reduced channel bandwidth of 10 MHz increases the guard interval size so that it can deal with the increased delay spread in the vehicular channel. If a 20 MHz bandwidth was used, the guard interval would be shorter than the delay spread, and thus would not adequately protect against inter-symbol interference [35].

In addition to the change in the channel bandwidth, the 802.11p amendment introduced stricter limits on the amount of out-of-channel emissions allowed. This is due to the measurements conducted in [55], completed during development, showing that adjacent vehicles transmitting in adjacent channels would interfere with each other.

In terms of error correction, 802.11p does not perform retransmissions, but does use Binary Convolutional Codes (BCC) for FEC. The absence of retransmissions is a function of 802.11p only supporting broadcast operation and the IEEE 802.11 family of standards not supporting broadcast acknowledgements.

At the MAC layer 802.11p introduces the WAVE mode (also known as OCB mode) which allows a device to transmit without being a member of a Basic Service Set (BSS). This is distinct from all previous IEEE 802.11 MAC standards, whose primary goal was to establish and maintain a cooperating group of devices in a BSS [35]. In a traditional IEEE 802.11 network, users typically have to join a BSS, which requires a number of steps and several seconds, before being able to broadcast frames to other users. This requirement exists as devices filter broadcast frames based on whether they are sent from within the same BSS [56]. The process of listening for a BSS beacon and negotiating to join would introduce too much overhead for safety-critical communications. In addition to the overhead of joining a BSS, the membership of any BSS would change frequently as vehicles move in and out of communication range. As such, 802.11p introduced the WAVE mode [9]. A radio in WAVE mode can transmit and receive data with the wildcard BSS Identification (BSSID). The BSSID is all 1's and allows two vehicles to immediately communicate with each other if they are in the same channel [35].

2.4.3.1 IEEE 802.11p MAC Protocol

802.11p uses the Enhanced Digital Channel Access (EDCA) MAC protocol designed as part of IEEE 802.11. The EDCA protocol is a variation of the Carrier Sense Medium Access with Collision Avoidance (CSMA/CA) protocol where the packet priority is

taken into account [57]. However unlike in pure EDCA, 802.11p removes the exponential backoff procedure, to reduce the maximum possible latency. That is, the contention window does not double in size when the transmission is not successful [10]. Thus, the MAC protocol becomes [57, 58]: when the transmitter has something to transmit, it listens to see whether any other device in its reception range is transmitting for one Arbitration Inter-Frame Space (AIFS). If no transmissions are detected, then the device can transmit its message immediately. If transmissions are detected, the backoff procedure begins.

The backoff procedure is a slotted wait procedure. First, the transmitter randomly draws the backoff counter from the uniformly distributed range $[0, W]$, where W is the contention window parameter set based on the Access Category (AC) of the data [59]. During each of the following slots, if the slot is idle the backoff counter is decremented. If a transmission is detected in a slot, the backoff procedure is halted until the transmission is over and the channel is idle for an added guard period. This guard period is one AIFS if the packet was received successfully, or if there were errors in the received packet, one Extended Inter-Frame Space (EIFS). When the backoff counter reaches zero, the station can finally transmit. After each transmission, the transmitter waits for a random backoff period before being eligible to transmit again.

To deal with different traffic priorities, the EDCA protocol categorises traffic into four different ACs. Each AC is maintained in its own internal queue, has a different AIFS length, and different contention window parameters. These parameters are summarised in Table 2.1. The AIFS length can be calculated using the following equation [57]:

$$t_{\text{AIFS}} = \text{AIFSN[AC]}t_{\text{slot}} + t_{\text{SIFS}}, \tag{2.3}$$

where AIFSN is a the number of slots each AC must wait, t_{slot} is the length of a single slot, and t_{SIFS} is the length of a Short Inter-Frame Space (SIFS). ACs with a higher priority use smaller AIFSN values, thus, their initial wait is shorter and can access the channel faster.

Each AC is maintained in its own separate queue and each queue functions as if it was an independent transmitter. Thus, there can be internal collisions between different AC queues. To resolve these collisions, the internal scheduler gives the transmission

Table 2.1 The different ACs EDCA parameters. For OFDM with a 10 MHz wide channel $W_{\text{min}} = 15$ and $W_{\text{max}} = 1023$ [59, p. 2321]. Based on data presented in [9]

AC	W_{min}[AC]	W_{max}[AC]	AIFSN[AC]
Background	W_{min}	W_{max}	9
Best Effort	W_{min}	W_{max}	6
Video	$\frac{W_{\text{min}}+1}{2} - 1$	W_{min}	3
Voice	$\frac{W_{\text{min}}+1}{4} - 1$	$\frac{W_{\text{min}}+1}{2} - 1$	2

opportunity to the higher priority AC. The lower priority AC then behaves as if there was an external collision, and begins the backoff procedure without setting the retry field in the MAC header [57]. In the case of an external collision, where two different devices transmit at the same time, the collided frames are deferred and the backoff procedure begins.

2.4.4 IEEE 802.11bd

IEEE 802.11bd (henceforth 802.11bd) is an evolution of 802.11p meant to update the 802.11p standard with the developments that have been deployed to IEEE 802.11a in IEEE 802.11n, IEEE 802.11ac, and IEEE 802.11ax. The aim is to increase the throughput at high relative velocities over longer ranges [36]. Unlike NR-V2X and C-V2X, 802.11bd is meant to be, at least partially, backwards compatible and interoperable with 802.11p. The current 802.11bd development plan requires that [60]:

- 802.11p devices can decode at least one of the transmission modes in 802.11bd
- 802.11bd devices can decode 802.11p transmissions
- 802.11p devices can detect 802.11bd transmissions and vice versa
- 802.11bd devices can interoperate with 802.11p devices
- 802.11p devices have the same channel access opportunities as 802.11bd

The new 802.11bd PHY has two different channel bandwidths available: 10 MHz and 20 MHz [61]. The 20 MHz channel is formed from two contiguous 10 MHz channels, on which the 802.11bd transmitter broadcasts the training and signal fields in parallel, before transmitting data symbols using the full 20 MHz channel (Figure 2.6). To take advantage of the two possible channel bandwidths, 802.11bd supports two different OFDM configurations: IEEE 802.11ac 40 MHz mode downclocked by two for 20 MHz channels, and IEEE 802.11ac 20 MHz, downclocked by two for 10 MHz channels [61]. Downclocking is where the system frequency is reduced by some factor. This has the added implication of increasing the time domain parameters by the same factor. Some of the OFDM parameters for each of the supported channel bandwidths are summarised in Table 2.2.

In addition to the changes to the OFDM structure, 802.11bd also includes new modulation and coding schemes. In IEEE 802.11ac 256-QAM support was introduced and this modulation scheme is also supported in 802.11bd. 802.11bd also supports a modulation scheme called BPSK dual sub-carrier modulation (DCM), where a rotated version of the signal is also transmitted, increasing diversity [63]. This increased diversity increases the effective signal-to-noise ratio, reducing the bit error rate.

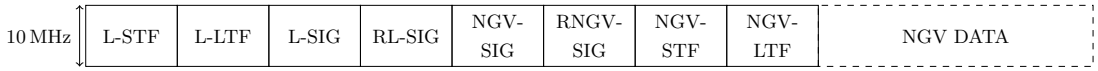

(a) 10 MHz wide channel

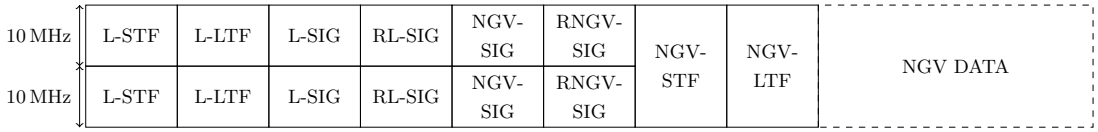

(b) 20 MHz wide channel

Figure 2.6 The physical protocol data units structures in 802.11bd for 10 MHz (a) and 20 MHz (b) channels [61].

Table 2.2 Select OFDM properties for both channel channel bandwidths supported by 802.11bd. Based on [61] and [62, p. 244–245]

	10 MHz	20 MHz
Number of sub-carriers	64	128
Number of pilot tones	4	6
Number of guard sub-carriers	8	8
Number of data carriers	52	108
Sub carrier spacing (kHz)	156.25	156.25

802.11bd supports two different FEC schemes: BCC and LDPC. The BCC, specified in [59, p. 2295–2296], is included primarily for backwards compatibility with 802.11p and other WiFi standards. The LDPC code follows the scheme specified in [59, p. 2377–2381] and is the only FEC used for protecting the data portion. Thus, 802.11p devices cannot decode the data portion of 802.11bd specific messages.

802.11bd also has introduced adaptive repetition, currently only for the 10 MHz channel mode [61]. Adaptive repetition is where there are optional retransmissions, dependent on how busy the channel is. The proposed parameters for 802.11bd's adaptive repetition mechanism are shown in Table 2.3. Retransmissions are seen differently between 802.11p stations and 802.11bd stations [64]. In 802.11p stations, the retransmissions are seen as independent messages, increasing the likelihood the message is correctly received at least once. For 802.11bd stations, the messages can be combined, repairing mistakes. Repairing the messages means that even if none of the individual copies of a message is received correctly, a fully copy of the message may be retrievable.

To allow 802.11bd to work at higher relative speeds than 802.11p (up to 500 $\mathrm{km\,h^{-1}}$), the standard now includes randomised midambles [61, 65]. Midambles are training symbols, periodically inserted into the data during transmission and are used to track the changes in the wireless channel due to vehicle mobility. The effect of adding midambles to 802.11bd was investigated in [66–68]. All three investigations found that midambles improved the amount of error free throughput and the Packet Error Rate (PER). 802.11bd will support three different midamble periods allowing a training symbol to be placed after every 4, 8, or 16 data symbols [61]. [66] found that in most cases the shorter midamble periods reduced the PER roughly the same amount as longer

Table 2.3 The proposed number of retransmissions based on the channel busy ratio (CBR). Adapted from [64].

Measured CBR	Number of Retransmissions
CBR ≥ 0.6	0
$0.3 \geq$ CBR < 0.6	0 or 1
$0.2 \geq$ CBR < 0.3	1
$0.15 \geq$ CBR < 0.2	2
CBR < 0.15	3

midamble periods. Thus, in most cases, the shorter midamble periods did not decrease error rates enough to compensate for the increased transmission time. The exception to this finding is the Highway Non Line of Sight (NLOS) case, where the performance of each midamble period diverged and the shorter period performed better than longer periods.

Like NR-V2X, 802.11bd will support mmWave operations [69] and some preliminary investigations have been completed in [70]. However, as the time of writing, the 802.11bd development group are still discussing what this support will look like. 802.11bd mmWave operations will likely be based on the high data rate mode in IEEE 802.11ad [71]. Similarly to NR-V2X, any mmWave support will not be discussed further due to this thesis' focus on the sub 6 GHz operation of V2X communication.

802.11bd will also support ranging, allowing vehicles to determine the distance to other 802.11bd-enabled vehicles [61]. There are two different ranging methods in the the standard, however not all 802.11bd stations may support both methods as one is optional [72].

2.4.4.1 IEEE 802.11bd MAC protocol

The MAC protocol in 802.11bd will look similar to the EDCA protocol presented in Section 2.4.3.1. To ensure fairness between 802.11bd and 802.11p, the EDCA protocol in 802.11bd will use the same parameters as 802.11p [73]. However, some changes are needed to deal with the combined 20 MHz channel. At the MAC, one of the 10 MHz channels is called the primary channel, the other is the secondary channel. Which channel is the primary channel is set by the higher layer protocols.

When using a 20 MHz channel, the channel access procedure is based off the states of the two channels. Each of the channels uses the same backoff procedure, and both use a joint backoff counter. However, the primary and secondary channels are treated differently if they are found to be busy [61]. If the primary channel is found to be busy, the backoff procedure for the 10 MHz channel is used. If the secondary channel is busy and the station knows how long the channel will be busy for, when the channel goes idle, the backoff procedure should resume after an AIFS interval. If the secondary channel is

detected to be busy, and the station does not know how long the channel is busy for, the backoff procedure resumes one EIFS after the channel goes idle.

2.5 WIRELESS CHANNEL MODELS

Wireless channel models are a key part of simulating wireless communication systems and are responsible for helping ensure simulated results represent reality. There are two major types of channel model: link-level, and network-level. Link-level models are used for link-level network simulations, which simulate the individual physical links between transceivers, and are important for determining the performance of PHY and data link layers. As such, link-level simulations generate waveform-level information of a systems performance on a sample-by-sample basis [74]. Channel models at this level of simulation are complex and focus on modelling the waveform-level distortions caused by propagation effects (e.g. reflection, scattering, multipath channel response, frequency selective fading) [75].

Network-level channel models are used for network simulation, which investigate the large-scale behaviour of many nodes in terms of throughput, end-to-end latency, congestion, and network capacity [76]. To study a network at scale there may be tens of thousands of end user and infrastructure devices which may send several thousand packets each [77]. To make simulating these large scale networks tractable, network simulators develop simplified, abstracted models for the lower layers of the system (typically the PHY and data link layer). As such network-level channel models do not provide an accurate characterisation of the channels effect on individual bits or samples in a waveform like in link-level simulators. Rather, channel models at this level model the general statistics of the channel and are used to determine the received signal-to-noise ratio. The signal-to-noise ratio is then related to a packet error rate tables generated from link-level simulators. This reduces the complexity of the calculations required.

This thesis focuses on network-level channel models as that is type of simulation best suited to answering the research questions posed in Chapter 1. As such, the remainder of this section will discuss only network-level channel models. Section 2.5.1 discusses the different factors which affect signal propagation and how they are modelled in network simulators. In Sections 2.5.2 and 2.5.3, the free space path loss model and empirical log-distance models are described. An empirical log-distance model is used to develop the warehouse channel model from measurements in Chapter 6. Finally, Section 2.5.4 discusses the WINNER II channel models, a set of wireless channel models commonly used when simulating V2X technologies. The WINNER II channel model is used for verifying the MAC layer of the C-V2X simulator in Section 5.2.2.

2.5.1 Factors Which Affect Signal Propagation

There are three main factors which affect signal propagation at the network simulator level: path loss, shadowing, and fast fading. Path loss describes the difference between the transmitted and received signal power [78]. This loss of energy arises from the signal either being absorbed or scattered by objects in the environment and the natural diffusion of radiating energy. Shadowing is an abstraction for variation in the large-scale propagation of wireless signals and is typically modelled using a log-normal distribution with mean one [79]. Shadowing is caused by large obstacles interfering with the path of the transmission and changing the received power. A stochastic process is used as the effect on signal strength is highly dependent on the environment: since we cannot know the environment completely the shadowing must be modelled statistically [75].

Fast fading deals with the effect of multi-path interference on the received signal. Specifically, it is an abstraction for many different scattered signals arriving at the receiver [75]. These scattered signals can even be the same signal delayed in time due to having travelled along a different path to the receiver. This can lead to large variations in the received power, typically up to 40 dB, over small distances and periods of time [80]. Since the behaviour of electromagnetic waves is bounded by physical laws, fast-fading is a deterministic process, however, to sufficiently model the behaviour the environment must be known in exact detail. This is not practical in most cases, so statistical descriptions are used [81]. Fast fading can be modelled by several different stochastic functions, e.g. Rayleigh fading and Nakagami-m fading [79].

2.5.2 Free Space Path Loss

The simplest path loss model is free space path loss based on the Friis equation. In the free space path loss model, there are no obstacles for the transmitted signals to reflect or scatter off, not even the transmitter and receivers themselves. As such, the transmitted signal radiates as a perfect sphere of energy and the path loss attenuation (PL) at d metres from the transmitter is [78]

$$PL = \left(\frac{4\pi d}{\lambda}\right)^2, \tag{2.4}$$

where λ is the wavelength of the signal (metres), calculated as

$$\lambda = \frac{c}{f}, \tag{2.5}$$

where c is the speed of light in a vacuum (metres per second), f is the frequency of the transmission (hertz). This can be expressed in the logarithmic domain as

$$\widehat{PL} = 20\log(4\pi) + 20\log(d) - 20\log(\lambda), \tag{2.6}$$

where $\widehat{PL}$ is the path loss attenuation in decibels.

Since there are no obstacles or items in the environment, fading and shadowing are not possible. Thus, the only factor effecting propagation is the distance between the transmitter and receiver.

2.5.3 Empirical Log-Distance Channel Models

Empirical log-distance path loss models are a class of path loss models parameterised using real world measurements [82]. These models are all roughly of the form

$$\widehat{PL} = \widehat{PL\,(d_0)} - 10\alpha \log\left(\frac{d}{d_0}\right), \tag{2.7}$$

where $\widehat{PL}$ is the path loss attenuation in decibels at distance d, $\widehat{PL\,(d_0)}$ the path loss at the reference distance d_0, and α is the path loss exponent. The reference distance is an arbitrarily chosen distance, close to the transmitter, at which the base path loss of the model is measured or defined. These models were created based on the observation that the signal strength is inversely related to some power of the distance. The parameters for these models are generated by fitting measurements to Equation (2.7).

However, despite being fitted to measured data, the path loss exponent (α) can have physical meaning. For example, if the reference distance is fixed to 1 m and the wavelength λ is constant, free space path loss model, presented in Equation (2.6), can be restated with

$$\widehat{PL\,(d_0)} = 20\log(4\pi) - 20\log(\lambda), \tag{2.8}$$

and

$$\alpha = 2. \tag{2.9}$$

This means that when the path loss exponent is two, the received signal strength is similar to being in free space. If the path loss exponent is greater than two, the path loss is worse than free space, and if it less, the path loss is worse. This provides an easy metric to compare the relative strength of attenuation in different channels.

To deal with shadowing, a log-normal random variable is included in the path loss equation in the logarithmic domain. This means the path loss equation becomes

$$\widehat{PL} = \widehat{PL\,(d_0)} - 10\alpha \log\left(\frac{d}{d_0}\right) + \widehat{\chi_\sigma}, \tag{2.10}$$

where $\widehat{\chi_\sigma}$ is a normally distributed random variable with zero mean, and a standard deviation of σ.[2] The value of σ, like the path loss exponent, is also fitted to the

[2] A log-normal random variable in the natural domain is normally distributed in the logarithmic domain.

measurement data. Since this models the large scale, long term variation of the signal, $\widehat{\chi_\sigma}$ is evaluated over long time scales.

Empirical log-distance channel models do not have a standardised way to generate fast-fading values as it is not within their scope. Some network-level models use Nakagami-m, Rician, or Rayleigh random variables to generate the effects of fading [79, 83, 84]. Like shadowing and path loss, the parameters for these random variables can be based on real-world measurements.

2.5.4 WINNER II Channel Models

The WINNER II channel models, documented in [85], cover a wide range of scenarios and frequencies (2–6 GHz) making them useful for simulating many different wireless technologies. The WINNER II channel models are two-dimensional empirical log-distance channel models, fitted to measurement data collected for each scenario at multiple locations [86]. In addition to the log-distance channel models for network-level simulations, the WINNER channel models also provide a procedure and parameters for generating link-level simulation models.

The WINNER II channel models form the basis of the 3GPP and ITU-R channel models [87,88]. However, the 3GPP model has been extended to include all three spatial dimensions and covers a wider range of frequencies (0.5–100 GHz) [87, 89].

Chapter 3

STATE OF THE ART

This chapter provides an overview of the current state of the art in V2X technologies. Section 3.1 discusses comparisons of the two technologies available in the academic literature and helps answer research question Q1, which explores the difference between the V2X technologies. Section 3.1 also provides context for the investigation into the effect of density (Q2) and the effect of MCS and transmit power choice (Q3) discussed in the remainder of the thesis. Section 3.2 reviews the current literature around deploying V2X technologies in industrial environments, highlighting the lack of research of applications in the warehouse environments. Then, Section 3.3 details previous efforts to characterise the warehouse wireless channel, contextualising the work performed in Chapter 6. Finally, Section 3.4 discusses previous work into intersection collision warning and avoidance systems, motivating the collision warning application used for evaluating the technologies described in Chapter 4.

3.1 COMPARISONS BETWEEN V2X TECHNOLOGIES

As each of the technologies covered in Section 2.4 have been released at different times there is varying amounts of literature available for each. As the oldest protocol 802.11p has the most literature dedicated to it and it has been thoroughly scrutinised through theoretical analysis [57], simulation [12], and real-world deployment [13, 14]. C-V2X is less studied as it is a younger technology. Most studies on C-V2X are based on simulations [10] as until recently hardware to support C-V2X was not available. As NR-V2X is newly released and 802.11bd is still under development there exists very little research into these technologies.

Bazzi et al. [39] found that C-V2X had a longer range than 802.11p at the expense of latency. They came to these conclusions via MATLAB simulations measuring the Packet Reception Ratio (PRR) — the ratio of correctly received to transmitted packets — and the Update Delay (UD) — the amount of time passed between two consecutive packets. The simulations are completed for a variety of road conditions and vehicle densities. In a six lane highway scenario where there are 25 neighbours within 200 m of

the transmitting vehicle, 802.11p achieves a PRR ratio greater than 90%, 90 m away from the transmitter. C-V2X mode 4 achieves the same PRR, in the same scenario up to 180 m away from the transmitter using the same transmit power.

[39] also attempts to address what 802.11bd's performance could look like by simulating the 802.11p MAC protocol grafted onto the C-V2X physical layer. The modified 802.11p is evaluated against C-V2X mode 3 and mode 4. With the PHY layer changes, across all evaluated distances 802.11p performs similarly in terms of PRR and update delay to C-V2X in mode 4, but worse than C-V2X mode 3. It is not clear whether in this mode, the packet repetition from the blind HARQ procedure is accounted for when calculating the PRR. Regardless, the improvement in range suggests the performance differences between the two technologies is due to the physical layer and the more global view the eNodeB has in C-V2X mode 3.

Anwar et al. [90] developed similar conclusions to Bazzi et al., using both a theoretical and a simulation-based approach. They develop theoretical minimum transmission latency and maximum data rates for 802.11p, a candidate for 802.11bd, C-V2X, and NR-V2X, and then simulate PER, PRR, and UD. In terms of latency, 802.11p and 802.11bd outperform both NR-V2X and LTE-V2X for 100 Byte (B) and 1500 B messages. NR-V2X had a higher maximum theoretical throughput than both 802.11p and 802.11bd. Their theoretical results for latencies are summarised in Table 3.1. The theoretical result for latency in NR-V2X has a major limitation: they only consider NR-V2X slots to be the smallest allocable unit of time. NR-V2X, however, has mini-slots which could reduce latency by a factor of seven for short messages.

From their simulations, Anwar et al. found that for 100 B messages the 802.11bd candidate outperformed the other technologies with respect to PER, due to the insertion of midambles. In the case of the 1500 B messages, NR-V2X and C-V2X performed better than standard 802.11bd due to the increased error correcting power of turbo and LDPC FEC codes. However, the DCM mode of 802.11bd still outperformed both the cellular V2X standards. For 100 B, 802.11p and 802.11bd achieve a PRR of 90% at 225 m, whereas NR-V2X and C-V2X achieve the same at 450 m. For 1500 B all technologies, except 802.11p, achieved a PRR of 90% 60 m sooner than in the 100 B case. In the case of 802.11p, a PRR of 90% was achieved at 80 m. For short messages (100 B) 802.11p, 802.11bd, and NR-V2X can all deliver UD of less than 1 ms up to 300 m. The DCM mode of 802.11bd, NR-V2X, and C-V2X can all deliver an UD of less than 10 ms up to 500 m away, whereas 802.11p and standard 802.11bd can only deliver this up to 450 m.

The figures Anwar et al. present are achieved in close to ideal conditions and only consist of two nodes, i.e. there are no other interfering nodes possibly causing collisions. This explains why their estimation of each technology's performance exceeds the findings presented in [39], which has a number of vehicles transmitting at the same time.

Table 3.1 Minimum and maximum latency results for the V2X communication summarised from Anwar et al. [90]. All results are provided in milliseconds.

Packet size	802.11p	802.11bd	802.11bd DCM	C-V2X	NR-V2X
100 B	0.104–0.344	0.100–0.336	0.212–0.600	1–1	0.25–0.75
1500 B	0.520–4.08	0.388–3.98	2.03–7.88	1–11	1–8

In [91], Mannoni et al. present a comparison between C-V2X and 802.11p based on their performance as the density of vehicles increases. Their comparison is based on a single link between two vehicles in the centre of a disk shaped network with other vehicles placed randomly around it, simulated for 5 s. All vehicles are static. The performance is measured using two different metrics: range at which a PER of 1% is achieved and resource access delay. In terms of range, initially, C-V2X outperforms 802.11p, achieving approximately 425 m in the presence of no other nodes. However, the range limit for C-V2X decreases linearly as vehicle density increases, whereas 11p's range decreases exponentially and reaches what appears to be limit of roughly 180 m. The complete results are in Figure 3.1.

The increased range seen at low densities in Figure 3.1 is due to the enhanced physical layer performance of C-V2X compared to 802.11p. This enhanced performance becomes less relevant to the range as the density, and thus the collision rate, increases. The dramatic loss in range for C-V2X is due to collisions. C-V2X transmitters assume they are the only one with a reservation for a specific resource and thus start transmitting immediately when their reservation begins. This assumption does not hold when the number of transmitters is increased as there is an increased likelihood there will be duplicate resource reservation, and thus a collision. 802.11p on the other hand, ensures the channel is at least locally free before transmitting, meaning that collisions occur less frequently.

It must be noted that the range figures presented in Mannoni et al. for zero vehicle density (i.e. no other interfering vehicles), match the results presented by Anwar et al. for both C-V2X and 802.11p. This direct comparison is possible because a PER of 1% corresponds to a PRR of 99% (Appendix A). Unfortunately, the results in Mannoni et al. cannot be compared to the results in Bazzi et al. as the scenarios used in [39] have densities far greater than in [91].

[91] also compares the average resource access delay between the two technologies. The resource access delay is how long each protocol spends trying to access the channel. C-V2X as expected, has a constant resource access delay as density increases due to the constant time performance of the resource reservation scheme. In 802.11p however, the resource access time increases with vehicle density, as there are more vehicles trying to access the channel at any given time.

In [93], the authors investigate the effect of periodic and aperiodic messages with variable lengths for both C-V2X and 802.11p. Like Bazzi et al., Anwar et al., and

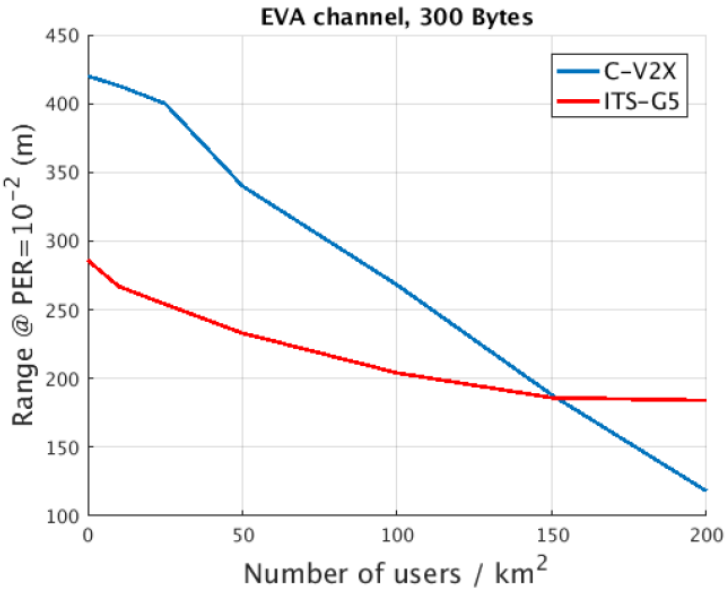

Figure 3.1 The range of C-V2X and IEEE 802.11p (ITS-G5) as a function of vehicle density. ITS-G5 is an alternate standardisation of IEEE 802.11p for the European Union which uses a different frequency range [92]. Source: [91] © 2019 IEEE.

Mannoni et al., they found that over shorter distances 802.11p performed better than C-V2X across the densities simulated for periodic and aperiodic messages of the same size. Over longer distances C-V2X performed a lot better due to the better physical layer performance when compared to 802.11p. In the case of aperiodic messages of variable size, C-V2X performs consistently worse than 802.11p, even over longer distances, as density increases. This is as frequent resource reselection increases the likelihood of collisions. With frequent changes in message sizes and periodicity, new resources must be reserved more often.

In addition to its exploration of periodicity and messages size, [93] also evaluates the claim that 802.11p's performance over long distances can be improved with changes to the physical layer. This claim is implied by Bazzi et al. and Mannoni et al., and stated in [12]. [93] explores this hypothesis by using the C-V2X block error rate performance to calculate the likelihood a packet is received for 802.11p. The authors found that the range of 802.11p is increased by the change in physical layer but still performs worse than C-V2X over long distances. They claim the difference in performance is due to the 802.11p transmissions being across the full 10 MHz channel and thus experiencing more noise than C-V2X, which only transmits across a subset of resource blocks.

The 5G Automobile Association (5GAA) present in [11] a comparison between C-V2X and 802.11p couched not in networking terms, but in application performance. Specifically, they look at the likelihood an alert message will be delivered in time and use this to estimate how many fatalities can be avoided with each system. They evaluate the technologies in urban, rural, and motorway scenarios. The authors define the probability

that an alert will be delivered in time as the PRR at the safe stopping distance for a range of speeds appropriate to the scenario.

To determine the PRR, the 5GAA use a network level simulator, with each scenario based on the 3GPP's simulation suite for evaluating V2X communication in [94]. In the six lane highway scenario C-V2X achieved a PRR of 80% at ≈150 m, whereas 802.11p achieved the same PRR at ≈100 m. These results are similar to the results presented by Bazzi et al. Overall, the 5GAA find C-V2X to be more likely to successfully deliver a warning message in all three scenarios. Based on these simulation results, the technology penetration rates, the crash rates, and the effectiveness of the messages the authors found that C-V2X could save 20 000 more lives, and avoid 300 000 more serious injuries than 802.11p. The authors of [11] state that C-V2X reduces fatalities and serious injuries more when compared to 802.11p due to better performance at the radio link level.

The claim that C-V2X has a longer range than 802.11p as reported by Bazzi et al., Anwar et al., and Mannoni et al. is refuted by Turley et al. in [12]. Turley et al. claim that their real-world, physical implementation of 802.11p can achieve a PRR of 90% over 500 m away. Simulation results based on measurements performed on their system in a highway scenario are compared to simulation results from Qualcomm in [95], which are similar to those presented by the 5GAA in [11]. These simulation results seem implausible as all the other estimates for 802.11p's range presented here are much lower. The results presented by Turley et al. are based on those presented in Alexander et al. in [96]. Both Turley et al. and Alexander et al. fail to identify why their implementation performs so much better than simulations in the literature, nor do they discuss how their simulation is structured.

With the notable exception of Turley et al. and Alexander et al., all the papers discussed here agree that 802.11p is worse than C-V2X over long distances. This is the main advantage of C-V2X over 802.11p. However, it is unlikely the improved range of C-V2X will be relevant in the warehouse environment this research focuses on.

3.2 V2X COMMUNICATION SYSTEMS IN INDUSTRIAL ENVIRONMENTS

There has been very limited work exploring V2X technologies in an warehouse environment. A very preliminary exploration is performed by Mustovic in [24], which evaluates 802.11p in a warehouse. However, Mustovic's investigation is restricted to very basic PRR measurements in a single warehouse and does not consider C-V2X. Other than this investigation, there are no other known works that look at using V2X technologies in warehouses.

In the context of a wider industrial environment, there are a few academic works which explore using V2X technologies for mining environments [97–99]. [97] and [98]

were performed together and investigated using 802.11p in an underground mining environment, with one analysing the performance at the link-level and the other determining where antennas should be placed on mining vehicles. [99] simulates the effect the choice of routing protocol has on the average end-to-end delay as the number of vehicles increases, when using 802.11p in an underground mining environment.

However, academic literature is not the only place where using V2X technologies for industrial environments is being explored. Currently there are several companies offering V2X and connected fleet solutions to mining operations. These systems are all based on 802.11p as, at the time of writing, C-V2X hardware has only recently become available. Of these systems, Cat's MineStar system has the most information publicly available. The Cat system supports both above- and below-ground mining operations and provides basic features such as proximity alerts, speed zone enforcement, and entry and exit notifications. The underground mining version of MineStar also supports advanced, bandwidth-intensive processes like teleoperation, which have strict quality-of-service requirements [10, 100]. This teleoperation technology is deployed in at least one mine: Newmont Goldberg's Tanami Mine in Northern Australia [18]. Achieving the performance requirements of teleoperation requires a lot of infrastructure. This is feasible in an underground mining scenario where there is already a lot of capital investment in deploying infrastructure. However, it is less feasible for a standard industrial or warehouse deployment.

In addition to the solutions offered by Cat and Cohda Wireless there are also solutions offered by ModularMine [101] and Wenco Mining Systems [102]. The solutions only offer basic proximity awareness and do not support any of the advanced features advertised by Cat.

3.3 THE WAREHOUSE WIRELESS CHANNEL

The warehouse wireless channel has not been very well characterised in the literature [106]. Even fewer papers have attempted to characterise the wireless channel in the frequency range V2X communications uses: 5.8–5.9 GHz. This section summarises some prior work investigating the warehouse channel.

Croonenbroeck et al. [103] presents measurements at 5.5–6.1 GHz meant for use with the IEEE 802.15.4a channel model. However, this paper characterises multiple industrial environments and does not give full treatment to the warehouse environment. Croonenbroeck et al. only perform Line Of Sight (LOS) and obstructed-LOS (OLOS) measurements in the warehouse, neglecting the NLOS case. Additionally the warehouse they studied was small and was primarily used as a workshop, with a large empty area at the front and limited racking at the back for storage. One interesting result of their study is that for transmission distances greater than 20 m, the coherence bandwidth — the bandwidth over which the channel can be considered to have similar fading

characteristics — was between 10 and 20 MHz. This is wider than the channels used in V2X technologies, meaning that the fading characteristics may be flat across the entirety of the channel. The authors also noted that often the path loss exponent was less than free-space path loss and that the small scale fading nearly matched Rayleigh fading.

Tanghe et al. in [104] perform measurements at 900 MHz, 2.4 GHz, and 5.2 GHz in four different industrial locations, two wood- and two metal-processing factories. In these facilities the equipment is organised into aisles, and there are some racked warehouse storage areas. One area in the warehouse stores large solid cardboard and wood boxes, stacked to form aisles. The resulting measurements are used to parameterise a empirical log-distance channel model and characterise the temporal fading in the warehouse channel. Similarly to Croonenbroeck et al., Tanghe et al. noted path loss exponents close to or less than the free space path. The authors attributed this to the industrial aisles acting as waveguides and they expect this behaviour to be enhanced by metal racking. The effect of industrial aisles acting as waveguides was also found by Bosselmann in [105], who observed the effect when modelling RFID systems for forklifts using a ray tracing simulator. When analysing the temporal fading, Tanghe et al. found it followed a Ricean distribution.

Sangodoyin et al. in [106] present measurements for a multiple-input and multiple-output (MIMO) ultra-wideband warehouse channel model. The measurements they report are for the 2–8 GHz frequency range and were conducted in a metal-racked warehouse with a low roof that primarily stores stationery, books, and computers. From these measurements they extract the key large scale parameters such as path loss exponent and the standard deviation due to shadowing. They also extract the small scale fading parameters to be used in a statistical geometric channel model such as the WINNER models. Like Tanghe et al. and Croonenbroeck et al., Sangodoyin et al. also present path loss exponents less than or close to free-space gain. However, the measurements provided are for 64 channels across the entire 6 GHz bandwidth, meaning their measurements are not useful for modelling narrowband channels. Additionally, none of the V2X technologies use MIMO technologies. Some of the authors of Sangodoyin et al. also produced measurements for a single-input and single-output system in [107], however, the same frequency resolution problem still applies.

Karaagac et al. in [108], present wireless channel measurements for a connected 2D shuttle system in a warehouse. These shuttles are designed to collect and move pallets around in a warehouse where there are no aisles between racks, increasing the storage density. However, these measurements were made at 868 MHz and 2.4 GHz, outside of the range of V2X communication. Unlike in [103, 104, 106, 107] the path loss exponents measured were close to 3 — higher than free space path loss. This can likely be attributed to the fact that the shuttles are inside the densely packed metal lattice of the racking.

Wang et al. [109] developed a ray tracing simulator to investigate the coverage of 5.8 GHz WiFi base stations in a warehouse for communicating with moving autonomous handling robots. The authors note that the main energy of the signal comes from the LOS path between the transmitter and receiver. When this direct path is disrupted, such as by racking, the received signal strength drops significantly.

3.4 INTERSECTION COLLISION PREVENTION AND WARNING SYSTEMS

There have been various approaches to intersection collision prevention and warning systems explored in the literature [4, 19, 110–112]. However, most do not rely on V2X technologies, relying on internal sensors or traditional wireless communication systems to coordinate with infrastructure. As such, this section focuses on the current state of infrastructure-free V2X-based solutions to intersection collision prevention.

To completely eliminate collisions from intersections, formal methods with provable safety have been explored by Hafner et al. [113]. They designed a purely distributed system, relying only on V2V communications. To achieve this, the algorithm creates a 'bad' set of speeds and positions that cause collisions, then (using a model of the vehicle's movements) it calculates the capture set, the set of all vehicle configurations which enter the bad set regardless of any throttle and brake inputs applied. From this capture set a control map can be constructed which defines what actions should be taken to avoid collisions by keeping the vehicle from entering the capture set. This means that the vehicle safety system only needs to take control of the vehicle when the vehicle touches the boundary of the capture set, leaving the human operator in control the remainder of the time.

To test their system, Hafner et al. built a prototype using DSRC and tested it using two vehicles on a test track at a T-intersection. In the test, vehicle A was travelling along the top of the T when vehicle B pulls out in front of it. The vehicle safety system detected vehicle B and applied the appropriate corrective action. In addition to testing the basic functionality, they also introduced imperfections into the state knowledge, representing performance when communication delays and sensor noise occur. In this case the algorithm performed similarly to the perfect state information case, and avoided the collision. Currently, the model presented in [113] does not scale to more than two vehicles, making it impractical for real world use.

One other approach to collision avoidance at intersections is Virtual Traffic Lights (VTLs) which introduces traffic-light-control into all intersections. Using VTLs was first proposed by Ferreira et al. [114], who were interested in reducing road congestion. However, VTLs have the effect of turning all uncontrolled intersections into controlled intersections, reducing the chance of collisions for rule-obeying drivers. In [114], Ferreira et al. propose a distributed V2V VTL system design and perform some simulations

to demonstrate the gains of the system. However, since their focus was on congestion reduction, their simulation metrics focused on this rather than any collision reductions. Their algorithm is as such: when multiple vehicles are approaching an intersection, they elect a leader who will act as temporary infrastructure. To be eligible to be a leader, the vehicle must be the closest vehicle in its cluster to the intersection and it must be presented with a red light whilst in control of the intersection. All vehicles but the leader are passive nodes in the protocol, only periodically updating their location. The vehicle node periodically broadcasts VTL messages, informing approaching vehicles of the current traffic light phase. When the lead vehicle detects no more vehicles attempting to enter the intersection from the direction with the green phase, it changes the VTL message to indicate the new phase. If the lead vehicle's lane is now in the green phase, it selects the first vehicle in a red phase queue to be the new leader. If there are no stopped vehicles (i.e. there are no vehicles on a red phase) the VTL can be disbanded as it is no longer required. This algorithm does not consider fairness of access to the intersection, meaning one stream can dominate access, however, this failing is addressed by Guo et al. in [115] who propose their own VTL algorithm.

Wang and Chen in [116] propose a collision warning algorithm that uses kinematic models of the vehicles to predict the minimal future distance between two vehicles. This is then used as a threshold (combined with the predicted vehicle speed) to trigger warnings to the drivers. There are two possible warnings under their system emergency- and normal-warnings, which are triggered based on different thresholds. Wang and Chen simulate their proposed algorithm for a T-intersection and found its performance acceptable, with false positive rate of 2.4% and a false negative rate of 3.6% for normal-warnings. They did not observe any instances of the algorithm failing with for cases where an emergency-warning was appropriate. The simulations performed in [116] did account for localisation error, but did not consider the effect V2V communications would have on the algorithm. Nor did it consider cases with more than two vehicles.

Joerer et al. [117] investigates an intersection collision prediction algorithm from a networking perspective, using the algorithm to investigate the effect of beacon frequency on 802.11p's ability to support a safety application. The algorithm they describe determines the overall probability of a collision occurring at a simple four-way intersection based on integrating over all possible acceleration values and determining if there will be a collision, weighted by the probability that acceleration will be picked. This algorithm performs well for the fixed path, no-turning scenario Joerer et al. explore, however, it is not clear whether this algorithm could be extended to handle the case where vehicles can turn. To evaluate 802.11p's performance, the collision probability threshold required to successfully warn drivers about 95% and 99% of collisions was determined for a range of beaconing frequencies. The authors found that that for low beaconing frequencies, the thresholds had to be very low, leading to many false positives. For higher beacon frequencies the thresholds were satisfactorily high, but the authors comment

that beaconing at these rates would overload the network.

Chapter 4

EVALUATION METHODOLOGY

This chapter discusses how the key research questions, posed in Chapter 1, will be answered. Specifically, it focuses on answering questions Q2 and Q3. Q2 addresses how the density of vehicles affects the performance of a collision warning application, whereas Q3 explores how the modulation and coding scheme and transmit power affects the performance of a collision warning application. These parameters are not the only ones which affect the algorithm's performance. For example, there is also the beaconing frequency (how often data is transmitted by each vehicle) and vehicle speed, both of which are treated as constant. Discussion of the remaining questions, Q1 and Q4, is left to Chapters 2 and 8. However, the results generated from this evaluation method will be used to inform the discussion around question Q4. Firstly, this chapter describes the methodology and scenario used to evaluate the two technologies. Then, it outlines the model warehouse environment the evaluation scenario uses. Finally, the collision prediction algorithm used is described.

4.1 EXPERIMENT SETUP

To answer research questions Q2 and Q3, the failure rate of a simple collision prediction algorithm was evaluated under each technology. The failure rate provides an application-specific metric defining how well (or poorly) each technology supports safety critical communication systems in an industrial environment. Specifically, the technologies will be evaluated for their ability to support an algorithm to predict aisle-end collisions between forklifts in warehouses (Figure 4.1). For this thesis, a collision is not defined as when two or more vehicles physically collide, but as when forklifts violate set safety distances. All other types of collisions are disregarded.

The specific collision prediction algorithm used to evaluate the technologies is discussed in Section 4.3. The algorithm has two possible failure modes: producing a false positive or producing a false negative. A false positive is where the algorithm mistakenly predicts a potential collision without one occurring. A false negative is the opposite, where the algorithm fails to predict a collision that does occur. Each error

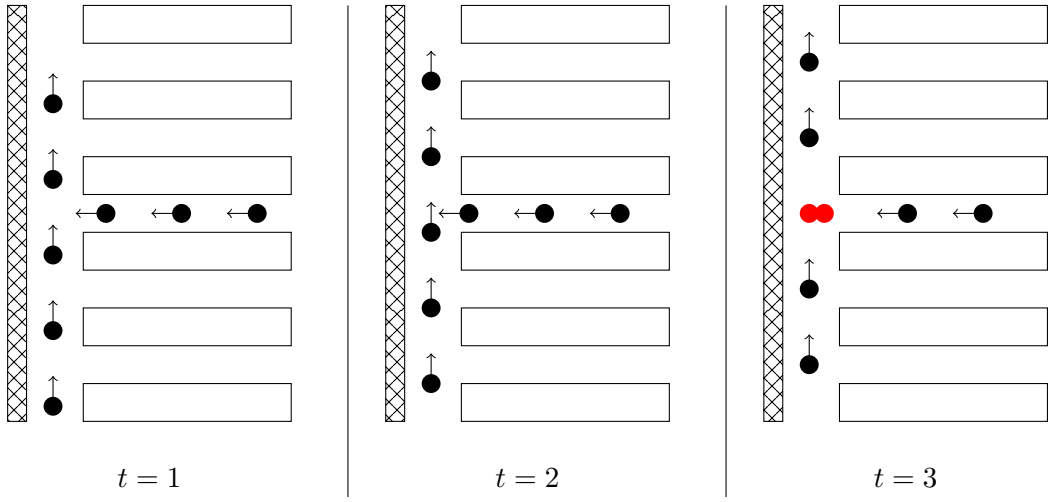

Figure 4.1 The collision scenario under consideration. The empty boxes represent racking and the hatched boxes represent an external warehouse wall.

class is dealt with independently as they have different safety implications and causes. Both false positive and false negative errors are can be caused by incorrectly predicting the position of the vehicle based on out-of-date information, which could be caused by missing a single beacon from vehicles. However, false negatives can also be caused by having no data about a vehicle as the collision prediction algorithm defaults to the intersection being safe and attempts to prove it unsafe to enter. As such, false positives cannot be caused by having no information about a vehicle. A vehicle being unaware of another vehicle is caused by either never correctly receiving beacons from it or missing too many consecutive beacons, so that the data about the other vehicle is stale.

Each stream of forklifts in the scenario was modelled simply, with every vehicle in the same stream following the same path and travelling at a constant speed. This choice of simple mobility was to avoid modelling realistic behaviours of forklift operators, as it seems unnecessary to model that level of detail to obtain answers to the key research questions. To introduce variation into each scenario, forklifts are added to each stream with a given probability each second, resulting in streams of vehicles distributed as a Bernoulli process. Without this variation (i.e. if constant introduction periods had been used) the number of possible collisions at a given introduction rate would be restricted or inflated, artificially increasing or decreasing the collision rate.

The algorithm is run when the forklift travelling along the terminating aisle is its safe stopping distance away from entering the intersection, allowing it enough time to safely stop before entering the intersection. This is the only point in the simulation where the collision prediction algorithm is run. Even if the outcome of the collision prediction algorithm indicates the intersection is not safe, the forklift enters the intersection and completes the turn. Always turning, without respect to safety, results in one part of the warehouse having on average twice as many forklifts, as the number of forklifts in

that section is the sum of the two Bernoulli process streams. This may not be realistic for high vehicle density scenarios, as it increases the contention for the radio channel and background noise beyond what could be reasonably expected. However, at lower forklift densities, this is a reasonable model. Furthermore, the added contention and background noise helps stress the technologies, allowing observation of their behaviour in adverse conditions.

It is worth briefly noting that, even accounting for the doubling of forklifts in one part of the warehouse, this simulation scenario is artificial and does not match real world forklift operator behaviour. However, the research questions Q2 and Q3 are not interested in modelling how forklift operators drive around in a warehouse, nor, are they interested in the optimisation of a collision prediction algorithm. Rather, Q2 and Q3 are interested in the ability of each communication system to support this particular safety application and exploring the factors which affect this ability. As such, even though the experiment scenario is artificial and unrealistic, it is still appropriate to answer the research questions.

4.2 MODEL WAREHOUSE AND FORKLIFT

This section defines the model warehouse parameters and some of its basic underpinning road rules. Additionally, the model forklift used for the experiments is defined and its key properties explored. For simplicity, this thesis assumes that forklift operators perfectly follow all rules and have perfect information about everything within in their line of sight.

For the purposes of modelling, the warehouse was reduced to the bare requirements for the scenario: a T-intersection (Figure 4.2). The model warehouse is not based on any real warehouse. Each arm of the T-intersection was 200 m long. The width of the aisle was not considered as this model warehouse is focused on forklift mobility, rather than modelling the effects of the racking. Modelling the effect of the racking, its contents, and the wider warehouse structure was left to the warehouse channel model described in Chapter 6.

For clarity, how the different parts of a T-intersection will be referred to is shown in Figure 4.3. The horizontal part of the T-intersection (red in Figure 4.3) will be referred to as the top of the intersection. The vertical part of the T-intersection (blue in Figure 4.3) will be referred to as the stalk of the intersection.

There are many different kinds of forklift, and the model forklift discussed here was loosely based on a popular type of stockpicker. The stockpicker is 3 m long and carrying its maximum design load travels at a maximum speed of 10.4 $\mathrm{km\,h^{-1}}$ (2.89 $\mathrm{m\,s^{-1}}$). The forklift has a worst case stopping distance of 3.13 m under full load. Assuming constant

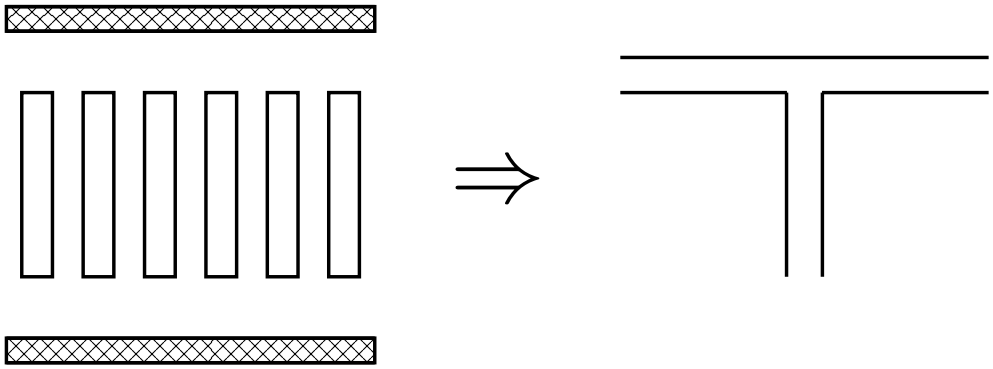

Figure 4.2 A typical layout of a warehouse (left) is reduced down to simple T-intersection (right) for the simulation scenario.

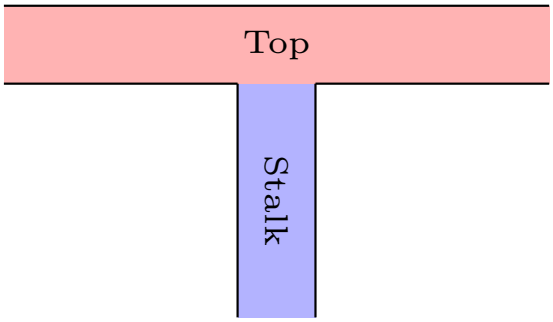

Figure 4.3 The anatomy of a T-intersection. The "top" of the intersection is highlighted in red and the "stalk" in blue.

deceleration, the stopping time can be calculated as

$$t_{\text{stopping}} = \frac{2d_{\text{stopping}}}{v_0}, \tag{4.1}$$

where t_{stopping} is deceleration time in seconds, d_{stopping} is the stopping distance in metres, and v_0 is the initial velocity in metres per second. Thus, at the forklift's maximum speed, the algorithm must determine if there will be a collision at least 2.17 s before one can occur. This critical point 3.13 m (2.17 s) away from the intersection is where the collision prediction algorithm is run in the simulation. Using this as the trigger point ignores drivers reaction time, meaning a real-world collision warning system would have to generate a warning before this point to allow operators to react and brake to prevent collisions. The time from a visual braking alert to beginning the braking process is on average 0.68 s according to [118], an order of magnitude less than the braking time, as such it is ignored as this scenario is not interested in modelling realistic driver behaviour. Additionally, it is highly unlikely the operator of a fully loaded forklift (as in this scenario) would be travelling at the maximum forklift speed towards an intersection where they would be making a 90° turn. Optimisation of the trigger point setting for real world implementation is not within the scope of this thesis, so it will be ignored.

When modelling the movement of forklifts around the warehouse, it was assumed

that New Zealand (NZ) road rules apply and that the intersection was uncontrolled. Under NZ road rules, at all uncontrolled T-intersections, vehicles on the stalk give-way to vehicles moving along the top [119]. This means forklifts on the stalk of the intersection will be responsible for stopping and giving way, and thus, will run the collision prediction algorithm. This rule does not reflect all warehouses as some warehouses treat all intersections as if they are controlled by a stop sign. This means vehicles on the stalk must come to a stop and give way to the top before proceeding [119]. This rule has not been modelled as with the ideal forklift operators assumed here, it prevents almost all collisions at T-junctions.

This thesis assumes that the safe following distance for a forklift is three vehicle lengths. This is a common following distance rule and is the minimum required under law in the United States of America [120]. This means the safe following distance for the model forklift is 9 m. However, this is measured from the end of one forklift's forks to the rear of the other vehicle (Figure 4.4), not to the internal point that the forklifts report as their position. For the model forklift, their position is reported as the centre point of the vehicle. Thus, the real safe following distance, based on coordinate to coordinate distance, is four vehicle lengths (12 m, Figure 4.4).

4.3 TEST COLLISION PREDICTION ALGORITHM

A test collision prediction algorithm has been designed for the evaluation scenario as all the previous work, explored in Section 3.4, has focused on predicting and then avoiding collisions, rather than pure detection. Again, the goal of this research is not to evaluate a collision prediction algorithm, but instead to use collision rate as a metric to compare how well each technology supports a safety application in a warehouse environment. With this in mind, all the prior solutions are too complex for the scope of this research. Most of the systems reviewed in Section 3.4 rely on vehicles having some level of autonomous control. This research assumes that the forklift has minimal autonomous capabilities, preferring operator input. However, this is not modelled to simplify the scenario and focus on the comparison of the performance of the V2X technologies.

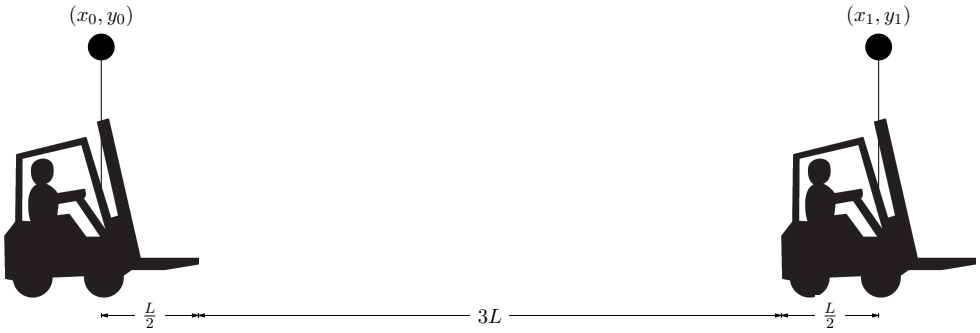

Figure 4.4 Determining safe following distance based on the vehicle length L.

The new collision prediction algorithm detects if there will be a large enough gap, between vehicles travelling along the top of the T-intersection, for a forklift on the stalk to safely begin to merge in. To do this, the algorithm predicts if, when the forklift travelling on the stalk enters the intersection, any vehicles will violate safe following distances rules. If such a vehicle exists, then a warning should be generated for the driver, however, for the purposes of the simulation, the result is simply recorded for later processing. Note that this algorithm does not check there will be no vehicles violating the safe following distances after the turn is complete, only that the instant the vehicle enters the intersection there are no vehicles which violate them. Whilst this may not be appropriate for a real-world system aiming to completely prevent collisions, that is not the goal of this system. This system is part of the test setup for the technologies, only aiming to explore the performance of the V2X technologies, as such, this limitation is acceptable.

There are two parts to the algorithm: data dissemination and data processing. Data dissemination is done by periodically broadcasting the forklifts unique ID, position, velocity data, and a timestamp. It is assumed that position, velocity, and timestamp data are perfectly accurate and that all vehicles share a common, synchronised clock source for timestamping. The assumption that location data is perfect is not unfounded, even though GPS is unreliable indoors, as there exist indoor positioning systems for warehouses which achieve centimetre level localisation accuracy (Section 2.3). Additionally, this scenario is setup to solely explore the performance of C-V2X and 802.11p in the warehouse environment. Thus, including the effect of localisation error is irrelevant in this context. When a vehicle successfully receives another vehicle's broadcast, it saves the data into a table of known vehicles replacing any data it may have received from the vehicle previously.

The data processing step determines if there is a safe gap for the vehicle to enter and is triggered when the vehicle crosses a pre-set threshold before each intersection based on the vehicle's speed and stopping distance. The vehicle speed and stopping distance for this scenario are specified in Section 4.2. A complete description of the algorithm is provided in Algorithm 1. Before this algorithm is run, the computing vehicle removes any stale data about other vehicles from its table – any data older than a timeout parameter. Despite the computing vehicle potentially forgetting about another vehicle, the simulator will still account for it when performing the ground truth calculation of whether the intersection was safe. Once the algorithm begins, the computing vehicle eliminates other vehicles which are not travelling along the top of the intersection. For each remaining vehicle in the table, the computing vehicle predicts the position of the other vehicle when it (the computing vehicle) is due to enter the intersection. When the future position of the vehicle is predicted, the time between a message being generated and being used is not accounted for. The predicted position is checked against one of two thresholds, based on the relative predicted position: if the predicted position is

ahead of the computing vehicle when it enters the intersection the fore-threshold is used, if it is behind the computing vehicle, the aft-threshold is used. If any vehicle violates either safety threshold, the safe-gap check fails and an unsafe gap is reported.

The *isOnTop* function used in Algorithm 1 is responsible for determining which vehicles to consider when calculating whether the intersection is safe to enter. It eliminates vehicles that are in the known vehicle database but are not relevant (i.e., forklifts that will not pass through the intersection and pose a threat to the computing forklift). The specific implementation of *isOnTop* is discussed in Section 5.1.5 as it is not necessary to describe the collision prediction algorithm more generally. In a real world implementation of this algorithm, determining which forklifts are of interest to the algorithm would require significant work on the *isOnTop* function. However, creating the *isOnTop* function is a mapping and localisation problem, outside of scope.

The collision prediction algorithm here is designed as part of the test rig, and thus makes several assumptions about the scenario. However, this does not affect the appropriateness of the algorithm for comparing the two technologies. In fact, the algorithm was created to exaggerate communication errors and is deliberately simple. To exaggerate the effect of communication failures, the other vehicles' position is not updated to reflect the distance travelled since the beacon was received. This punishes vehicles for missing single beacons by increasing the error on the predicted vehicle position, but is not as severe as missing multiple beacons in a row which causes data time-out. This is appropriate in this context as the collision prediction algorithm is intended to be part of the test scenario, aiming to expose flaws in the communication technologies, rather than enable a suitable collision warning application.

To simplify the algorithm, it only considers the x-direction when calculating the following distance, as the calculation is begun before the turn has started and thus the computing vehicle cannot predict its eventual y-position. This is also acceptable in this scenario as the predefined and fixed paths means that vehicles should end up in the same y-position after the turn is completed, and thus the only term affecting the following distance is the lateral following distance. This simplification, whilst unrealistic, is allowable as the aim of this is to create a suitable test metric to compare the two technologies, not create a real-world collision warning application.

In fact, a real world implementation of Algorithm 1 is inadvisable. The algorithm is not generalised and is specific to the simulation scenario described in Section 4.1. In particular, algorithm has an implicit orientation matching the right-turning simulation scenario and only cares about lateral separation between the vehicles, not true Euclidean distance, making it unsuitable for situations where vertical variation is possible. Additionally, in this scenario only the vehicle on the stalk of the intersection performs this calculation, as it has the responsibility to give way. In a real world implementation, both vehicles should perform the calculation to provide warnings to both operators to

Algorithm 1: Determine if the intersection is safe to enter. The function $isOnTop(\cdot)$ returns true if an input vehicle is on the top of the T-intersection in question.

Input: List of n known vehicles, $V = \{(\overrightarrow{s_0}, \overrightarrow{p_0}), \ldots, (\overrightarrow{s_n}, \overrightarrow{p_n})\}$ where $\overrightarrow{s} = (s_x, s_y)$ is the vehicle velocity vector and $\overrightarrow{p} = (p_x, p_y)$ is the position vector
Input: Our velocity vector $\overrightarrow{s}^* = (s_x^*, s_y^*)$
Input: Out position vector $\overrightarrow{p}^* = (p_x^*, p_y^*)$
Input: Time until we enter the intersection, t
Result: Is it safe to enter the intersection

```
V' = ∅;
// Remove vehicles that are not moving along the top of the
   intersection
for (s, p) ∈ V do
    if isOnTop(s, p) then
        V' = V' ∪ {(s, p)};
    end
end
if V' = ∅ then
    // If there are no vehicles travelling across our path we're
       safe
    return SAFE;
else
    for (s, p) ∈ V' do
        // Predict the location of the other vehicle when we enter
           the intersection (assuming it does not change its
           velocity)
        p' = p + t s;
        if p'_x < p*_x then
            // If the vehicle is supposed to be behind us, check the
               rear safety distance is not violated
            if p*_x − p'_x < REARSAFETYDISTANCE then
                return UNSAFE;
            end
        else
            // If the vehicle is supposed to be behind us, check the
               front safety distance is not violated
            if p'_x − p*_x < FRONTSAFETYDISTANCE then
                return UNSAFE;
            end
        end
    end
    // If no vehicles violate the safety distances, we're clear to
       enter the intersection
    return SAFE;
end
```

stop and prevent a collision. This algorithm will not easily generalise to the case where a vehicle on the top is the computing vehicle, as more information about the path of a turning vehicle will be required to determine the distance after it completes its turn. A general, real-world implementable algorithm could be designed based on the skeleton of Algorithm 1. However, neither of these factors, which make the algorithm unsuitable for real-world usage, affect its suitability for evaluating the performance of each technology.

Currently, this algorithm relies on all vehicles travelling at a constant speed and on a deterministic path to predict potential collisions. This is not realistic as each forklift operates independently and is driven by a human operator who, when compared to the simulated forklifts, is erratic and unpredictable. One possible method to overcome this limitation is predicting the future path and velocity of the forklift using Kalman filters and an appropriate kinematic model of the forklifts. This approach to path prediction for general vehicular networking has been explored in [121, 122] and a general survey of other path prediction techniques for vehicular networks is available in [123].

Chapter 5

SIMULATOR DESIGN AND VERIFICATION

This chapter details the design of the simulator discussed in Chapter 4. The simulator designed and verified here will be used to help investigate research question Q2 and research question Q3 (Section 1.1). Respectively, these questions focus on the effect of vehicle density, and the effects of the MCS and transmit power settings on the collision prediction algorithm failure rate. Development of the simulator will also provide information to discuss Q4, which explores what improvements may be possible with the development of the next generation V2X technologies.

The first section of this chapter describes the design of the simulator including: discussing the different simulation models that are available, the overall structure of the simulator, and how each technology's model is structured. The second section details and discusses the verification of the chosen simulator. Verifying simulators is a key part of any simulation research, as it ensures that the output of the simulators matches the model.

5.1 SIMULATOR DESIGN

This section discusses the overall design of the simulator used to investigate research questions Q2 and Q3. A single simulator will be designed to simulate both C-V2X and 802.11p. First, the available V2X simulation models are described. Then, the overall structure of the simulator is detailed, followed by discussions of the simulation models for each technology. Finally, the module which implements the collision prediction algorithm defined in Chapter 4 is discussed.

5.1.1 Available V2X Simulators

Three different simulators are available for simulating V2X technologies.

5.1.1.1 OMNeT++

OMNeT++ is an event-driven C++ simulation library, designed to simulate distributed and communications systems [124]. Often billed as a network simulator, OMNeT++ on its own does not support any communication specific modules. Rather, all communication-specific modules are separate projects, building upon the simulation framework provided by OMNeT++ [125]. For example, the INET project adds support for various wired and wireless communication technologies and protocols to OMNeT++ [126].

To support V2X communication and simulation the Veins project adds support for vehicle mobility, IEEE 1609, and 802.11p simulation into OMNeT++ [127, 128]. Vehicle mobility is introduced in Veins using the Simulation of Urban MObility (SUMO) framework [129]. SUMO defines the road network and has different mobility models of idealised representations of real-world drivers, allowing large, complex traffic networks to be simulated. The SimuLTE library introduces support for LTE and LTE-based device-to-device communication into INET [130]. However, as of writing, the SimuLTE module does not include for support mode 3 and 4 device-to-device communications [131], and thus cannot be used to simulate C-V2X communications.

Currently there are two projects working to provide support for mode 4 infrastructure-free device-to-device communication in SimuLTE: OpenCV2X [132] and Artery-C [133]. However, at the time of writing, only OpenCV2X is open-source and available to members of the public. The authors of Artery-C plan to release the project under an open-source license but have not done so yet.

Currently there are no OMNeT++ packages supporting 802.11bd or 5G communications.

5.1.1.2 NS-3

NS-3 is an event driven network simulator written in C++ [134]. Initially developed as a replacement for the NS-2 network simulator, it is a result of combining elements of prior simulators to form a new one. NS-3 currently has direct support for 802.11p [135] and a diverse range of vehicle mobility simulators [136]. NS-3 currently does not have support for 802.11bd communications.

NS-3 has a module designed for simulating LTE communications, however, this module does not support device-to-device communication and thus does not enable C-V2X simulation. Eckermann et al. introduced support for C-V2X mode 4 to the NS-3 simulator in [137], allowing it to be used to simulate C-V2X systems.

The LENA project, responsible for developing NS-3's LTE model [138], is currently in the process of developing a 5G model [139]. In November 2019 the project received funding from the National Institute of Standards and Technology (NIST) to develop an

NR-V2X model [140]. This development will, in the future, allow 5G V2X communications to be explored using the NS-3 simulator. Additionally, in February 2020 an NS-3 based simulator for mmWave NR-V2X was released [51]. This simulator is not suitable for simulating the 5.9 GHz frequency band of NR-V2X.

5.1.1.3 LTEV2VSim

LTEV2VSim is a MATLAB based V2V communication simulator, designed to investigate the performance of C-V2X and 802.11p together [141]. It has been used multiple times in the literature to explore different resource allocation schemes for C-V2X [39, 142, 143]. Since this simulator is interested in resource allocation algorithms the application layer functionality is fixed, generating beacons of a parameterised size at a parameterised frequency. This makes it unsuitable for the application level investigation scenario designed in Chapter 4.

5.1.1.4 Chosen Simulator Platform

OMNeT++ is selected as the simulation platform to answer research questions Q2 and Q3. This is as there is support for both C-V2X and 802.11p, allowing a single simulator to handle both technologies. Whilst NS-3 also supports both technologies, there are fewer works in the literature using it to investigate 802.11p and a smaller overall user base.

5.1.2 Simulator Structure Overview

The simulator to answer Q2 and Q3 is built using the Veins and OpenCV2X models in OMNeT++. The overall structure of a model forklift node is shown in Figure 5.1 and the overall structure of the simulator packages is shown in Figure 5.2. There is one unified `GapDetector` module for both technologies which implements the collision prediction algorithm described in Chapter 4. Additionally, it is responsible for periodically broadcasting safety messages and storing safety messages it receives from other vehicles.

Depending on which mode the simulator is in, the `GapDetector` module interacts with either a 802.11p or C-V2X specific adapter. The adapters provide a unified interface for interacting with each technology's Network Interface Card (NIC), and translate the signals received from the SUMO mobility modules indicating the vehicle's current position. A unique adapter is required for each technology as each technology's NIC has a different module interface and requirements to translate the messages generated by the `GapDetector` module into a suitable format. The adapters interface with their respective technology's NIC, which handle simulating the technology and interface with an implementation of the warehouse channel model discussed in Chapter 6. Each

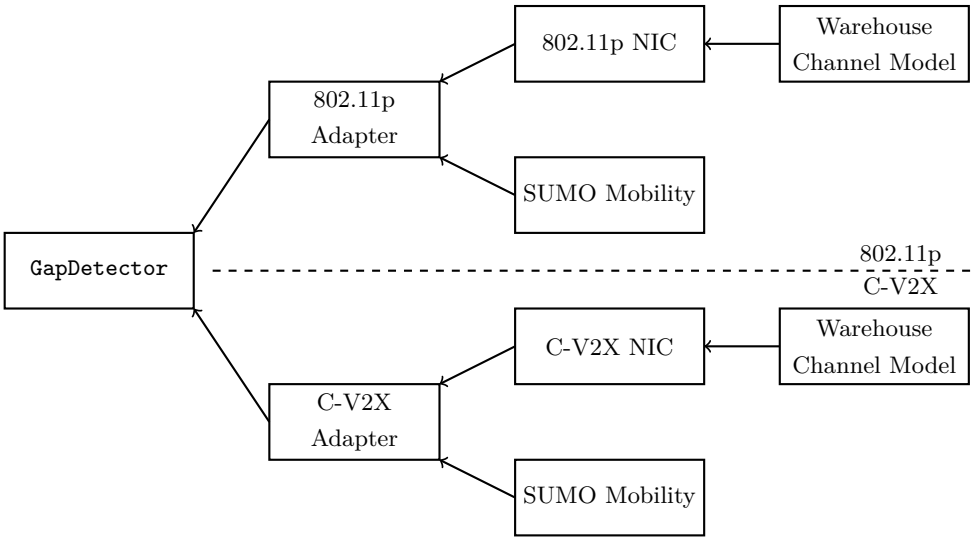

Figure 5.1 The structure of a forklift node. Since each simulation interacts with SUMO through a slightly different interface the SUMO module is not shared between the simulator modes.

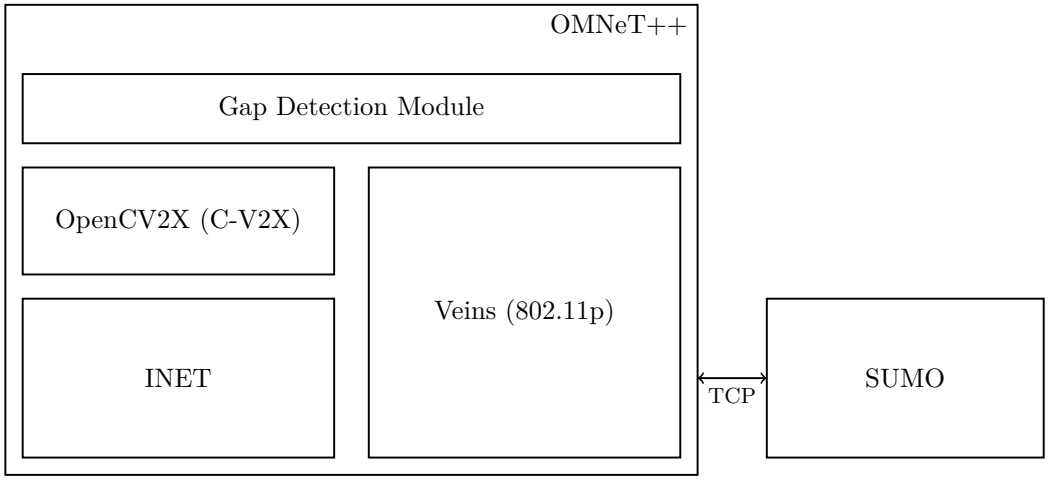

Figure 5.2 The structure of the software packages used in the simulator. SUMO interacts with Veins and OpenCV2X using a local TCP connection.

technology uses its own implementation of the channel model due to differences in the physical-layer-channel-model interface.

5.1.3 C-V2X Simulator

The C-V2X simulator used is called OpenCV2X [132] and is based on the SimuLTE LTE simulator for OMNeT++. Figure 5.3 shows the different sub-modules in an LTE NIC and highlights which have been altered to simulate C-V2X. Within the LTE protocol stack there are several different layers in addition to the Medium Access Control layer (MAC) and physical layer (PHY) discussed in Chapter 2. These are: the Radio Resource Control (RRC) layer [144], the Packet Data Convergence Protocol (PDCP) [145], and the Radio Link Control (RLC) layer [146].

The RRC layer interfaces between applications and the LTE protocol stack and is responsible for handling mobility and cell tower handover when operating in normal LTE or C-V2X mode 3 [147]. The PDCP layer encrypts the data carried by the packets and optionally compresses the headers. This encryption functionality is disabled for device-to-device communication, but is still used when communicating with the eNodeB for normal LTE operation or C-V2X mode 3 scheduling [145]. In the simulator these layers are combined into one module as they are focused around capabilities which do not need to be modelled for a communications-level description of LTE system behaviour.

The RLC layer is responsible for packet segmentation and reassembly, duplicate deletion, and error correction through Automatic Repeat reQuests (ARQ) [146]. ARQ is a system where retransmissions are requested if data is incorrectly received and is separate from the Hybrid ARQ (HARQ) process implemented by the PHY (Section 2.4.1). RLC has three operational modes: acknowledged mode, unacknowledged mode, and transparent mode. In acknowledged mode, the RLC layer will perform segmentation and error correction through ARQ. C-V2X operates in the unacknowledged RLC mode, where the RLC layer will segment large packets but will not perform any error correction through ARQ. In transparent mode the RLC layer simply acts as a buffer and does not do any packet segmentation or reassembly.

To simulate C-V2X, OpenCV2X changes a lot of the MAC and PHY of the SimuLTE simulator to implement the semi-persistent scheduling algorithm (summarised in Section 2.4.1). To adapt to the PHY changes for C-V2X, two new BLock Error Rate

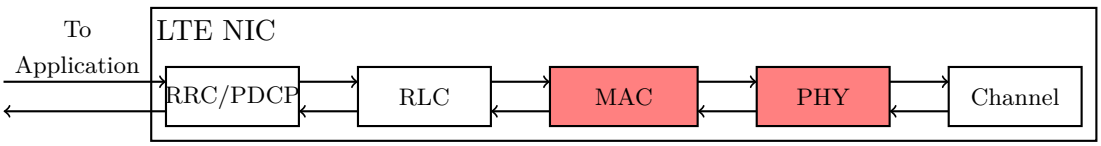

Figure 5.3 The LTE NIC structure in OpenCV2X. The boxes highlighted in red are heavily changed to simulate C-V2X.

(BLER) curves are included. BLER curves are used to calculate the probability of a given block having an error. The new BLER data sets come from two different sources: a NIST project investigating mode 1 and mode 2 device-to-device communication in LTE [148] and a Huawei report to the 3GPP around the number of DeModulation Reference Symbols (DMRS) to use in C-V2X transmissions [149]. However, these curves are significantly different. This can be attributed to the different channel models used to generate them, with the NIST report using a simple Additive White Gaussian Noise (AWGN) channel, and the Huawei report using the ITU-R Urban Micro (UMi) channel model which includes the effects of vehicle mobility. The NIST data set will be used for the modulation and coding scheme (MCS) comparisons as it covers all of the MCSs available in C-V2X, unlike the Huawei data set, which only has three different MCSs available ($\frac{1}{2}$-QPSK, 0.7-QPSK, and $\frac{1}{2}$-16QAM).

Since the NIST BLER data set is generated using an AWGN channel, the BLER assumes that all noise is independently and uniformly distributed across the whole channel [78]. This assumption ignores the multipath nature of the wireless channel, where reflection and scattering of radio waves propagating in the environment causes delayed copies of signals to interfere at the receiver. Since the warehouse channel is expected to be highly reflective, given the large regular metal structure of racking, using a BLER data set from an AWGN channel will not be representative of the warehouse radio environment. However, as there are no other data sets available to explore the effect of MCS on the collision prediction algorithm failure rate (Q3), this is unavoidable.

5.1.4 IEEE 802.11p Simulator

The 802.11p simulator is implemented by the Veins project and a complete description of the simulator can be found in [150]. This section summarises the key details to provide a basic background of the structure of the 802.11p NIC.

The 802.11p NIC has two parts, the MAC and the PHY implementing the respective MAC and PHY responsibilities. The MAC implements the EDCA algorithm (Section 2.4.3.1) and instructs the PHY to transmit packets and check the channel state as appropriate. The PHY module is responsible for keeping track of the channel state, transmitting packets, and determining if packets would have been correctly received. To track the channel state, the PHY must record all transmissions currently ongoing, even if a real node would not be able to hear it due to being out of range. This channel information is used not only to determine if the channel is busy, but to calculate the amount of noise a packet experiences as part of determining whether a packet is successfully received.

5.1.5 Gap Detection Module

This module implements the collision prediction algorithm in Algorithm 1 (Chapter 4). It also implements the system to check if the algorithm produced a correct result. This check is simple and is performed immediately as the turning forklift enters the intersection. The check searches through every vehicle on the top of the intersection and determines if they are further away than the safe-following distance. If any are closer than the safe following distance, then a collision has occurred. A single vehicle turning can only result in a single collision, even if multiple vehicles are within the safety bounds, or the collision state continues along the rest of the aisle. This check cannot detect violations of the safe following distance rule during or after the turn, however, these are only possible for vehicles behind the turning vehicle (Appendix B).

Algorithm 1 requires an implementation-defined helper function, $isOnTop$, to determine if a forklift is on the top of the intersection (Chapter 4). This was left undefined in Chapter 4, as how the simulator determines whether a vehicle is on top was irrelevant to the algorithms description. To implement $isOnTop$, the simulation checks if the the target vehicle is predicted to have a y-coordinate above the intersection decision threshold when the computing vehicle has finished its turn. This handles the case where vehicles are only a few seconds apart on the stalk and will enter the intersection together, violating the safe-following distance rule.

To prevent vehicle beaconing times all being synchronised to the vehicle generation process, a random delay is introduced before a vehicle sends its first beacon. The random delay is drawn from a uniform distribution in the range of zero to the beacon period. After this initial delay, the vehicle beacons at a constant rate with no jitter or randomisation.

5.2 SIMULATOR VERIFICATION

This section details the verification of the technology layer of the simulator stack. As there are two different components to the technology layer (the 802.11p technology stack and the C-V2X technology stack) they must be verified independently of each other. The 802.11p technology stack is part of the Veins project which has been extensively used in the literature [150–155] and so it is accepted as being correct. The OpenCV2X stack is new with no strong verification in the literature. As such, the stack is verified in this section. However, OpenCV2X project is based on the SimuLTE project which like Veins has been extensively used and verified in the literature [130]. Therefore, only the changes between OpenCV2X and SimuLTE must be considered.

The major changes between OpenCV2X and the SimuLTE project are focused at the MAC and PHY, implementing the semi-persistent scheduling algorithm. Thus, only

the MAC and PHY will be verified here. The following subsections detail the procedures used to verify the PHY and MAC independently.

5.2.1 Physical Layer Verification

The PHY verification is focused around the receive path of the transceiver, ensuring that the packet sensing and error generation module is correct. To verify this, a Packet Reception Ratio (PRR) test simulation was developed and compared against the analytical values calculated from the raw BLER data sets included in the simulator. PHY verification will be completed using both the Huawei and NIST data set as the Huawei data set is needed for the MAC verification in Section 5.2.2.

The PRR simulation setup is simple and consists of two nodes, a single transmitter and a single receiver. The transmitter transmits a packet once every 10 ms and advances towards the receiver over a distance of 850 m. This advancing approach was selected to allow PRR data for all transmitter-receiver distances to be collected in a single simulation replication. As it transmits, it records where each packet was sent. When the receiver successfully receives a packet, it records the sequence number of the packet. These are used to determine the PRR data for 1 m long segments, with approximately 1000 packets per segment. The full set of simulation parameters are included in Table 5.1.

The analytical PRR can be stated as:

$$PRR\left(d\right) = \left(1 - BLER_{\text{SCI}}\left(d\right)\right)\left(1 - BLER_{\text{payload}}\left(d\right)\right), \tag{5.1}$$

where $BLER_{\text{SCI}}\left(d\right)$ is the BLER for the SCI when the transmitter is d metres away from the receiver, and $BLER_{\text{payload}}\left(d\right)$ is the BLER for the chosen MCS when the transmitter is d metres away from the receiver. This is because C-V2X packets are sent in two parts: the SCI containing the control information (e.g the MCS used to transmit the payload) and the payload itself (Section 2.4.1). The SCI is always sent independently using MCS 0 (0.13-QPSK), whereas the payload can be sent with any available MCS and can be a lot longer than the SCI. The Huawei BLER data set does not provide a BLER curve for MCS 0, so the NIST curve for MCS 0 will be used as $BLER_{\text{SCI}}\left(d\right)$ for both data sets.

Since the provided BLER data sets are functions of SINR in the logarithmic domain, Equation (5.1) becomes,

$$PRR\left(d\right) = \left(1 - BLER_{\text{SCI}}\left(\widehat{SINR}\left(d\right)\right)\right)\left(1 - BLER_{\text{payload}}\left(\widehat{SINR}\left(d\right)\right)\right), \tag{5.2}$$

where $\widehat{SINR}\left(d\right)$ is the the SINR in decibels of one sub-carrier in a resource block when the transmitter and receiver are d metres apart. Since there is only one transmitter in this scenario, there is no interference. Therefore, assuming isotropic antennas, the

SINR can be calculated as

$$\widehat{SINR}\,(d) = 10\log\left(\frac{P_{\text{tx,SC}}}{PL(d)N_{\text{rx}}N_0}\right), \tag{5.3}$$

where $P_{\text{tx,SC}}$ is the transmitted power per resource block, calculated as

$$P_{\text{tx,SC}} = \frac{P_{\text{tx}}}{12L}, \tag{5.4}$$

where P_{tx} is the overall transmit power and L is the number of resource blocks used for the transmission, $PL(d)$ is the path loss over distance d, N_{rx} is the noise figure of the receiver, and N_0 is the noise power across the sub-carrier bandwidth (15 kHz).

The analytical PRR, computed using Equations (5.2) and (5.3) and the BLER tables included in Appendix C, is compared with the simulated PRR in Figure 5.4. The simulated results agree with the analytical values for both the Huawei and NIST data set. Thus, the PHY matches the analytical expectation.

This verification method does not conclude whether the PHY tasks required for the semi-persistent scheduling algorithm are correct (i.e. correctly selecting/rejecting candidate resource blocks and correctly calculating CBR). This result is left for the MAC verification section, as any errors in these procedures are only detectable through observing the MAC level behaviour.

Table 5.1 The simulation parameters used to verify the simulator PRR results against the theoretical performance.

Parameter	Value
Transmit power ($\widehat{P_{\text{tx}}}$)	10 dBm
MCS	9 (0.73-QPSK)
Packet size	190 B
Beacon frequency	100 Hz
Channel model	Free Space
BLER data set	Huawei [149], NIST [148]
Carrier frequency	5.89 GHz
UE antenna gain	0 dBi
UE noise figure ($\widehat{N_{\text{rx}}}$)	6 dB
Thermal noise	-174 dB Hz^{-1}
Receiver sensitivity	-110 dB
Number of replications	250
Number of RBs (L)	16
Probability to keep resources	0.8
Vehicle model	Model forklift (Section 4.2)
Vehicle speed	0.1 m s^{-1}

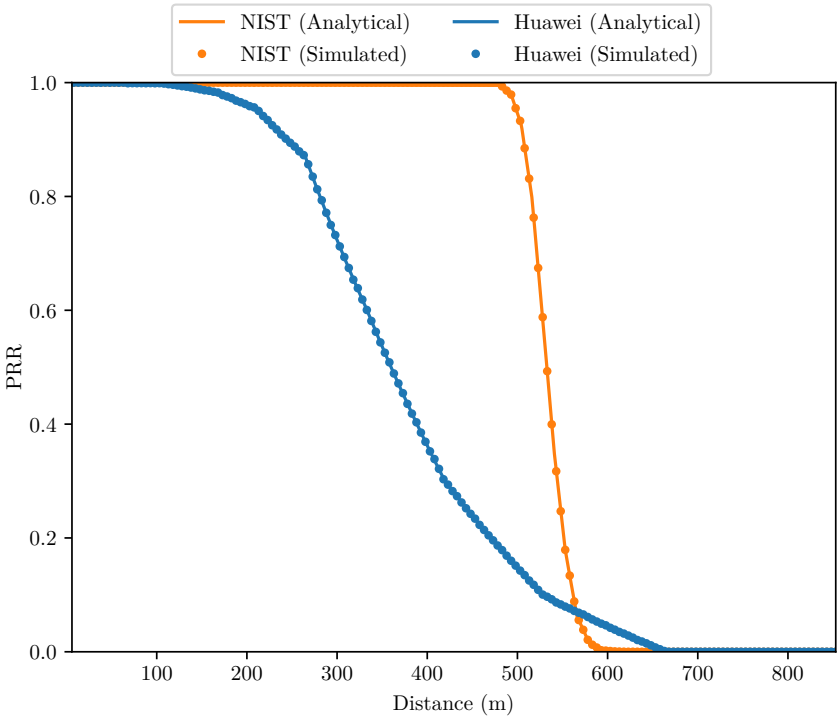

Figure 5.4 The simulated PRR of 0.73-QPSK (MCS 9) compared to the analytically determined PRR.

5.2.2 Medium Access Control Verification

To verify the MAC of the C-V2X simulator, the packet collision rate and channel busy ratio (CBR) was compared to analytical results presented in [156]. For this, a modified version of the verification scenario which comes with the simulator was used. However, the scenario developed in [156] was not directly replicated as the verification scenario here. Since the scenario in [156] uses 6000 vehicles, it was not feasible to fully recreate the scenario with the computing resources available. As such, the scenario is a one-tenth model with the addition of an extra lane in each direction. This means that instead of the simulation environment being a 20 km long, four-lane highway with 2000–6000 vehicles, the model was a 2 km long, six-lane highway with 200–600 vehicles. The added lanes are to support free vehicle flows as without them the vehicles are congested and move slower than their maximum speed.

Other than scaling the simulation environment down, all communication parameters are set the same as in [156]. However, all of these are not clearly presented in the paper, so best guesses have been set based on default configuration and the code available on GitHub [157]. Additionally, the authors of [156] do not state the amount of time or the number of replications simulated. The simulation runs presented here were run for 12 s of in-scenario time and 10 replications were performed. The simulation length was selected based on the convergence of the CBR to a steady state value plus 10 s of

steady state. Since the data showed very little variation between replications, only 10 replications were completed. A full summary of the simulation parameters is given in Table 5.2, with best guess parameters marked with asterisks.

The verification results for packet collision rate are presented in Figure 5.5. In [156], packet collision rate is presented as a function of the distance between the transmitter and receiver and as a function of vehicle density (β) in vehicles per metre (vpm). The curves in Figure 5.5 closely match the shape of the results in [156] (Figure 5.6). Whilst the exact values do not match, they are not expected to, with any difference possibly being explained by the one-tenth scale scenario and unknown simulation length. In the case β=0.1 vpm, the shape of the packet collision rate matches the expected shape poorly. This is likely due to there not being enough vehicles in the simulation to provide enough data points per replication. This conclusion is backed up by the half-duplex error rate, packet collisions where packets are not received because the vehicles are transmitting at the same time. For β=0.1 vpm, the simulated results matches the expected half-duplex error rate the least, when compared to β=0.2 vpm and β=0.3 vpm (Figure 5.7). The CBR steady state value for β=0.2 vpm and β=0.3 vpm scenarios match closely (within 4%) with the analytical steady state values presented in [156] (Figure 5.8). Similar to the packet collision rate, the CBR for the β=0.1 vpm case does not match the analytical value. This is likely also explained by the scale difference between the scenario here and in the scenario in [156].

5.2.3 Discussion

Verifying simulators is key to developing trust that the results generated by the simulator are representative of the model. As such, this section discusses the verification process and why certain benchmarks were selected to verify the simulator against. Verification of the 802.11p simulator has been skipped, as so many other works use and rely on the simulator that it is accepted as being correct. This is in steep contrast to the C-V2X simulator. OpenCV2X is relatively new and unused when compared to the 802.11p simulator. Thus, verification of the C-V2X simulator was needed to gain confidence in the results it produced.

Verification of the C-V2X PHY was performed by comparing the output of a single transmitter approaching a single receiver. Since there are no other sources of error, i.e. interference from other transmitters, the resulting PRR is purely a function on the received signal strength. As such the results can be directly compared to the expected PRR as calculated from the BLER data sets. This is as the aim of this verification is not to verify that the BLER data sets are correct, as they are from pre-existing verified literature, but to verify that the C-V2X simulator's packet method and calculations are correct and consistent with the simple analytical model of packet errors.

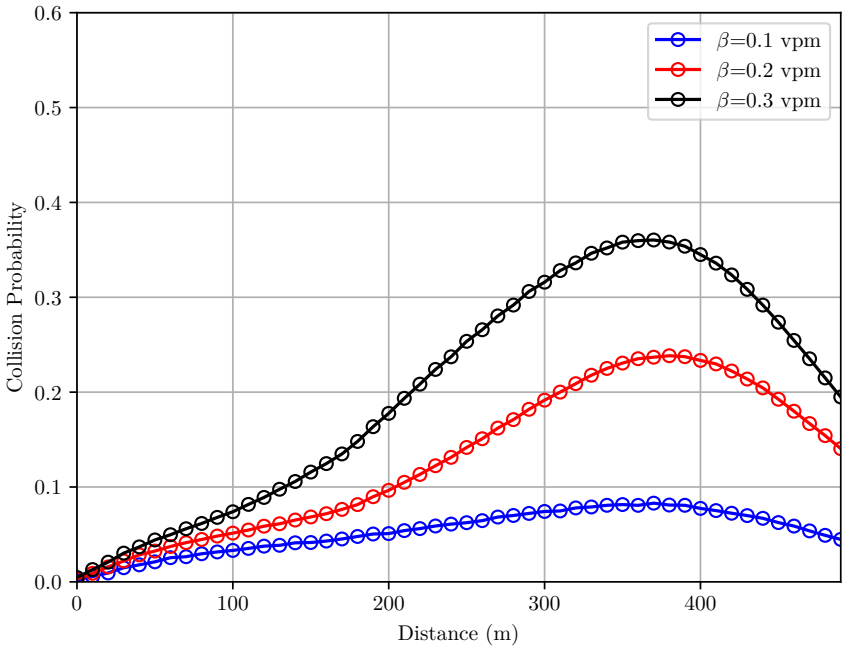

Figure 5.5 The packet collision rates for the verification scenario from the OpenCV2X simulator. They are presented as a function of distance between transmitter and receiver, for the three different vehicle densities simulated (β, vpm).

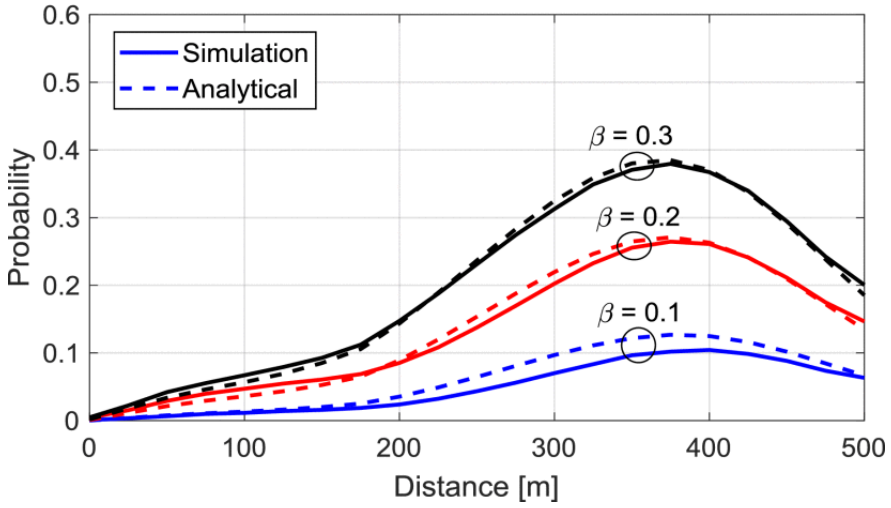

Figure 5.6 The expected packet collision rate as a function of distance between the receiver and transmitter for three different vehicle densities (β, vpm). Reproduced from [156] © 2019 IEEE.

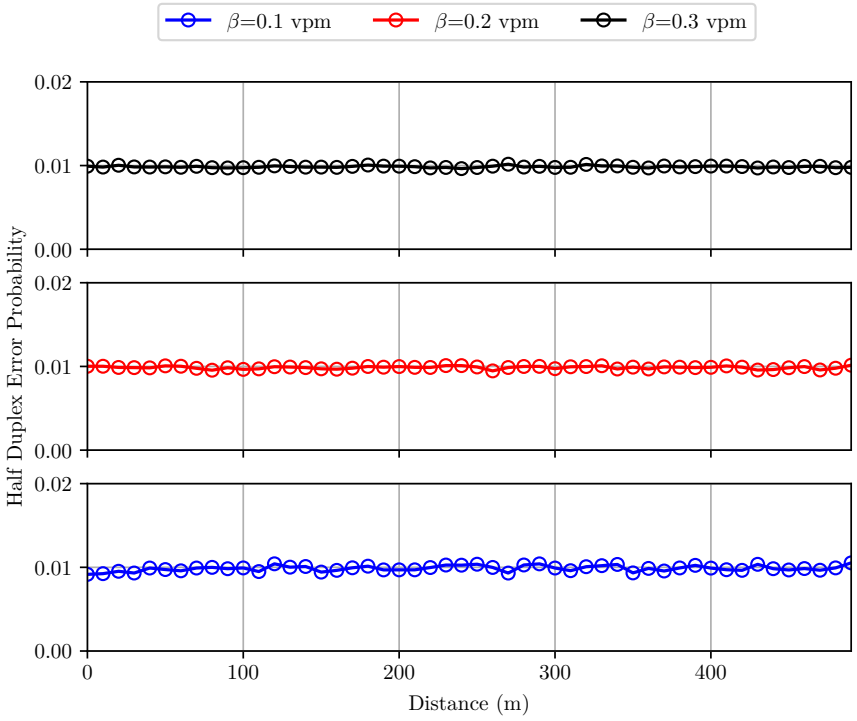

Figure 5.7 The half duplex error rate as a function of distance which should be 0.01 across all distances [156]. The half-duplex collision value for β=0.1 vpm case is less smooth than the values for β=0.2 vpm and β=0.3 vpm, indicating that there is not enough vehicles in the simulation to get an adequate idea of the vehicle behaviour given the run time and replication count.

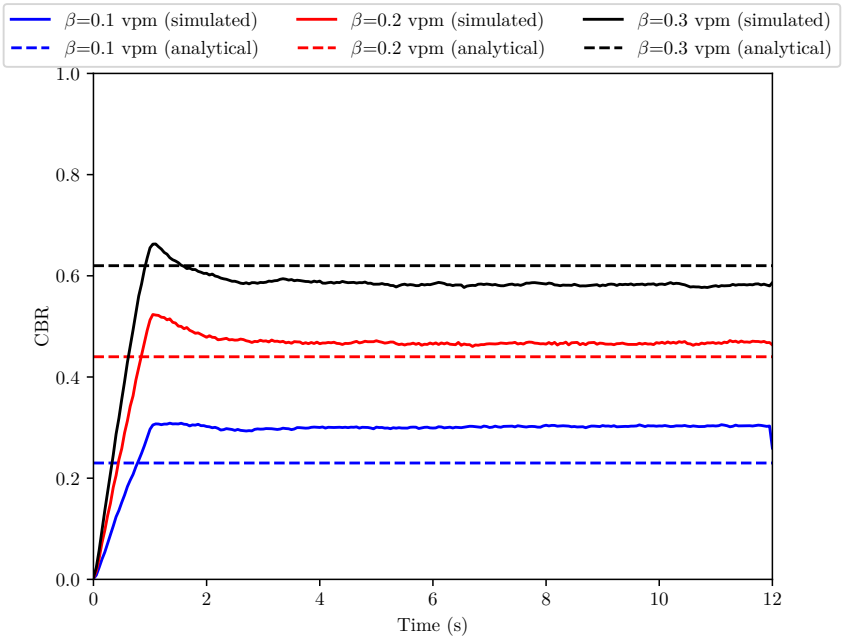

Figure 5.8 The simulated CBR for all three scenarios compared to the analytical values derived in [156].

Table 5.2 The simulation parameters used to replicate the scenario in [156] and verify the MAC. Parameters marked with asterisks (*) are best-guesses based on the open-source code in [157].

Parameter	Value
Maximum vehicle speed	11.84 m s^{-1}
Number of vehicles	204, 402, 600
Vehicle density (β)	0.1, 0.2, 0.3 vpm
Road length	2000 m
Number of lanes	6 (3 in each direction)
BLER data set	Huawei [149]
Channel model	WINNER B1 model [85]
Carrier frequency*	5.91 GHz
UE antenna gain*	3 dBi
UE noise figure*	9 dB
Receiver sensitivity*	-90.5 dB
Thermal noise*	-174 dB Hz^{-1}
Transmit power	20 dBm
MCS	9 (0.73-QPSK)
Number of sub-channels	4
Number of RBs per sub-channel	12
Packet size	190 B
Resource reselection probability	1
Beacon frequency	10 Hz
Simulation time	12 s
Number of replications	10

As discussed in Section 5.1.3, the sources of the BLER data set were a Huawei and NIST study, respectively. The Huawei data set is treated as verified as it was created from simulations performed during the standardisation process for C-V2X [149] and has been used in the literature as such [156,158]. Like the Huawei BLER data set, the NIST BLER data set was created by simulation; however, unlike the Huawei BLER data set, which was explicitly created to evaluate C-V2X, the NIST data set was created for studying mode 1 and 2 PC5 communication [148]. As such, the NIST BLER data set models the mode 1 and mode 2 Public Sidelink Shared Channel (PSSCH) specification, which only includes one DMRS per resource block. However, the modes 3 and 4 PSSCH use four DMRS per resource block [159,160]. Modes 3 and 4 use more DMRS to account for the rapidly changing channel caused by the highly mobile nature of vehicles.

This would normally make the NIST data set an inappropriate BLER model for the mode 4 PSSCH, however, the NIST data set explores the behaviour of a static AWGN channel. This means including the extra DMRS would not significantly change the outcome of any given block, as the channel is not varying and there is no need for the extra DMRS. Thus, it is hereon assumed that the NIST data set is an appropriate approximation of the PSSCH. This assumption is not unfounded in the literature, as both McCarthy and O'Driscoll [132] and Eckermann et al. [137] use it for their simulation work but do not explicitly state so.

To verify the C-V2X MAC, the simulator packet collision rate and CBR results were compared to Gonzalez-Martin et al. [156] who developed an analytical model for the behaviour of C-V2X. This paper was chosen as it provides clearly derived and independent development of a C-V2X model and verifies it against an internally developed MATLAB based simulation. It was selected over two other papers: McCarthy and O'Driscoll [132], which presents the OpenCV2X simulator used here, and Eckermann et al. [137], which developed the NS-3 C-V2X model discussed in Section 5.1.1. In McCarthy and O'Driscoll, the authors do not independently verify their model against any other literature. Rather, they chose to verify themselves using a scenario proposed in the 3GPP simulation guidelines [94], but do not directly compare themselves to any other published work. Additionally, whilst performing verification of the model for this thesis, two issues at the PHY were discovered and reported to the authors which have since been fixed. The two PHY errors were:

- When calculating the received power per resource block for the SCI, the overall transmit power was spread only across the two resource blocks for the SCI, rather than the whole transmission.
- To determine whether a packet was dropped due to signal strength, interference, or both, the PHY compared expected drop rate against two different random variables, rather than a single one. Thus, in the absence of interference, the probability of dropping a packet became:

$$PRR = \left(1 - BLER_{\text{SCI}}\right)^2 \left(1 - BLER_{\text{payload}}\right)^2, \tag{5.5}$$

  rather than the correct probability, presented in Equation (5.1).

These errors are included in the results of [132], reducing its credibility as a verification source. Unlike McCarthy and O'Driscoll, Eckermann et al. rely on the verification of the previous NS-3 LTE model for mode 1 and mode 2 device-to-device communication, developed by NIST in [161], to demonstrate their model is correct. However, this correctness is not transitive to the mode 4 operating mode which is very different to operating modes 1 and 2.

The PHY of the OpenCV2X matches the calculated analytical values (Figure 5.4). However, there is a discrepancy between the MAC verification scenario results produced by the OpenCV2X simulator and the results presented in [156] (Figure 5.5 and Figure 5.8). This discrepancy is that the values from the simulator do not exactly match. However, an exact value match between the two cannot be expected due to the scale difference in the simulation, the unknown simulation length, and the missing simulation parameters. Since the trend and shape of the results presented in Section 5.2.2 match the trend and shape presented in [156], the MAC can be accepted as verified. Thus, since both MAC and PHY of C-V2X match their theoretical expectations, the C-V2X simulator

is verified. As such, the simulation results presented in Chapter 7 will reflect the theoretical expectation of each technology's performance.

Chapter 6

A WAREHOUSE AISLE-END CHANNEL MODEL

This chapter details the design and parameter characterisation of a warehouse wireless channel model. Designing and correctly parameterising a warehouse channel model will allow research questions Q2 and Q3 (Section 1.1) to be explored using the simulators discussed and designed in Chapter 5. While this thesis generally refers to the channel model as a warehouse channel model, more accurately, this model is a warehouse aisle-end wireless channel model. The model focuses on aisle-end communication in a warehouse and does not capture the effects of inter-aisle communication, nor does it take into account the variability of warehouse contents.

The following sections detail the structure of the model, a measurement campaign to find the parameters of two warehouses, validation of the model, and a discussion of the resulting model in relation to the literature, the limitations of the model, and some suggestions for future improvements.

6.1 MODEL DESCRIPTION

This model aims to capture the behaviour of the warehouse wireless channel for end-of-aisle communication. Specifically the case where vehicles in an aisle are communicating with vehicles moving past the end of the same aisle. To do this, the model defines three zones (Figure 6.1) with three different log-distance path loss equations of the form [82]:

$$\widehat{PL}(d) = \widehat{PL\,(d_0)} + 10\alpha \log_{10}\left(\frac{d}{d_0}\right), \tag{6.1}$$

where $\widehat{PL}(d)$ is the path-loss attenuation at d metres, $\widehat{PL\,(d_0)}$ is the reference path loss, or the path loss measured at the reference distance d_0 in metres, and α is the path loss exponent. Which zone a transmission belongs to, and thus which path loss equation is used, is determined by the location of the vehicle moving along the top of the T-intersection. If both vehicles are on the same branch they use the zone 1 path loss. The distance from the centre-line of the stalk of the T-intersection in metres is used to define which zone a vehicle along the top of the T-intersection is currently in.

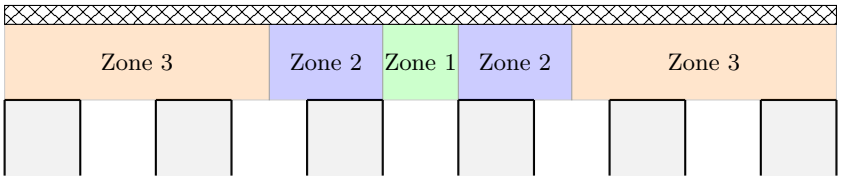

Figure 6.1 The different zones in the warehouse channel model. The aisle of interest is the centre aisle, in line with zone 1.

The choice to use three zones is to roughly parallel LOS, obstructed LOS, and NLOS states used in some other models [104, 162]. Additionally, defining three cases for vehicles position along the top of the intersection to three cases reduces the number of measurements required to parameterise the model.

6.2 WAREHOUSE MEASUREMENT CAMPAIGN

To set the parameters of the model described above, a measurement campaign to measure the path loss along an aisle was completed at two different locations. The Packet Reception Ratio (PRR) was also measured to provide a benchmark to compare the resulting model against. This section details the path loss measurement equipment used during the campaign in Section 6.2.1 and the path loss measurement methodology is described in Section 6.2.2. Sections 6.2.3 and 6.2.4 discuss the PRR measurement equipment and procedure, respectively. Section 6.2.5 is dedicated to describing the two locations investigated in the measurement campaign. Finally, Sections 6.2.6 and 6.2.7 respectively detail and discuss the path loss and PRR results for the locations investigated.

6.2.1 Path Loss Measurement Equipment

To determine the path loss exponent and reference path loss a portable test rig was developed consisting of a Keysight N9432C spectrum analyser [163] and a Cohda MK5 On Board Unit (OBU) [164]. The OBU acts as a signal generator by continuously transmitting maximum length IEEE 802.11p packets centred at 5.89 GHz. The OBU uses an omnidirectional SMW-303/MGW-303 DSRC antenna [165], where the MGW-303 is a magnetic mount version of the SMW-303 with the same antenna pattern. The OBU is powered via an external Lithium-Polymer (LiPo) battery and is controlled using a laptop is connected via Ethernet. The spectrum analyser uses a 5.8 GHz SpiroNET antenna (0.95 dBic) [166] and is powered off an internal battery.

The received power measurements are recorded by the spectrum analyser to a laptop over Ethernet via the virtual instrument software architecture API. However, the spectrum analyser does not record the path loss of the centre frequency, rather a stable spur created by the OBU within 30 kHz of the centre frequency. This is done as the OBU is not a signal generator creating a clean tone at the centre frequency, rather

it is an IEEE 802.11p transmitter and thus there is no carrier at the centre frequency to measure [59]. The output of the OBU, measured at roughly 1 m away, is shown in Figure 6.2.

Notable in Figure 6.2 is the lack of the spur that the path loss is measured against. Over long sweep times the spur cannot be seen, however when set to a fine enough resolution bandwidth (RBW) and a short enough sweep time it becomes visible. The cause of the spur is unknown, however it is a suitable reference point for path loss measurements as it is relatively stable in both amplitude and frequency, and is close to the centre frequency of the channel. To verify that the spur is not a result of the spectrum analyser measurement routine, its existence was confirmed using two different spectrum analysers: the N9342C used in the rest of the experiment, and a Hewlett-Packard 8593E spectrum analyser [167] (Figure 6.3).

Measurements were taken at two different locations, described in Section 6.2.5. At Location 2 an external 435 x 420 mm sheet metal ground plane was used for the transmitting SMW-303 antenna. It was not used at Location 1 as it was believed the internal ground plane of the antenna would be sufficient to ensure the radiation pattern was consistent with the one provided by the manufacturer in [168]. The validity of this radiation pattern is key as the SMW-303 antenna is not perfectly omnidirectional, in fact, the SMW-303 antenna gain varies by over 10 dBi over the range of angles between the signal generator and the spectrum analyser [168]. Using the ground plane at Location 2 helped ensure this assumption holds, more closely mimicking the radiation pattern test environment.

6.2.2 Path Loss Measurement Methodology

To fully parameterise the warehouse channel model three different measurement sets must be taken for each scenario — one set of measurements for each zone. A scenario is one test area within the wider warehouse location and the specific scenarios investigated at each locations are described in Section 6.2.5. The general plan of the measurements is shown in Figure 6.4. Specific measurement plans for each location are provided in Appendix D.

To perform the measurements for one zone, the OBU transmitter is placed corresponding to one of the red dots in Figure 6.4. The receiver system is placed on a movable plastic trolley which is wheeled down the aisle and stopped at set positions down the aisle, represented by the black dots. At each position, the receiver system takes 250 measurements of received signal strength over roughly one minute. These measurements are averaged to form a single point in a measurement set. This process is repeated for the remaining two zones for each scenario.

As discussed in Section 6.2.1 the measurement setup does not use a traditional signal generator and instead at each location the spectrum analyser measures a stable

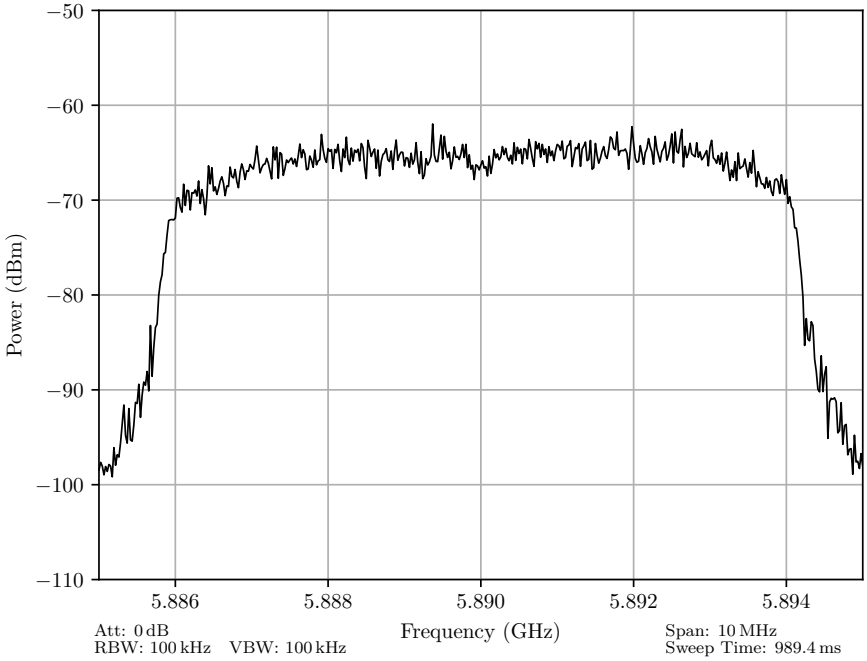

Figure 6.2 The output of the Cohda Mk5 OBU transmitting at 0 dBm, measured approximately 1 m away using the N9342C spectrum analyser. The measurement was taken LOS in an open office environment.

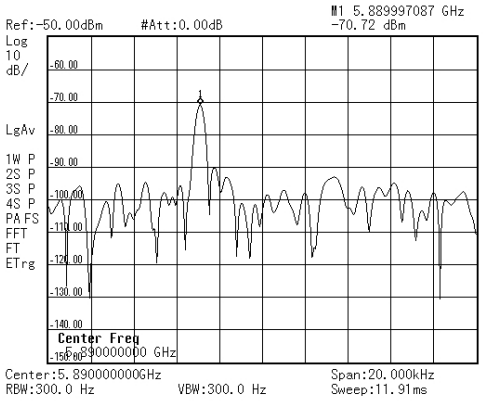

(a)

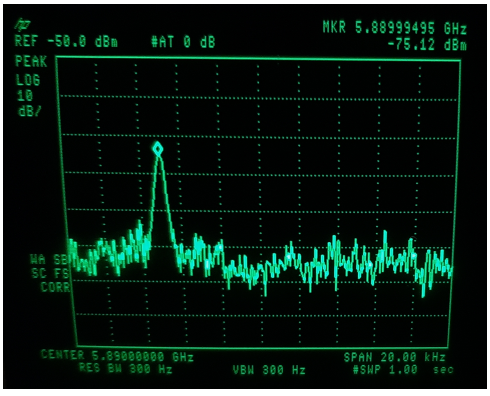

(b)

Figure 6.3 Confirming the existence of the spur with both the (a) N9342C spectrum analyser and the (b) 8593E spectrum analyser.

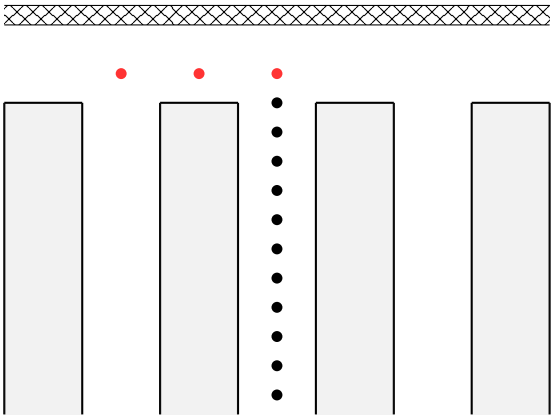

Figure 6.4 The general layout of the warehouse measurements for one intersection. The red dots represent the locations the transmitter is placed to quantify each zone.

spur produced by the Cohda OBU. This spur is not perfectly frequency stable, drifting a little over time. To account for this the channel measurement looks at the 20 kHz range around the centre frequency and selects the dominant peak in the range as the spur location. Selecting a 20 kHz range leads to a noise floor of around -130 dBm. A RBW of 300 Hz was used for all measurements.

Using the OBU as a signal generator changes how the path loss is calculated from the measured received signal strength values. To convert the measured received power values into path losses for analysis the following link budget is used:

$$\widehat{PL} = \widehat{P_{\text{tx}}} + \widehat{G_{\text{tx}}}(\theta) + \widehat{G_{\text{rx}}} - \widehat{L_{\text{tx}}} - \widehat{L_{\text{rx}}} - \widehat{P_{\text{rx}}} \tag{6.2}$$

where $\widehat{PL}$ is the path loss, $\widehat{P_{\text{tx}}}$ is the transmit power in dBm, $\widehat{G_{\text{tx}}}(\theta)$ is the transmit antenna gain at the angle θ between the receiver to the transmitter, $\widehat{G_{\text{rx}}}$ is the gain from the receiver's antenna, $\widehat{L_{\text{tx}}}$ and $\widehat{L_{\text{rx}}}$ are the cable losses at the transmitter and receiver, and $\widehat{P_{\text{rx}}}$ is the power measured by the spectrum analyser. Since the OBU does not generate a single pure tone as an output, rather producing an 8.8 MHz wide OFDM signal, the output power of the OBU is not equal to $\widehat{P_{\text{tx}}}$. To calculate $\widehat{P_{\text{tx}}}$ the transmit power of the OBU must be spread over the entire signal bandwidth. Assuming that the overall transmit power is uniformly distributed across the overall signal bandwidth (BW_{signal}), $\widehat{P_{\text{tx}}}$ can be estimated as

$$\widehat{P_{\text{tx}}} = \widehat{P_{\text{OBU}}} - 10\log_{10} BW_{\text{signal}} + 10\log_{10} BW_{\text{RBW}} \tag{6.3}$$

where $\widehat{P_{\text{OBU}}}$ is the overall transmit power of the OBU and BW_{RBW} is the RBW of the spectrum analyser. This assumption is based on the observation the that 802.11p signal in Figure 6.2 is relatively flat across its 8.8 MHz observed bandwidth. $\widehat{G_{\text{tx}}}(\theta)$ is used to adapt for the directionality of the SMW-303 antenna and is linearly interpolated across 5° intervals based on the antenna pattern provided by the manufacturer in [168].

Values for $\widehat{G_{\text{rx}}}$, $\widehat{L_{\text{tx}}}$, $\widehat{L_{\text{rx}}}$ were retrieved from the data sheets provided by the respective component manufacturers. It was assumed that all adapters were perfect and had 0 dB losses.

Once the measurements have been converted into path losses, the values for each measurement point in each measurement set are averaged. The averaged values are then fitted to the log-distance path loss equation (Equation (6.1)) using non-linear least-squares. Both the reference path loss, $\widehat{PL\,(d_0)}$, and the path loss exponent, α, are outcomes of the fit. The reference distance (d_0) is fixed at 1 m for the fitting process. The resulting reference path losses and path loss exponents for each measurement set are then used to form the warehouse channel model described in Section 6.1.

6.2.3 Packet Reception Rate Measurement Equipment

To measure the PRR along the aisle a test rig was developed using two Cohda MK5 OBU, one as a transmitter and the other as a receiver. Each OBU had an identical hardware setup using a SMW-303 DSRC antenna and controlled by a laptop over Ethernet (Figure 6.5). Both transmitter and receiver were powered using LiPo batteries. At measurement Location 2 an external 430 x 420 mm sheet metal ground plane was used on both the transmitter and receiver test rigs.

6.2.4 Packet Reception Rate Measurement Procedure and Validation

To characterise the PRR along the aisle in each zone, the PRR test rigs are placed in a similar fashion to the path loss measurement procedure described in Section 6.2.2. However, there are two differences. Firstly, the position of the transmitter and receiver are reversed. Secondly, the spatial density of data points is halved so measurements are only taken at every other black dot in Figure 6.4. Reversing the position of the transmitter and receiver so that the transmitter is movable and in the aisle allows the measurements to be completed by a single person. Halving the number of data points reduced the time it takes to complete the measurements as it takes roughly two minutes to complete one data point — twice as long as for the path loss measurements.

At each packet loss sample point the transmitter unit inside the aisle sends a series of 180 B long packets to the receiver. Each packet has a Protocol ID (PID), unique to each measurement point, included with it. The transmitter records the PID at each location along with current position and the number of packets sent. The receiver, outside the aisle on the red dots in Figure 6.4 forwards the packets it receives to its controlling laptop which records the entire packet into a `.PCAPNG` file using Wireshark. The parameters used by the transmitter at each location are include in Table 6.1. The 180 B packet length includes both the header and data component of the packet.

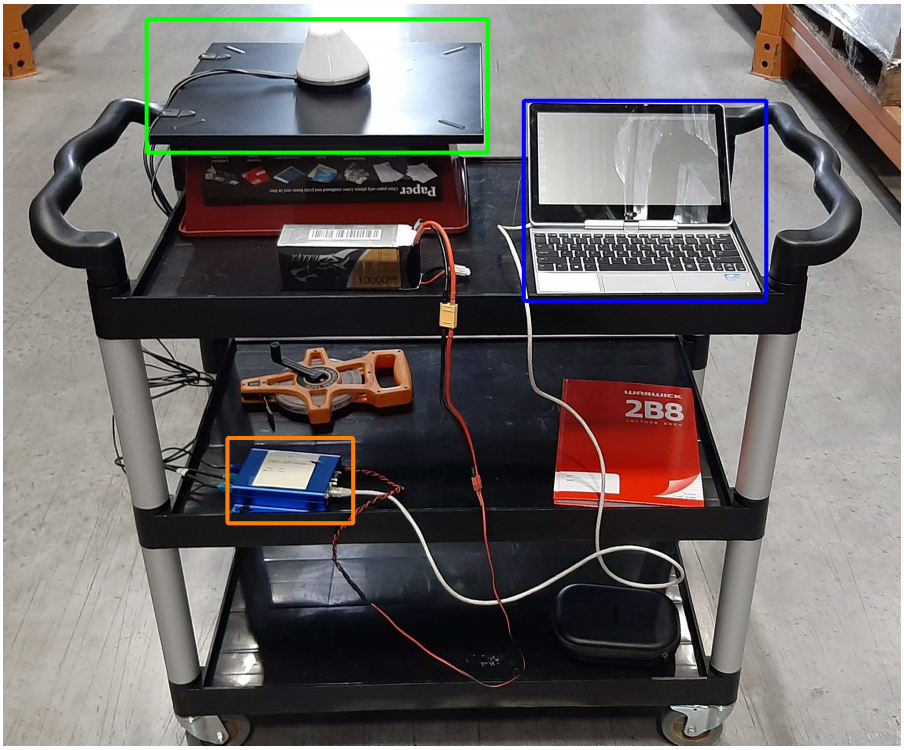

Figure 6.5 One of the PRR measurement test rigs at Location 2. The green box indicates the SMW-303 antenna and its ground plane, the orange box indicate the Cohda MK5 OBU, and the blue box indicates the laptop.

Table 6.1 The settings used for the PRR measurements

Parameter	Location 1	Location 2
Technology	802.11p	802.11p
Packet length (B)	180	180
Transmit rate (packets per second)	100	750
Number of packets	10000	100000
MCS	$\frac{1}{2}$-QPSK	$\frac{1}{2}$-QPSK
Frequency	5.89 GHz (Ch 178)	5.89 GHz (Ch 178)
Transmit power (dBm)	0	0

At Location 2, the packet rate and number of packets set were increased. This was because the measurements at Location 1 revealed that the minimum packet loss rate was lower than 10^{-3}, meaning it could not be detected. When discussing high PRR values, its complement packet loss rate or packet error rate is often used as it is easier to notate in text. A proof that packet loss rate is the complement of PRR is provided in Appendix A. To detect packet loss rates as low as 10^{-4} at Location 2, the number of packets sent were increased to 10 000. The packet transmit rate was also increased to 750 packets per second to reduce the time required to take a single measurement with the 10 000 packets, compared to the 100 packet per second transmit rate.

To calculate the PRR, the PID and packet decoding outcome are exported to a `.csv` file. Knowledge of whether a packet was correctly decoded is necessary as the Cohda OBU will forward any packet it receives in full to the laptop, regardless of whether it was correctly decoded or not. A packet is determined to be correctly decoded if it passes the cyclic redundancy check. The number of successfully received packets is then counted per PID and mapped to measurement points using the PIDs recorded by the transmitter. The PRR is then calculated as the number of packets received per measurement point divided by the number of packets transmitted at that location.

6.2.4.1 Validating the Packet Reception Rate Measurement Procedure

To validate the packet loss measurement procedure and equipment two million 180 B long packets were sent at 750 packets per second to measure the baseline PRR when the transmitters where 2 m apart from each other in an office environment. At this separation only eight packets out of the two million packets were lost. This verifies that any packet losses above this rate are not due to the measurement procedure, rather they are caused by the environment. Additional trials were performed around the University of Canterbury campus verifying that the measurement procedure was correct and did not result in additional errors.

6.2.5 Warehouses Investigated

Channel measurements were taken at two different warehouses both of which are discussed below. In addition to the brief descriptions included here, complete plans of the measurement environments and location are included in Appendix D. The results from each of these is summarised in Section 6.2.6 and are presented in full alongside the descriptions in Appendix D.

6.2.5.1 Measurement Location 1

Location 1 is a testing warehouse for warehouse equipment based in South Auckland. It consists of a large open area, with a limited area of racking along one side. A floor plan

of the location is included in Figure 6.6. The roof of Location 1 is made of corrugated metal panels with periodic transparent corrugated plastic sections to allow natural light in.

Since this location is a test warehouse there was more flexibility for investigating different possible scenarios for warehouse contents. This allowed the following scenarios to be investigated:

S1. Clear space: taken in the open area away from the racking.

S2. Empty racking: the racking was empty.

S3. Highly absorbent: lowest level of the racking filled with tap water-filled intermediate bulk containers (IBCs).

S4. Highly reflective: the lower warehouse racking was blocked off with large aluminium panels.

S5. Mixed: a mix of materials was used to fill the lower levels of the racks. These materials included paper filled crates, packaged food items, packaged bar soap, wooden crates and pallets, forklift components, water filled IBCs, aluminium panels, and computers. A full and more specific description is available in Appendix D.

6.2.5.2 Measurement Location 2

Location 2 is a commercial logistics centre based in Rolleston, a town south of Christchurch, New Zealand. The company which owns and operates the warehouse offers complete supply chain solutions and uses the warehouse as a centre for their general logistics operations. As such Location 2 contains a wide variety of materials, primarily retail food goods and plastic pellets for manufacturing.

Since Location 2 is an active commercial logistics warehouse, measurements were performed on a Saturday to minimise disruption to the operation of the facility. However, limited work was still ongoing whilst the measurements were completed.

Measurements were completed in two different aisles in at Locations 2:

S6. An aisle primarily consisting of Ultra High Temperature (UHT) milk in paper cartons for export on lower levels and bags of Polyethylene pellets on higher levels. The contents of the aisles either side were of a similar make up.

S7. An aisle with chips/crisps in boxes on pallets. The aisles on either side were made up of a similar variety of chips but also had UHT milk in some bays.

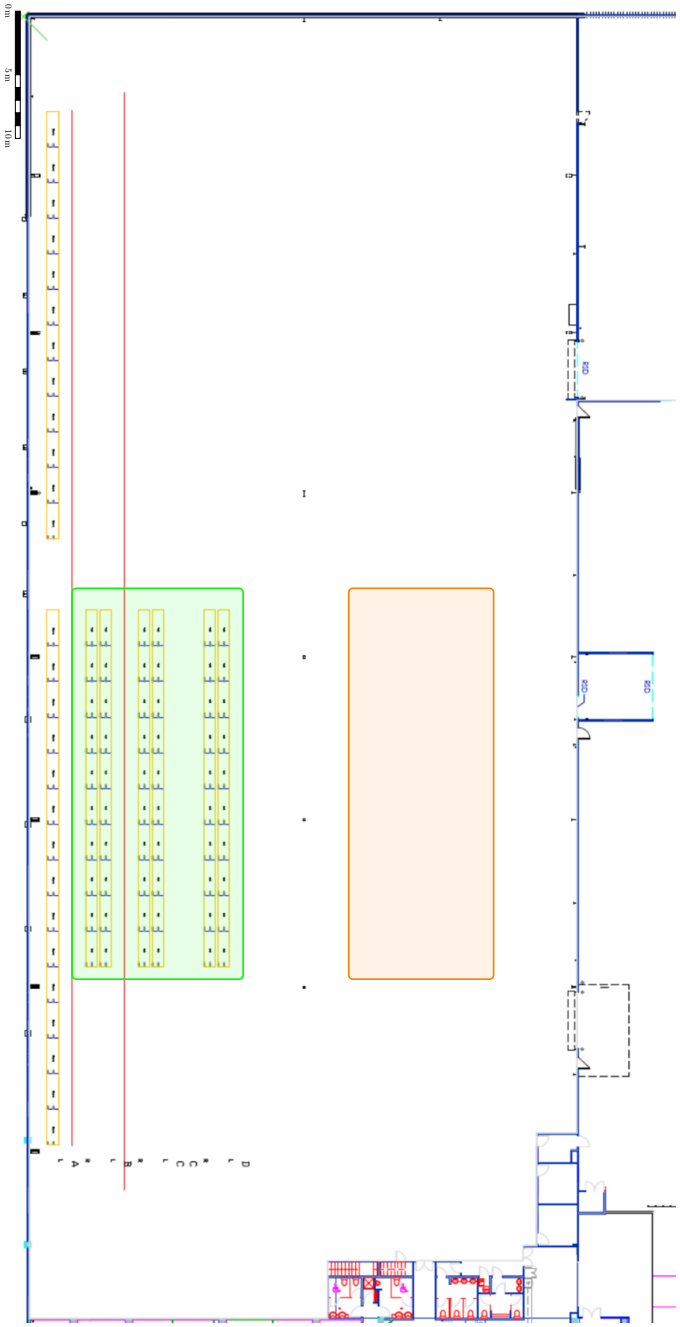

Figure 6.6 The floor plan of Location 1 with the area for the clear space experiment (S1) highlighted in orange and the racked area (S2–S5) highlighted in green.

An indicative floor plan showing the major areas of the Location and the location of each aisle is in Figure 6.7. Appendix D contains a more thorough description of the environment and pictures of each location.

The roof of Location 2 is different to that of Location 1. Location 2 has a drop ceiling with fluorescent lighting and sprinkler system. Sections of the drop ceiling are made of transparent plastic panels, allowing sunlight from clear panels in the roof through, helping light the warehouse. The roof of the warehouse is made of metal corrugated roofing panels with clear plastic panels matching the clear panels in the drop ceiling.

6.2.6 Resulting Model Parameters

The channel model parameters ($\widehat{PL\left(d_0\right)}$ and α) for Location 1 and Location 2 were extracted using the method described in Section 6.2.2. These results are summarised in Table 6.2. Select results are included in Figures 6.8 and 6.9. Full results are included in Appendix D alongside descriptions and pictures of each of the scenarios.

Scenarios S1 and S2 explore the path loss of empty industrial areas and empty racking respectively. The reference path loss and path loss exponent values for S1 are all roughly consistent with each other (Figure 6.8). This is expected as there is no obstructions and it is open LOS propagation. The path loss in zone 1 of S2 is similar to this LOS propagation, if slightly worse at the reference distance. This could just be statistical differences, however since the zone 1 reference path loss is consistently between 36–40 dB for scenarios S2–S5 it is likely due to the differences between the two environments (e.g. the large concrete wall on one side of the test aisle).

The effect of the racking is brought into sharp contrast when comparing the variation between zones 2 and 3 and zone 1 in S2. This demonstrates that even empty racking can have a quite severe effect on the path loss at these frequencies. This is not unexpected as the repeated, sharp, metallic edges of the of the racking provide plenty of opportunities for scattering and reflection, reducing the received signal energy.

Scenario S3 explored the effect of a highly absorbent environment. The path loss in zone 2 is significantly higher than in zones 1 and 3, as the direct path will have been blocked by the water-filled IBCs. However, the decrease in path loss exponent between zone 2 and zone 3 is interesting and is likely caused by the main signal path changing to no longer propagate through the absorbent IBCs. A change in the main signal path also explains the increased reference path loss and path loss exponent compared to zone 1.

Scenario S4 investigated the effect of a highly reflective aisle, akin to metal bins stored on racking. Zone 1 has a similar reference path loss to other scenarios, however the path loss exponent is a lot smaller and is less than one. This suggests the reflective racking may be acting as a waveguide as discussed in [104, 105]. In zone 2, the opposite happens and the large reflective sheets prevent the signal from directly propagating:

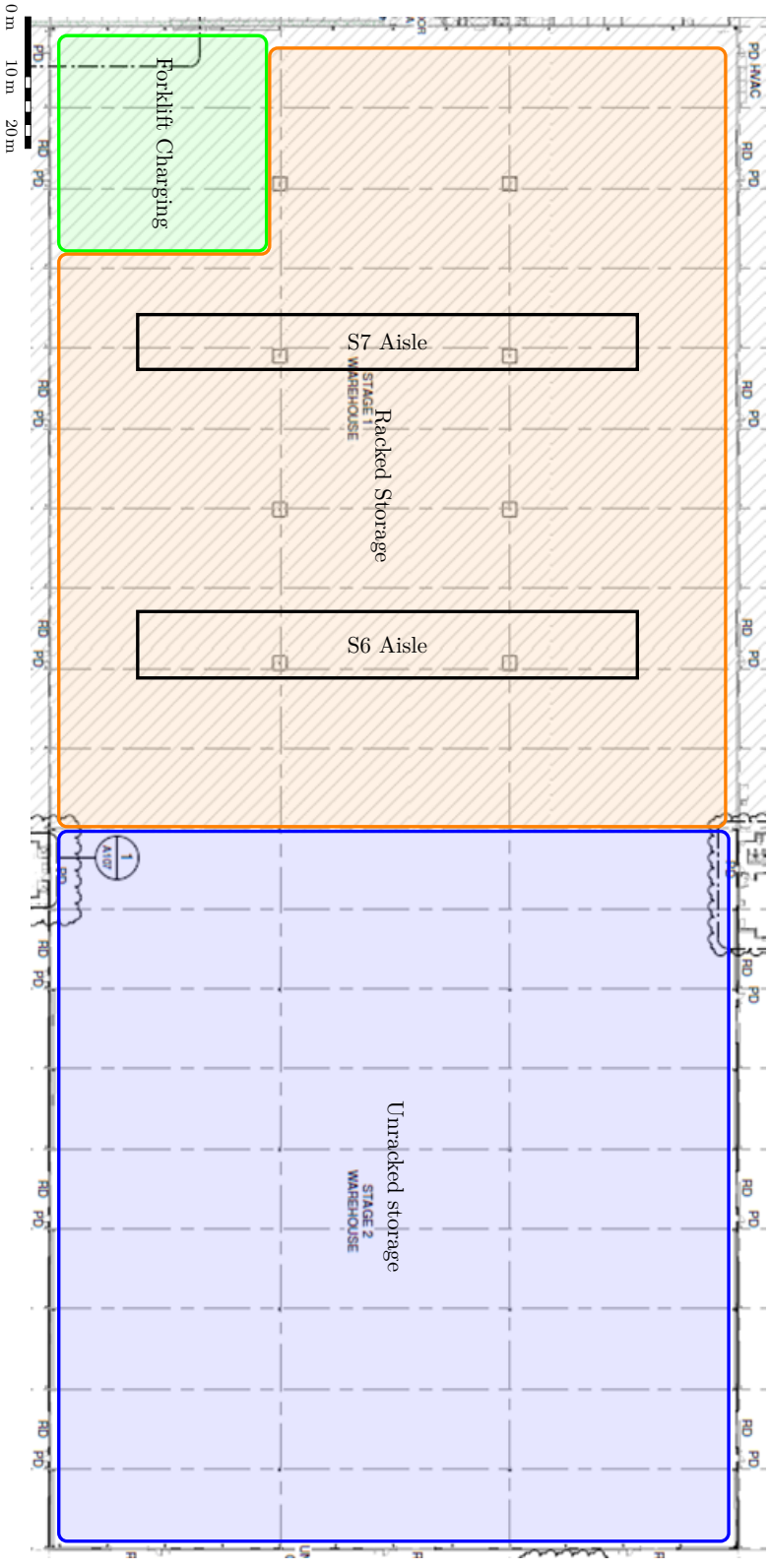

Figure 6.7 The floor plan of Location 2 with the different areas of the warehouse labelled. The scale is accurate for the building floor plan, however, the indicated areas are not exact. RD and PD stand for roller-door and pedestrian-door, respectively.

Table 6.2 The warehouse channel model parameters for Location 1 and Location 2.

Location	Scenario	Zone	Zone Boundary (m)	$\widehat{PL(d_0)}$ (dB)	d_0 (m)	α
1	S1	1	2.61	33.38	1.0	1.306
		2	4.71	32.01	1.0	1.658
		3	—	38.30	1.0	1.116
	S2	1	1.59	36.80	1.0	1.304
		2	4.71	22.16	1.0	2.835
		3	—	19.05	1.0	3.065
	S3	1	1.59	36.55	1.0	1.468
		2	4.71	17.60	1.0	3.641
		3	—	39.24	1.0	1.641
	S4	1	1.59	39.67	1.0	0.677
		2	4.71	26.66	1.0	2.681
		3	—	51.17	1.0	0.090
	S5	1	1.59	36.81	1.0	1.911
		2	4.71	35.24	1.0	1.902
		3	—	20.57	1.0	3.329
2	S6	1	1.50	34.04	1.0	1.595
		2	8.10	31.17	1.0	2.211
		3	—	23.62	1.0	2.865
	S7	1	1.50	32.16	1.0	1.434
		2	6.40	26.98	1.0	2.079
		3	—	21.34	1.0	2.651

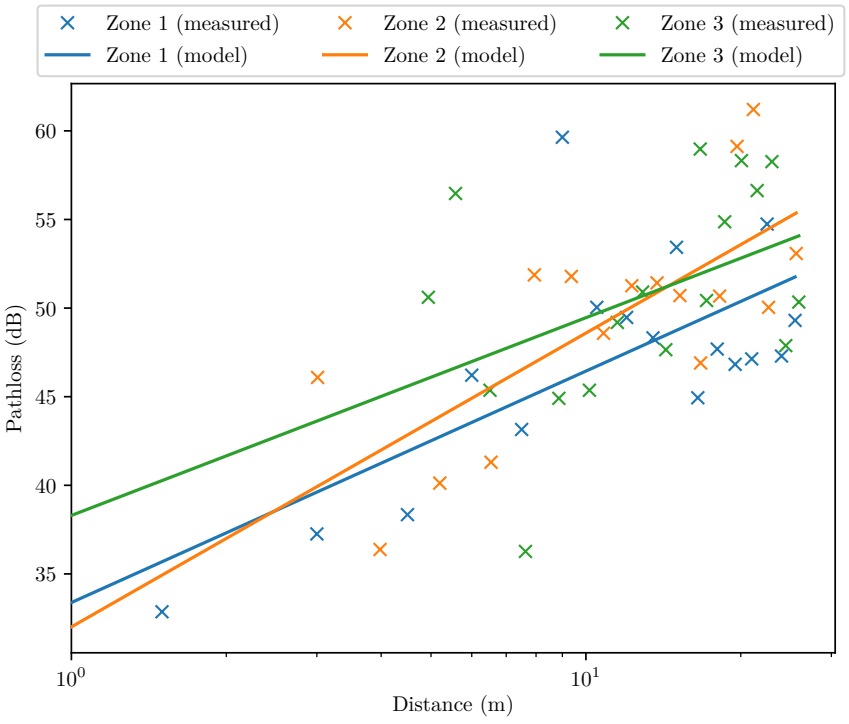

Figure 6.8 The results for Scenario 1.

this results in a higher reference path loss than other scenarios at Location 1 and a relatively high path loss exponent. The path loss along the aisle in zone 3 of S4 is very flat and uniform, having a path loss exponent of 0.090. This indicates that the path loss is not highly dependent on the separation between the transmitter and receiver. The received signal strength is dominated by the reference path loss, and thus, the main power of the received signal is likely from reflections. These reflections could be from the building walls or the corrugated metal roof.

Scenario S5 is the scenario most representative of a real commercial warehouse at Location 1. However, when compared to S6 and S7 (measurements taken at a commercial warehouse) they are substantially different. Note, the absolute values between each of these scenarios cannot be directly compared as each represents a different environment. Additionally, each zone is defined differently due to the setup of the racking in each scenario being unique. However, the internal trend in values across the zones can be compared. In S5 the reference path loss and path loss exponent are consistent across zone 1 and zone 2. This is not observed in S6 and S7 where there is a distinct increase in the path loss exponent between the two zones. Additionally, the path loss in zone 3 of S5 is significantly worse than zone 3 of S6 and S7 with higher path loss exponent for a roughly similar reference path loss. These differences between S5 and the scenarios at Location 2 make it a potentially bad representation of a real-world commercial warehouse, however, this cannot be stated with any certainty as there are no sites other the Location 2 available to compare it against.

Scenarios S6 and S7 are very consistent with each other. This can been seen in Figure 6.9 where all of the fitted path loss curves are slightly offset from each other. This is due to the similarity of the path loss exponent for each zone, so any difference between the two scenarios is due to the reference path loss rather than the path loss exponent. The similarity of the path loss exponents indicates that the material in the racking does not have a strong effect on the path loss exponent, rather the main effect could be from the warehouse structure and racking. However, this cannot be stated with any certainty as the path loss properties of UHT milk and chips are not well studied, so this could be an expected result due to similar material properties.[1] Further measurements will be required to determine whether this effect can be generalised.

For the purposes of modelling the warehouse wireless channel for simulation and evaluating each technology, one set of parameters must be selected. The scenario S6 — the UHT aisle at Location 2 — is selected, as it is from a commercial site and has a full packet loss measurement set available. A single scenario to mimic is adopted over an average or statistical model due to the limited measurements available.

[1] If this relationship exists it would be very surprising as milk is an extremely lossy RF material ($\tan\delta = 0.20$–0.35 [169, 170]) compared to cardboard boxes ($\tan\delta = 0.03$–0.04 [171, 172]) filled with plastic potato chip packets (which are made from polypropylene which has $\tan\delta = 0.002$ [173]). $\tan\delta$ is called the loss tangent and as it increases more energy is lost to heat generation in a material as a signal propagates through it.

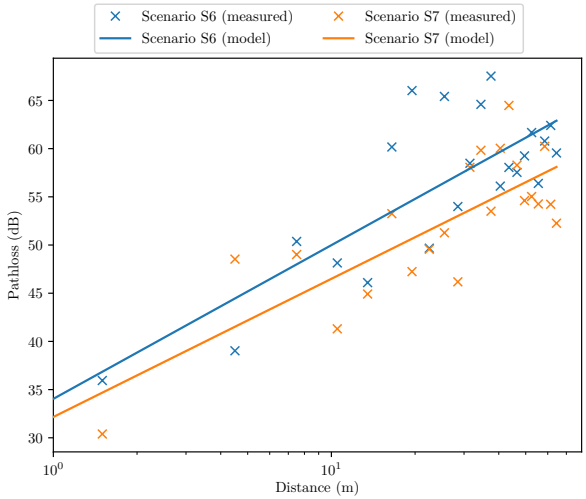

(a) Zone 1

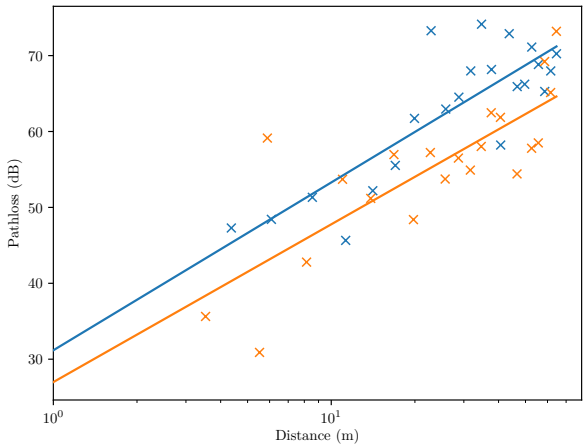

(b) Zone 2

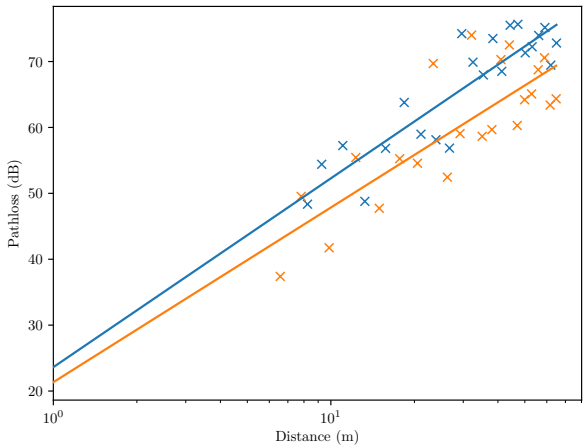

(c) Zone 3

Figure 6.9 Comparing the different zones in scenarios S6 and S7.

6.2.7 Packet Loss Measurement Results

This section details the packet loss measurements completed for each scenario. At Location 1, only 10 000 packets were sent at each measurement point, meaning that error rates below 10^{-3} could not be assessed. Only 10 000 packets were sent as preliminary testing at the University of Canterbury campus indicated the packet error rate would be above this level; it was not. There were no significant packet drops during any of the scenarios at Location 1 — meaning that for the distances tested the packet drop rate is less than 10^{-3}.

At Location 2, an increased number of packets were sent at a higher rate (100 000 packets at 750 packets per second) which allows the detection of lower error rates. Additionally, measurements were completed over longer distances covering locations where the signal strength is weaker and thus (all else being equal) are more likely to have errors. Figure 6.10 shows the packet reception results for S6. Unfortunately, due to time constraints and equipment malfunction, packet loss measurements were not performed for S7.

The main feature noticeable in the PRR measurements for S6 is the drop in zone 2 and zone 3 around 60 m along the aisle. This is likely caused by an obstacle in the environment for the following reasons:

- The artefacts appear in more than one zone at around the same distance.
- The PRR recovers in the final data point in zone 3.
- There is a lead in to the dip, possibly caused by partial occlusion of the main signal strength from an obstacle.

Surprisingly, there is not a corresponding drop in path loss at these locations for each zone. This is possibly caused by more the signal strength coming from reflections and scattering from the racking, rather than the main path of the signal. This can lead the data on the signal being irretrievable but the overall signal strength not reducing. This is likely exacerbated by the received signal being so close to the noise-floor of the OBU, meaning that any obstruction of the main signal path will have a greater effect.

6.3 MODEL VALIDATION

To validate the model described and parameterised above, the model will be implemented in the simulator and packet loss simulations completed. The results from these simulations will be compared to both analytical results for each technology and the observed PRR presented in Section 6.2.7.

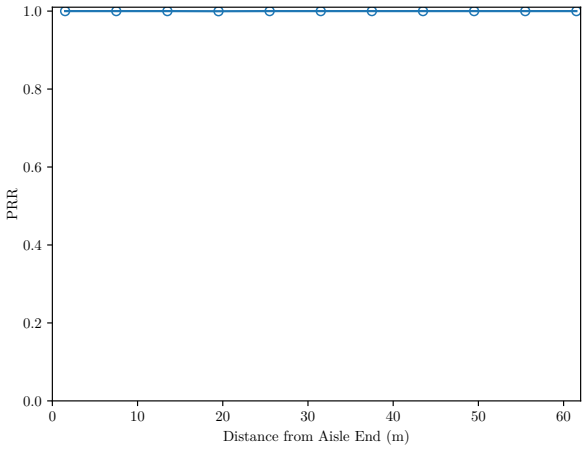

(a) Zone 1

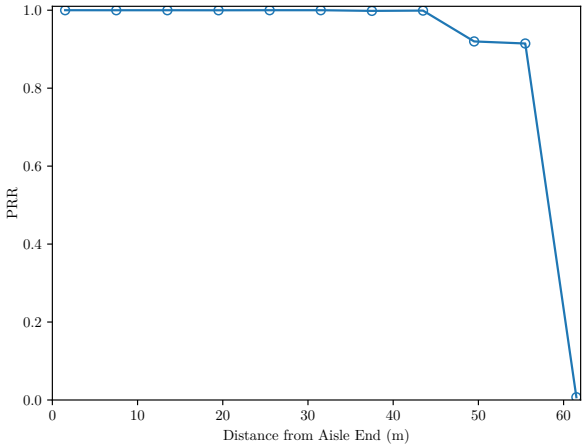

(b) Zone 2

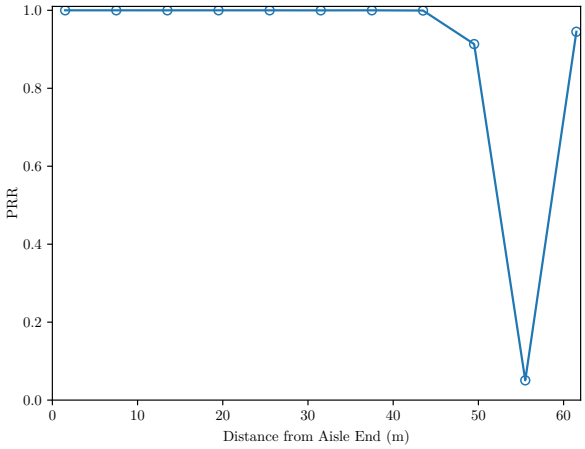

(c) Zone 3

Figure 6.10 PRR measurements for Scenario S6.

6.3.1 Comparison to Analytical Results

The warehouse channel model proposed in Section 6.1 was implemented in both the C-V2X and 802.11p simulators. To validate the model, the output of the simulators will be compared to theoretical results. Since analytical results only exist for the Bit Error Rate (BER) performance of 802.11p, the correctness of C-V2X's model will be validated by comparing the expected output computed from the Block Error Rate (BLER) tables provided by NIST [148] and Huawei [149]. A method of calculating the expected PRR for C-V2X is provided in Section 5.2.1, so this section will only discuss how to calculate the PRR for 802.11p.

To generate appropriate PRR curves from the simulator, a setup similar to the one used to verify the PHY in Section 5.2.1 was developed. In that scenario there is a single transmitter and receiver. However, for this scenario one transmitter and three receivers, one for each zone, are used. To ensure the correct zone parameters were applied to each receiver, and thus the implementation was correct, the receivers were all placed in different zones.

The theoretical PRR for 802.11p can be calculated from the Bit Error Rate (BER) as the probability that every bit in a transmitted packet is received correctly. Thus the PRR as a function of distance is,

$$PRR(d) = (1 - BER(d))^l, \tag{6.4}$$

where $PRR(d)$ is the PRR when the transmitter is d metres away from the receiver, $BER(d)$ is the Bit Error Rate (BER) at distance d, and l is the length of the packet in bits. Note that Equation (6.4) only holds for independently and identically distributed bit errors in the absence of error control coding. Since BER is as a function of the Signal-to-Noise Ratio (SNR), Equation (6.4) can be restated as,

$$PRR(d) = (1 - BER(SNR(d))^l, \tag{6.5}$$

where $SNR(d)$ is the SNR at distance d. The $\frac{1}{2}$-QPSK MCS was used for all the PRR measurements performed at warehouses, so it will be used for the verification as well. The BER performance of QPSK is well known as [78],

$$BER_{\text{QPSK}} = \mathrm{Q}\left(\sqrt{SNR\,(d)}\right), \tag{6.6}$$

where $\mathrm{Q}\,(x)$ is the complementary probability distribution function for a normal distribution,

$$\mathrm{Q}\,(x) = \frac{1}{\sqrt{2\pi}} \int_x^\infty e^{\frac{-t^2}{2}}\, dt = \frac{1}{2}\,\mathrm{erfc}\left(\frac{x}{\sqrt{2}}\right), \tag{6.7}$$

where $\mathrm{erfc}\,(\cdot)$ is the complimentary error function [174]. However, the BER after the error correction coding is not as definite and theoretical results only place an upper

bound on the BER. The upper error bound for hard decision decoding of $\frac{1}{2}$-QPSK is [175],

$$BER_{\frac{1}{2}\text{-QPSK}} < \frac{1}{2}\sum_{i=10}^{\infty}\beta_i D^i, \tag{6.8}$$

where

$$D = \sqrt{4BER_{\text{QPSK}}(1 - BER_{\text{QPSK}})}, \tag{6.9}$$

and β_i are weights derived from the transfer function of the convolutional code used by 802.11p. The convolutional code 802.11p uses is the same as the remainder of the 802.11 standard, for which appropriate weights are presented in [176] and are reproduced in Table 6.3.

To confirm the warehouse channel model is implemented correctly for 802.11p, the theoretical upper bound presented in Equation (6.8) will be assumed to be equal to the BER. Thus, substituting Equation (6.8) into Equation (6.5),

$$PRR\,(d) = \left(1 - \frac{1}{2}\sum_{i=10}^{\infty}\beta_i D^i\,(d)\right)^l, \tag{6.10}$$

where, substituting Equation (6.6) into Equation (6.9),

$$D\,(d) = \sqrt{4\,\mathrm{Q}\left(\sqrt{SNR\,(d)}\right)\left(1 - \mathrm{Q}\left(\sqrt{SNR\,(d)}\right)\right)}. \tag{6.11}$$

Since there is only one transmitter in the validation simulation scenario, there is no interference. Therefore, assuming isotropic antennas, the SNR can be calculated as,

$$SNR\,(d) = \frac{P_{\text{tx}}}{N_0 N_{\text{rx}} PL(d)}, \tag{6.12}$$

where P_{tx} is the transmit power, $PL(d)$ is the path loss experienced when the transmitter and receiver are d m apart, N_0 is the thermal noise across the bandwidth of the transmission, and N_{rx} is the noise figure of the transmitter.

This validation simulation scenario had 50 replications completed for both C-V2X and 802.11p. Since C-V2X has two different BLER data sets, both are used for validation. Tables 6.4 and 6.5 detail the settings used for the simulation runs. For both simulations the PRR is calculated by allocating packets into 1 m wide bins.

The simulated results for 802.11p are compared against the analytical result in Figure 6.11. There is little deviation between the two curves as the 802.11psimulator also assumes that the upper bound on the BER after error correction is the real experienced BER. Figure 6.12 compares the expected PRR to the C-V2X simulator using the warehouse channel model. Since both simulators match the expected values the model is judged to match the theoretical expectations.

Table 6.3 The non-zero weights used to estimate the $\frac{1}{2}$-QPSK MCS used in 802.11p. Reproduced from [176, Table 1 row m=6].

i	β_i
10	36
12	211
14	1 404
16	11 633
18	77 433
20	502 690
22	3 322 763
24	21 292 910
26	134 365 911

Table 6.4 The simulation parameters used to validate the warehouse channel model. The two different noise figure values are selected so that all PRR transition of all three zones can be clearly shown for each technology.

Parameter	802.11p	C-V2X
Transmit power	0 dBm	
Packet size	190 B	
Beacon frequency	100 Hz	
Channel model	Table 6.5	
Carrier frequency	5.89 GHz	
Receiver sensitivity	-110 dB	
Number of replications	50	
Antenna gain	0 dBi	
Thermal noise	-174 dB/Hz	
Vehicle used	Model forklift (Section 4.2)	
Vehicle speed	0.1 m s^{-1}	
Noise figure (dB)	12	22
MCS	3 ($\frac{1}{2}$-QPSK)	9 (0.73-QPSK)
Number of RBs per sub-channel (L)	—	16
Number of sub-channels	—	3
Resource reselection probability	—	0.8
Number of retransmissions	—	0

Table 6.5 The channel model parameters used for validate the warehouse channel model.

Zone	Zone Boundary (m)	$\widehat{PL(d_0)}$ (dB)	d_0 (m)	α
1	1.50	34.04	1.0	1.595
2	8.10	31.17	1.0	2.211
3	—	23.62	1.0	2.865

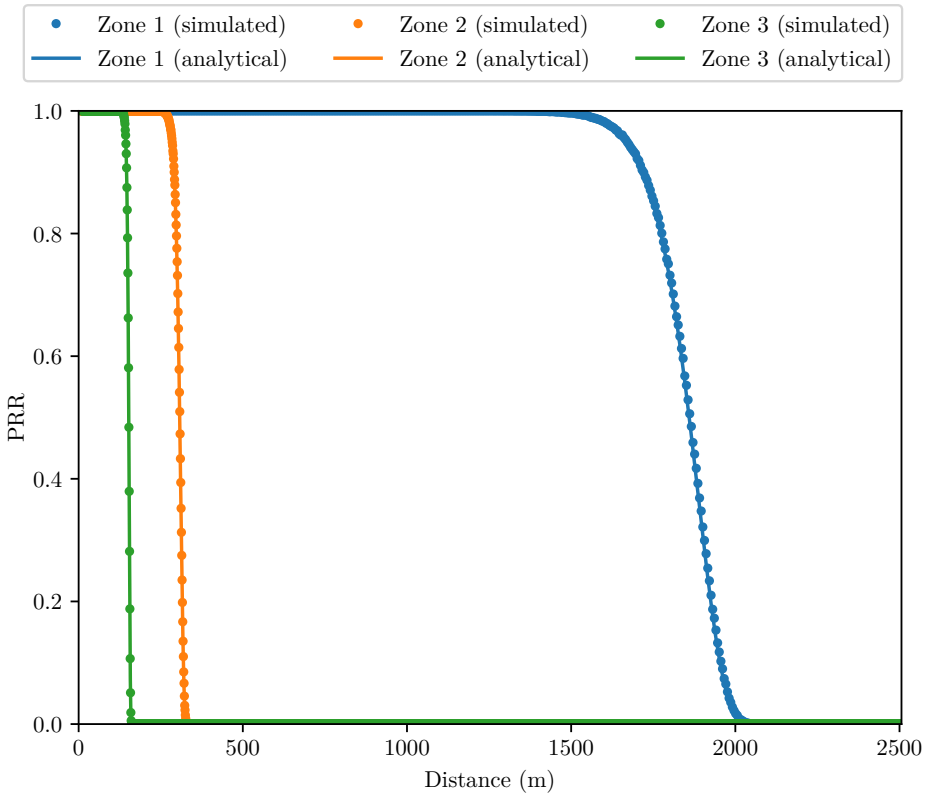

Figure 6.11 The PRR of the 802.11p simulator using the warehouse channel model compared to the expected analytical results calculated using Equations (6.10)–(6.12).

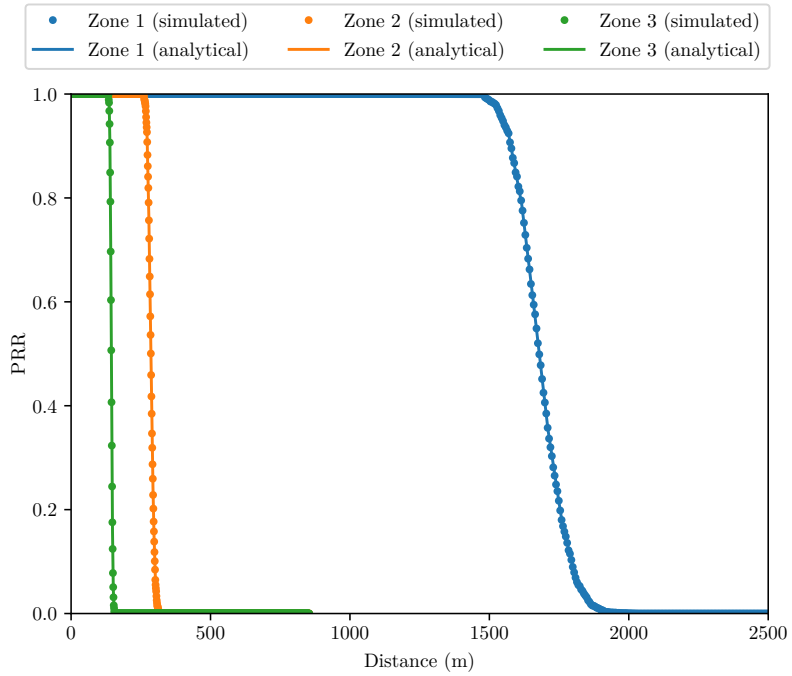

(a) The PRR for the NIST data set. Whilst the PRR has been calculated at 1 m intervals, the zone 1 data has been thinned to only show every fifth data point to make the figure easier to read.

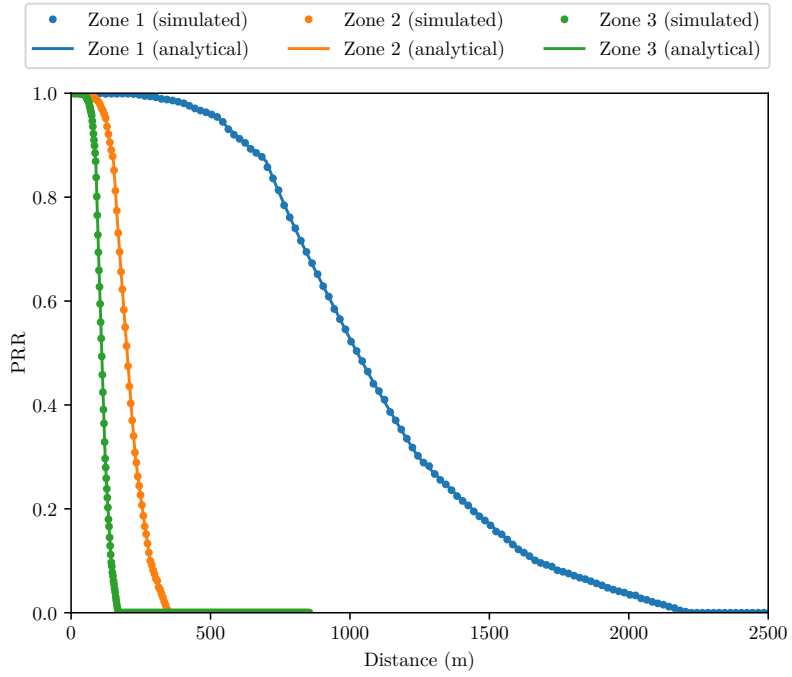

(b) The PRR for the Huawei data set. Whilst the PRR has been calculated at 1 m intervals, the data for zones 1, 2, and 3 has been thinned to only show every twentieth, fifth, and second data point, respectively, to make the figure easier to read.

Figure 6.12 The PRR of the C-V2X simulator using the warehouse channel model compared to the expected analytical results calculated using the method in Section 5.2.1. For both data sets, zone 2 and 3 are only simulated for distances up to 850 m to reduce the required simulation time.

6.3.2 Comparing Simulator to the Real World

To determine how representative the warehouse channel model is of the real packet loss measurements, a PRR simulation was constructed and compared to the real-world measured PRR in Section 6.2.7. The PRR simulation was based on the setup used above, however, the transmitter and receiver were configured to mimic the Cohda Mk5 OBU. The simulation parameters used are included in Table 6.6.

Figure 6.13 shows the results of the simulator. For the channel model to be reflective of the environment, the simulator and real-world measurements should generally match. Since there is such limited measured PRR data, the main criteria is that the simulated PRR is 100% along the measured aisle length. This does hold, however it tells us very little about the performance of the channel model at mimicking the real world, primarily informing us that the model does not disagree over the small slice of information gathered here.

6.4 DISCUSSION

The channel model formed here is unique and as discussed in Section 3.3, has few works to be compared against in the literature. The most relevant paper are Tanghe et al. [104] and Croonenbroeck et al. [103]. Tanghe et al. discusses a production warehouse at 5.2 GHz. The results presented here are in line with their results with path loss exponents less than two for LOS transmissions. However, Tanghe et al. report the path loss exponents less than two for light and heavily obstructed paths, whereas the measurements here indicate they are worse than free space transmission. This difference is caused by the measurement setup in Tanghe et al.: the transmitter and receiver height are significantly different. In Tanghe et al., the transmitter is 6 m from the floor and the racking in some situations is shorter than this, allowing the signal to diffract off the contents of the racking and propagate between aisles. Though this is not the case in all of their measurements, the remaining discrepancy is possibly explained by the types of warehouses measured: metal and wood processing facilities. These facilities will be very different and are likely to have more homogeneous materials in the racking, when compared to the warehouses measured in this thesis.

Croonenbroeck et al. [103] perform channel measurements at 5.8 GHz in a warehouse environment. The environment is similar to scenario S5, consisting of a limited area of racking at the back of a workshop. They perform two sets of measurements for the LOS case, with path loss exponents between 1.64 and 1.79, and the obstructed LOS case, with path loss exponents between 1.83 and 1.97. The LOS and obstructed LOS case roughly parallel the zone 1 and zone 2 measurements conducted here. For zone 1 of S5, the path loss exponent is significantly higher than what Croonenbroeck et al. present for the LOS case. However, the path loss exponent for zone 2 is within the range they present

Table 6.6 The simulation parameters used to validate the warehouse channel model against the real world PRR measurements.

Parameter	802.11p
Transmit power	0 dBm
Packet size	180 B
Beacon frequency	100 Hz
Channel model	Table 6.5
Carrier frequency	5.89 GHz
Receiver sensitivity	-96 dB
Receiver noise figure	6 dB
Number of replications	50
Antenna gain	0 dBi
Thermal noise	-174 dB Hz^{-1}
Vehicle used	Model forklift (Section 4.2)
Vehicle speed	0.1 m s^{-1}
MCS	1 ($\frac{1}{2}$-BPSK)

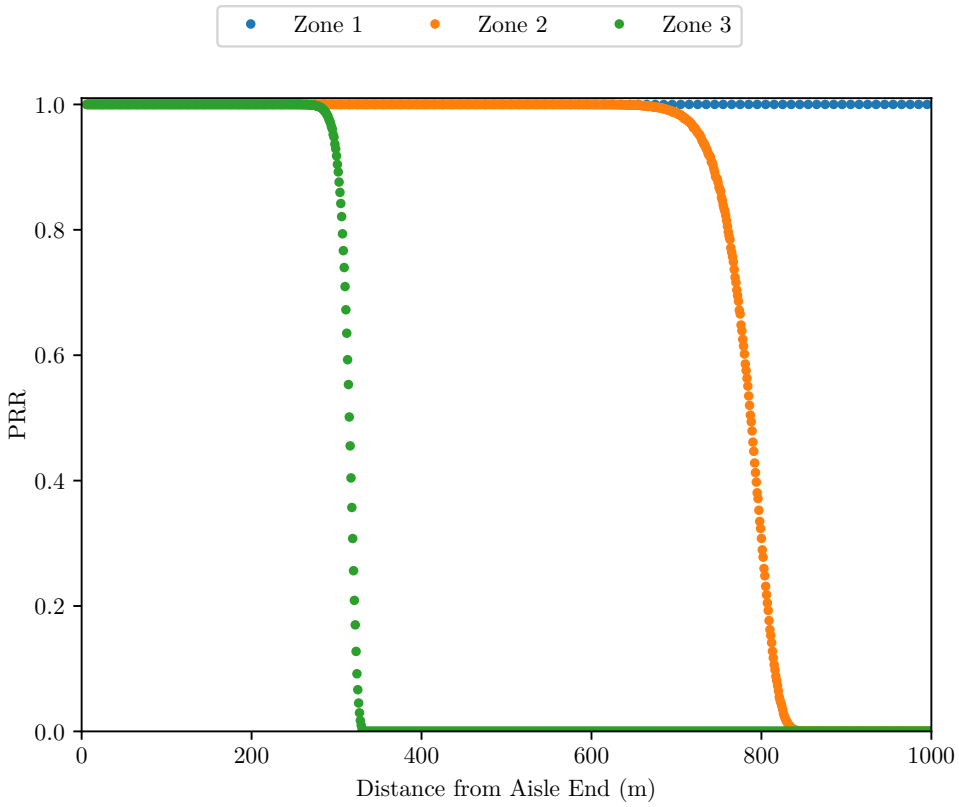

Figure 6.13 The PRR results when the simulator is setup to mimic the Cohda OBU. These are only plotted for the first 1000 m and as such, zone 1 has a a PRR of 100% for the entire simulated length.

for the OLOS case. Scenarios S6 and S7 do not match the results in Croonenbroeck et al., however this is likely due to the differences in measured environment.

Upon initial inspection the results in Table 6.2 are surprising: there are path loss exponents significantly less than free space and the reference path loss varies per zone. However both of these can be explained. Path loss exponents less than free space have been repeatedly reported in the literature for industrial channels and are caused by multipath effects and the racking acting as a waveguide [103–106]. The reference path loss varying per zone is caused the increased path loss exponent per zone, forcing the reference path loss down when it is projected back to 1 m. Correspondingly, where the path loss exponent does not increase between zones, the reference path loss is similar (e.g. comparing scenario S3's zone 1 and zone 3 and S5's zone 1 and zone 2) and any difference is likely due to the statistical variation in measurements.

Section 6.2.6 briefly discusses why a single scenario is adopted for the channel model parameters, rather than averaging across the measurements taken. This is due to the limited number of sites measured within this thesis and the highly variant nature of warehouse contents. Once more measurements are conducted, a statistically averaged warehouse could be constructed. One problem with this is that warehouses themselves, not just the contents, vary a lot. This is due to the building's construction and material makeup, the spacing between racks, and what the racking is constructed from. For example, even within Location 2 the warehouse racking varied a lot with different aisles having different depth racking bays from 2–4 units deep.

This raises the important question of whether it is possible to form a generic model of warehouse intersection and its usefulness. This thesis does not answer this question as it is beyond the scope, however it does recommend some possible future research. A more useful representation of a warehouse could be gained through not just focusing on aisle-ends but focusing on developing a more generic path loss curves for different environmental elements (e.g. single racking, empty space, empty racking) and then using a piecewise sum of the distance a signal propagates through each medium to determine the path loss. To handle variation of warehouse contents, a series of different curves could be developed for each environmental element and then randomly selected or assigned to different elements in the environments. This approach is applied to traditional road networks and buildings in [177]. To handle the multipath and reflective nature of the warehouse channel, an additional fast fading parameter for the channel should be investigated. This would include addressing what type of fading distribution (and possibly what combinations of fading distributions) are present in a warehouse, and measuring the parameters. This could be done in parallel to the medium characterisation process. Another approach could be to form a statistical-geometric model for a warehouse similar to the WINNER II channel models [85]. This would require using a full channel sounder, but would provide not only a channel model for network level simulations but a model also suitable used for link-level simulations of

warehouses.

The channel model developed in this chapter was implemented in the simulator and has been validated against theoretical results and real world measurements. However, this is not complete validation of the model. This is as the PRR data presented in Section 6.2.7 is not over a long enough distance to definitively state that it behaves similarly. Using theoretical results did not improve the validation significantly either, as the C-V2X simulator uses the same BLER data set and the 802.11p simulator uses the same method to calculate the packet drop rate for a given SNR. This does not mean the validation process undertaken in this chapter was worthless. Undergoing this process allows the implementation to be exercised and shows that the model matches the assumptions it is built under, but not that these assumptions are good approximations of the real world. To fully validate this model more packet loss measurements should be conducted over longer distances, using more packets, and a higher MCS. Using a higher index MCS increases the likelihood that any given bit will be in error for the same SNR compared to lower MCS settings.

The warehouse channel model described in Section 6.1 and parameterised in Section 6.2.6, is suitable for evaluating the performance of 802.11p and C-V2X in a warehouse environment. The evaluation method and simulator that it will be used with to complete this evaluation are discussed in Chapters 4 and 5, respectively. The results of the evaluation are presented and discussed in Chapter 7.

Chapter 7

COLLISION DETECTION SIMULATION CAMPAIGN

This chapter covers the execution of a simulation campaign to answer research questions Q2 and Q3. These questions address the effect of the average spacing between vehicles and the technology settings on the error rate of a collision warning application, respectively. The scenario this chapter simulates was designed in Chapter 4 and the simulator and channel model used are described in Chapters 5 and 6.

First, Section 7.1 establishes a baseline algorithm failure rate under perfect communication conditions. Then, Section 7.2 determines how many vehicles are in the simulation to provide context for the simulation results presented in following sections. Section 7.3 details the simulation methodology and analyses the expected relative impact of each factor. Sections 7.4–7.6 present the results of the simulation campaign, exploring the effect of density, Modulation and Coding Scheme (MCS), and transmit power on the error rate of a collision warning application. Finally, Section 7.7 discusses these results and answers research questions Q2 and Q3.

7.1 ESTABLISHING A BASELINE ALGORITHM FAILURE RATE

Establishing a baseline collision rate is important as the algorithm, even with perfect communication, will fail occasionally. These failures are caused by the collision prediction algorithm not extrapolating the other forklift's position, accounting for the distance travelled since the last beacon was received, before predicting the other forklift's future position. Not adjusting the vehicle's position for the delay between transmission and usage penalises vehicles for missing messages. This penalty is necessary as all vehicles in the simulation move with a constant speed, thus, the position of the vehicle can be accurately predicted for any time. In a real scenario, this would not be the case as the forklift speed and direction will vary due to the human operator. This penalty works in tandem with the stale data timeout, which penalises vehicles harshly for missing multiple beacons in a row by making them forget vehicles. For all simulations the beacon period is 100 ms and the stale data timeout is set to 200 ms. This setup means there can be up to 0.29 m of positioning error, even if all the beacons are correctly

received, when using the model forklift in Section 4.2 and a beacon period of 100 ms.

To determine the baseline collision rate, a perfect information distribution mode was setup in the 802.11p simulator. This mode intercepts a forklift's transmissions at the 802.11p adapter layer before they are sent to the 802.11p NIC (Section 5.1.2). The 802.11p adapter then directly sends them to the `GapDetector` modules of all other vehicles in the simulation. This means that there is no packet loss or delay in receiving messages, creating a perfect communication system. Only one of the technologies needs to implement this mode as the scenario setup is identical for each technology and is the only cause of any algorithm failures.

The perfect information distribution simulation was run for a range of different densities and the full parameter set used is in Table 7.1. The density has been controlled by setting the average introduction period (AIP) between vehicles. Figure 7.1 shows the baseline false positive error rate, i.e. where the intersection is declared unsafe, when in reality it is safe to enter. Figure 7.2 presents the baseline false negative rate, i.e. where the intersection is declared safe to enter, when in reality it is unsafe.

Figures 7.1 and 7.2 show that the baseline error rate is not constant for all densities. For the 10–40 s AIP, the baseline false positive and false negative error rates are possibly the same as there is a region where the 95% confidence intervals overlap. The increasing confidence interval size with increasing AIP is likely due to fewer forklifts passing through the intersection in each individual replication, increasing the variability of the mean error rates per replication. For the 4–8 s AIP, the false positive and false negative failure rates are decreasing and do not line up with the 10–40 s AIP. This is as in the 4–8 s AIP, vehicles are on average closer together and, thus, the intersection is less likely to be borderline safe. Only when the intersection is borderline safe can small errors, created by not accounting for the distance travelled between beaconing and data use, cause algorithm failures. Additionally, there are more likely to be multiple vehicles causing the intersection to be unsafe, and thus more opportunities for the system to correctly detect the state, further reducing the false negative error rate.

This establishes a baseline algorithm failure rate. Any collision prediction algorithm failures above this rate are caused by the technologies, and can be used to evaluate them.

Table 7.1 The parameters used to establish the baseline error rate of the collision prediction algorithm.

Parameter	Value
AIP (s)	4, 5, 7, 8, 10, 20, 30, 40
Number of replications	250
In-scenario time	2 hours
Forward safety distance	12 m
Rear safety distance	12 m
Vehicle model	Model forklift (Section 4.2)

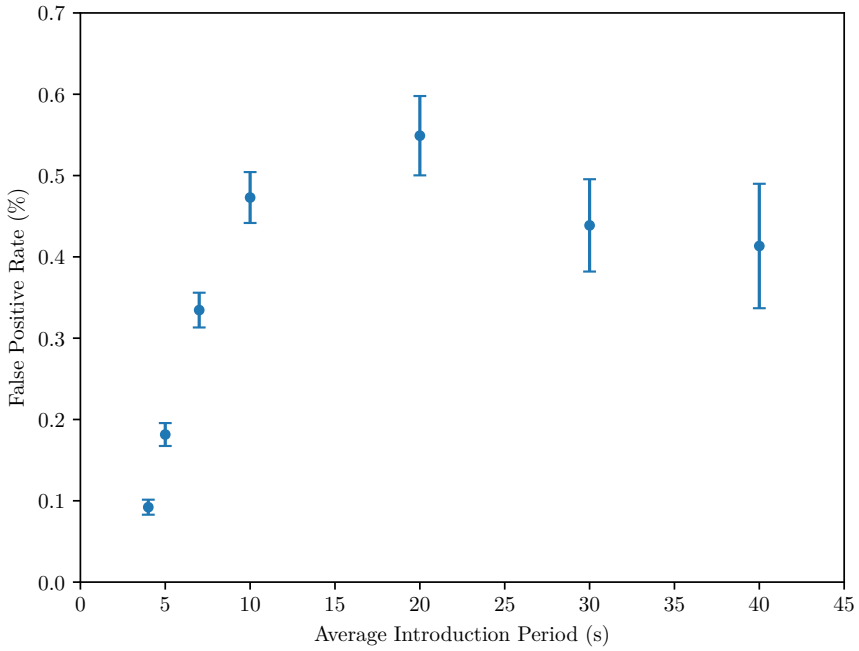

Figure 7.1 The baseline false positive rate for the collision prediction algorithm. The error bars show the 95% confidence intervals.

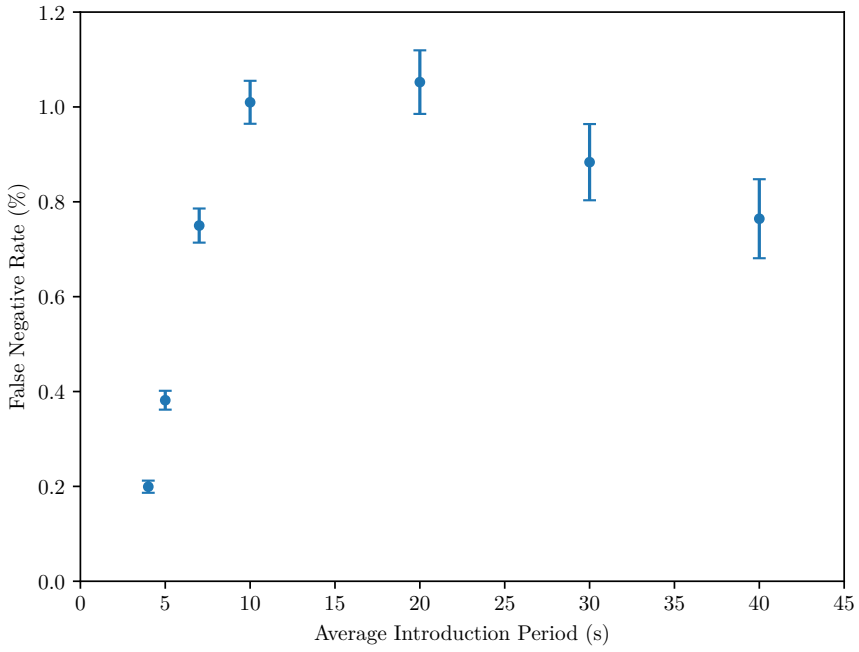

Figure 7.2 The baseline false negative rate for the collision prediction algorithm. The error bars show the 95% confidence intervals.

7.2 NUMBER OF VEHICLES IN EACH SIMULATION

To establish how many vehicles are in the simulation at any time, the system can be viewed as a queue. The average number of items in any queue at any point in time can be calculated using Little's law [178]:

$$N = \lambda W, \tag{7.1}$$

where N is the average number of items in a queue, λ is the average rate at which items are added to the queue, and W is the average waiting time of an item in the queue. Little's law holds regardless of the distribution of arrival period or wait time. For the simulated scenario, there are two independent streams of forklifts which will be treated as two separate queues with equal average arrival rate and waiting time. Thus, the average number of vehicles in the simulation at any given time is,

$$N = 2\lambda W, \tag{7.2}$$

where λ is the inverse of the AIP and W is the time for the vehicle to leave the queue. W is constant for all AIP values and is the time each vehicle spends in the simulation. As such, W is the time it takes for a forklift to travel along two 200 m long aisles (Section 4.2),

$$W = \frac{\text{distance travelled}}{\text{vehicle speed}} = \frac{400}{2.889} = 138.46\,\text{s}. \tag{7.3}$$

Table 7.2 presents the average number of vehicles in the simulation scenario for the AIP values in Table 7.1.

7.3 SIMULATION METHODOLOGY

To explore the impact of density, MCS, and transmit power a number of replications of each parameter set were run. To ensure each run was statistically independent, each run had a different random number generator seed, automatically selected from the

Table 7.2 The average number of vehicles in the simulation scenario per AIP.

AIP ($\frac{1}{\lambda}$, seconds)	Number of Vehicles (N)
4	69.2
5	55.4
7	39.6
8	34.6
10	27.7
20	13.8
30	9.2
40	6.9

OMNeT++ built-in set of seeds.

The main simulation campaign was conducted in two steps: an initial pilot run and then a larger bulk simulation run. The pilot run used a 2^k-factorial experimental design to evaluate relative impact of each parameter (transmit power, MCS, and density) on the technologies' performance. A 2^k-factorial experimental design explores the two extremes of k parameters to determine the strength of the influence of a parameter on the outcome of the experiment [179]. The strength is calculated by determining what percentage of variation in the experiment outcome is explained by a change in each parameter. However, as it is possible that combinations of factors have a larger impact than either factor individually, 2^k-factorial analysis also analyses the impact of parameters combinations. The exact method used to calculate these values is described in [179, pp 284–292].

The parameters in Table 7.3 were used for the pilot run. An AIP (density) of 30 s was selected as the lowest value of density, over the 40 s case, due to its smaller confidence interval size. The overall resulting influence of the parameters is shown in Table 7.4. The false positive error rates for C-V2X and both false positive and false negative error rates for 802.11p all agree density is the factor with the most impact on the error rate (72–75%). However, for the false negative error rate of C-V2X, the most important factor is transmit power (60.1%). This is anomalous and its cause is explored in Section 7.6.

Since it appears that the density has the largest effect on the resulting error rates, it will be explored in depth over a wide range of density values. Transmit power and MCS choice contribute less to the change in performance, so a sparser set of simulations will be completed. The remainder of the simulations completed in this chapter all use 160 replications for each parameter set. 160 replications was selected based on the number of simulations required to reduce the 95% confidence intervals to make a statistically significant distinction between the two different C-V2X MCS options explored in the forklift density simulations (Section 7.4). All simulations in this chapter use 190 B long packets (including header), have a beacon period of 100 ms, a stale data timeout of 200 ms, and use a rear and forward safe following distance of 12 m. For all C-V2X MCS values used, the mapping from MCS index to scheme is taken from Table 3 in [39].

Table 7.3 The simulation parameters used for the pilot run.

Parameter	Value	
	802.11p	C-V2X
Number of replications	20	
Packet length (including headers)	190 B	
AIP (s)	4, 30	
Transmit power (dBm)	0, 30	
Thermal noise	-174 dB Hz^{-1}	
Noise figure	6 dB	
Receiver sensitivity	-100 dB	
Antenna gain	0 dBi	
Frequency	5.89 GHz	
Channel model	Warehouse channel (Chapter 6)	
Vehicle model	Model forklift (Section 4.2)	
Rear safety distance	12 m	
Forward safety distance	12 m	
Beacon timeout	200 ms	
MCS	$\frac{1}{2}$-BPSK (MCS1) $\frac{3}{4}$-64QAM (MCS8)	0.27-QPSK (MCS3) 16-QAM (MCS20)
Bandwidth	10 MHz	10.08 MHz
Number of resource blocks	—	56
Number of sub-channels	—	1
Resource reselection probability	—	0.2
Channel busy threshold	—	-92 dB
BLER data set	—	NIST [148]

Table 7.4 The impact of each factor on the False Positive (FP) and False Negative (FN) error rates. All values are percentages.

Factor	802.11p		C-V2X	
	FP	FN	FP	FN
Density	75.2	74.5	72.3	26.13
Transmit Power	6.46	5.03	8.71	60.1
MCS	1.87	7.04	3.34	0.16
Transmit Power and Density	5.10	7.12	6.27	13.3
MCS and Density	0.19	6.17	0.37	0.29
MCS and Transmit Power	5.99	0.00	4.89	0.02
All	5.237	0.11	4.14	0.00

7.4 EFFECT OF VEHICLE DENSITY

To study the effect of forklift density, the average introduction period will be varied from 4–30 s. Since transmit power has such little effect on the outcome of the experiment it is fixed to 15 dBm (Table 7.4). The simulation parameters used are included in Table 7.5. Figure 7.3 presents the false positive algorithm failure rates as a function of density. Figure 7.4 includes the same for the false negative failure rate.

Based on the false positive failure rate shown in Figure 7.3, there is no statistical difference between C-V2X, 802.11p, and the base line false positive error rate. When considering the false negative error rate in Figure 7.4, C-V2X performs significantly worse than both 802.11p and the baseline. 802.11p does not perform significantly different to the baseline false negative rate. An interesting thing to note is that for C-V2X at higher densities the performance of each MCS diverges. This is likely due to the increased noise due to forklifts on the edges of the simulation transmitting and interfering with vehicles near the intersection. In this case a more noise-tolerant MCS, like MCS3, can handle this added interference, but a less noise-tolerant MCS, like MCS20, will be more susceptible to errors, causing an increase in algorithm failure rate.

To determine whether the error rate increases, relative to the baseline as the AIP decreases, the percentage increase on baseline is included in Figure 7.5. There are no statistically significant differences or trends for either technology in the false positive data. For the false negative data, whilst there are no statistically significant changes in the percentage of baseline across both technologies, there is a clear trend of an increasing false negative rate for C-V2X in MCS20 as density increases (AIP decreases). This indicates that for C-V2X as the AIP decreases, the false negative rate worsens relative to the baseline performance for each density. 802.11p matches the baseline across all densities for both false positive and false negative error rates, indicating that it does not introduce any extra errors within the resolution of this experiment.

Table 7.5 The simulations parameters used to explore the effect of forklift density on the performance of the algorithm.

Parameter	Value	
	802.11p	C-V2X
AIP (s)	4, 7, 10, 20, 30	
Run time (h)	1, 1, 2, 2, 2, 2	
Transmit power (dBm)	15	
Thermal noise	-174 dB Hz^{-1}	
Noise figure	6 dB	
Receiver sensitivity	-100 dB	
Frequency	5.89 GHz	
Channel model	Warehouse channel (Chapter 6)	
Vehicle model	Model forklift (Section 4.2)	
MCS	$\frac{1}{2}$-BPSK (MCS1) $\frac{3}{4}$-64QAM (MCS8)	0.27-QPSK (MCS3) 16-QAM (MCS20)
Bandwidth	10 MHz	10.08 MHz
Number of resource blocks	—	56
Number of sub-channels	—	1
Resource reselection probability	—	0.2
Channel busy threshold	—	-92 dB
BLER data set	—	NIST [148]

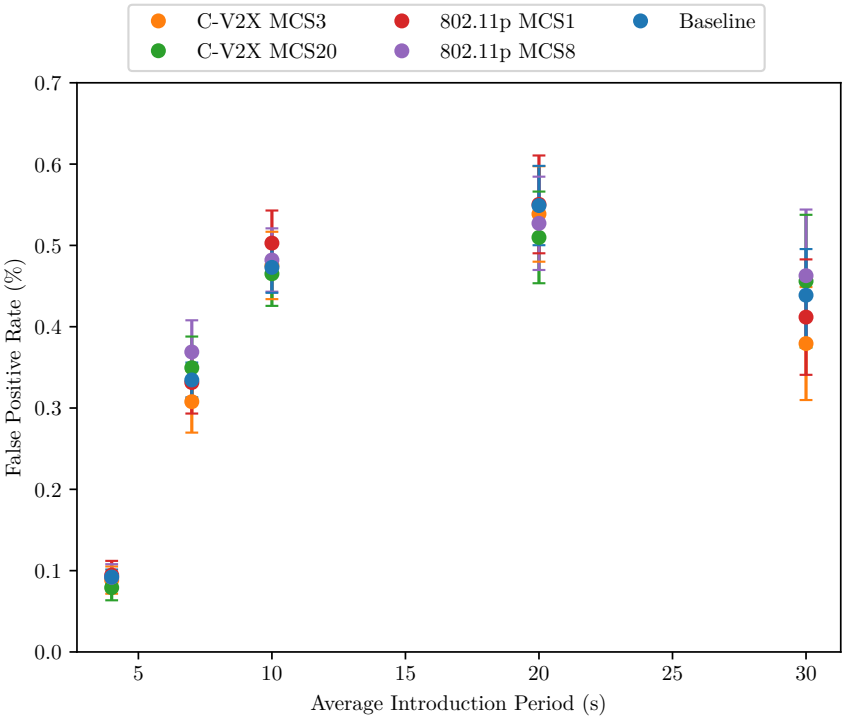

Figure 7.3 The false positive failure rate of the collision prediction algorithm as a function of density. The error bars show the 95% confidence intervals.

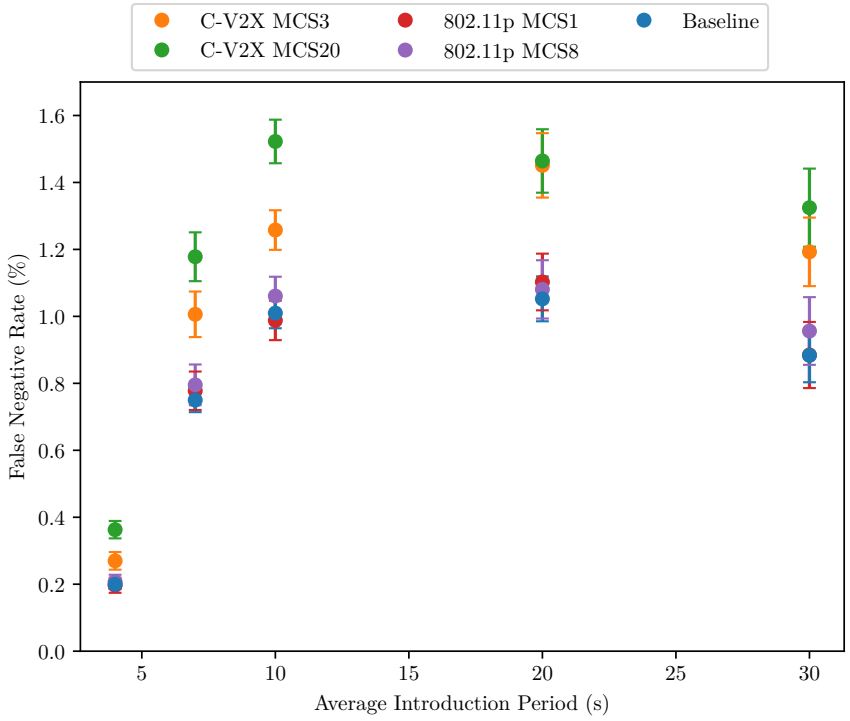

Figure 7.4 The false negative failure rate of the collision prediction algorithm as a function of density. The error bars show the 95% confidence intervals.

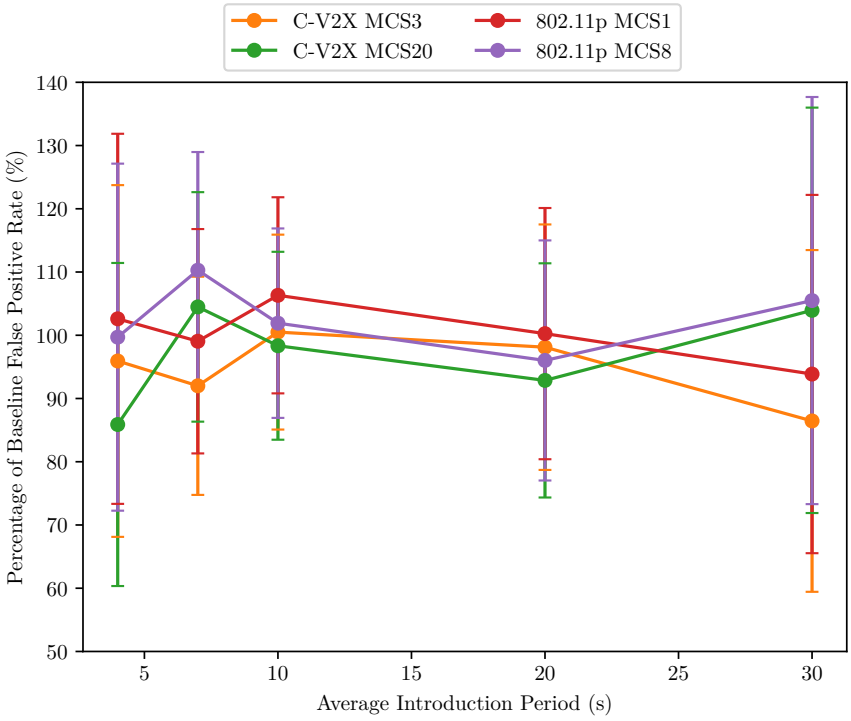

(a) False positive error rate

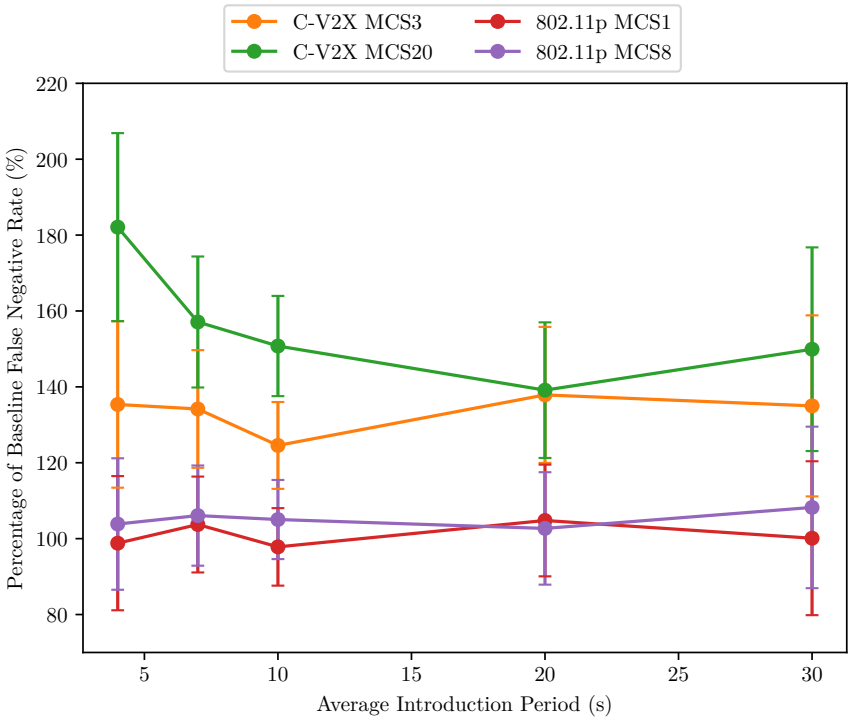

(b) False negative error rate

Figure 7.5 The percentage of baseline error rate for the false positive error rate (a) and false negative error rate (b) as a function of density. The error bars indicate the uncertainty on the factor, calculated using the 95% confidence intervals. The baseline error rate is at 100%

7.5 EFFECT OF MODULATION AND CODING SCHEME

To explore the effect of Modulation and Coding Scheme (MCS) on the application, several MCS settings for both technologies were simulated. The settings for these simulations are included in Table 7.6, with the different MCS settings outlined in Table 7.7. These MCS values were selected to allow the technologies to be directly compared, or as the two extremes of the possible MCS. The results of these simulations are shown in Figures 7.6–7.8.

For the 20 s and 30 s AIP, there are no statistically significant differences between MCS choice for either technology, across both false positive and false negative error rates. Similarly, there is no statistically significant difference based on the choice of MCS across both technologies for the false positive error rate, in the 10 s AIP case (Figure 7.8). However, for the 30 s and 10 s AIP, there is a clear trend of increasing false negative error rate as the MCS index increases. As the MCS index increases, higher rate codes are used and these (usually) have an increased BER/BLER for the same SNR. For 160 replications this trend is not statistically significant, however the difference between the start, end, and some intermediary points are, indicating this trend does likely exist. 802.11p possibly also exhibits this behaviour for the same AIP values. However, the trend is not as strong and there is no statistically significant difference in the false negative error rate based on the choice of MCS.

The increase in failure rate as MCS index increases is likely due to the similarly increasing noise susceptibility of MCS as the MCS index increases. This means weaker noise, caused by packet collisions from vehicles on the fringes of the simulation, can increase the block error rate, increasing the chances a beacon is lost. These interfering vehicles must be on the fringe of the simulation as, if they were close the receiver which must be near the intersection for interference to have an effect on the application error rate, the beacon would be completely lost irrespective of the MCS selection.

Table 7.6 The simulation parameters used to explore the effect of MCS choice on the collision prediction algorithm error rate.

Parameter	Value	
	802.11p	C-V2X
AIP (s)	10, 20, 30	
Run time (h)	2	
Transmit power (dBm)	15	
Thermal noise	-174 dB Hz^{-1}	
Noise figure	6 dB	
Receiver sensitivity	-100 dB	
Frequency	5.89 GHz	
Channel model	Warehouse channel (Chapter 6)	
Vehicle model	Model forklift (Section 4.2)	
MCS	Table 7.7	
Bandwidth	10 MHz	10.08 MHz
Number of resource blocks	—	56
Number of sub-channels	—	1
Resource reselection probability	—	0.2
Channel busy threshold	—	-92 dB
BLER data set	—	NIST [148]

Table 7.7 The different MCS settings evaluated. The mapping from MCS index to C-V2X MCS is taken from [39].

802.11p		C-V2X	
Index	MCS	Index	MCS
1	$\frac{1}{2}$-BPSK	3	0.27-QPSK
3	$\frac{1}{2}$-QPSK	6	0.48-QPSK
5	$\frac{1}{2}$-16QAM	13	0.52-16QAM
6	$\frac{3}{4}$-16QAM	17	0.75-16QAM
8	$\frac{3}{4}$-64QAM	20	16-QAM

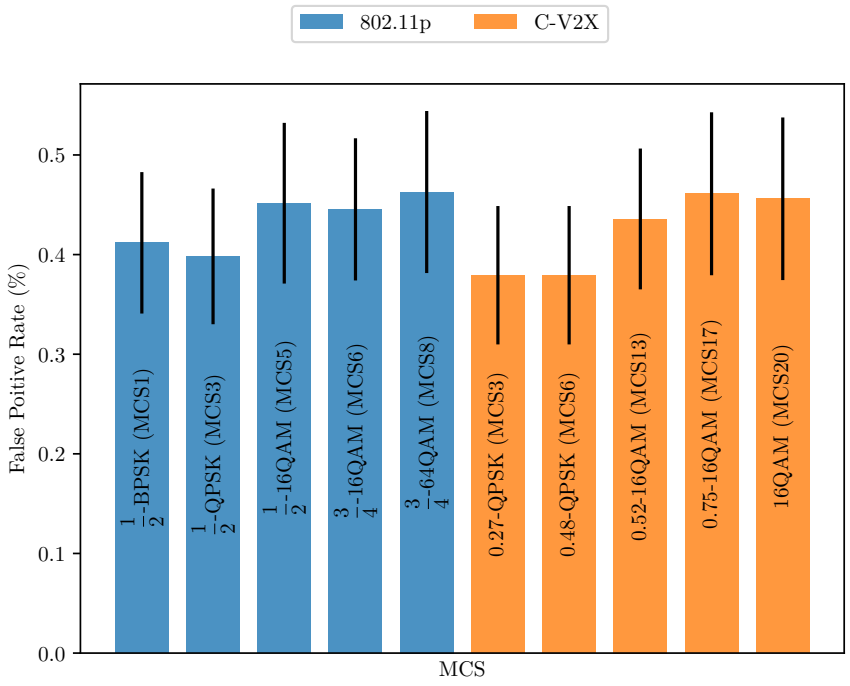

(a) False positive error rate.

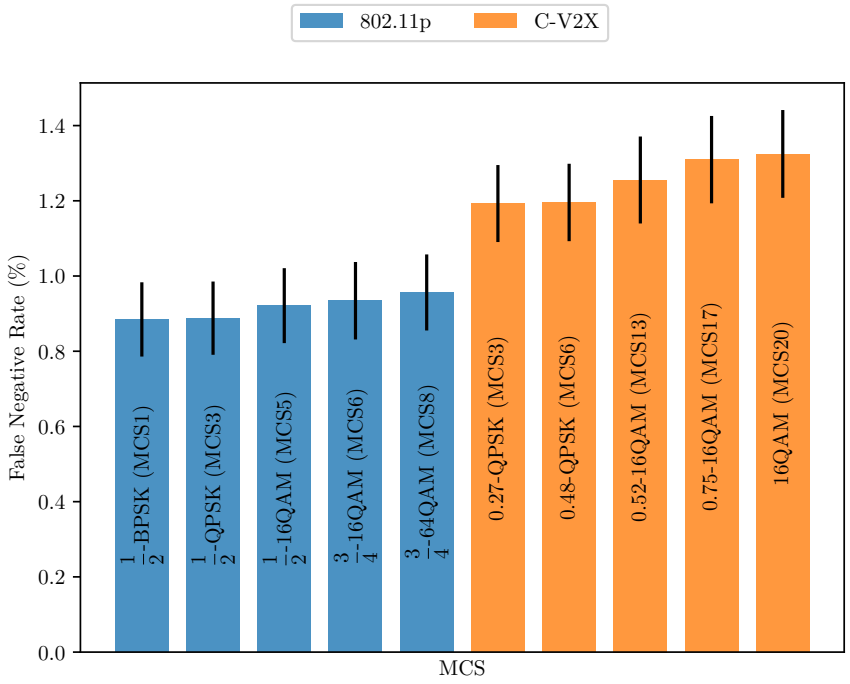

(b) False negative error rate.

Figure 7.6 The effect of MCS on the false positive error rate (a) and false negative error rate (b) for the 30 s AIP. The error bars show the 95% confidence intervals.

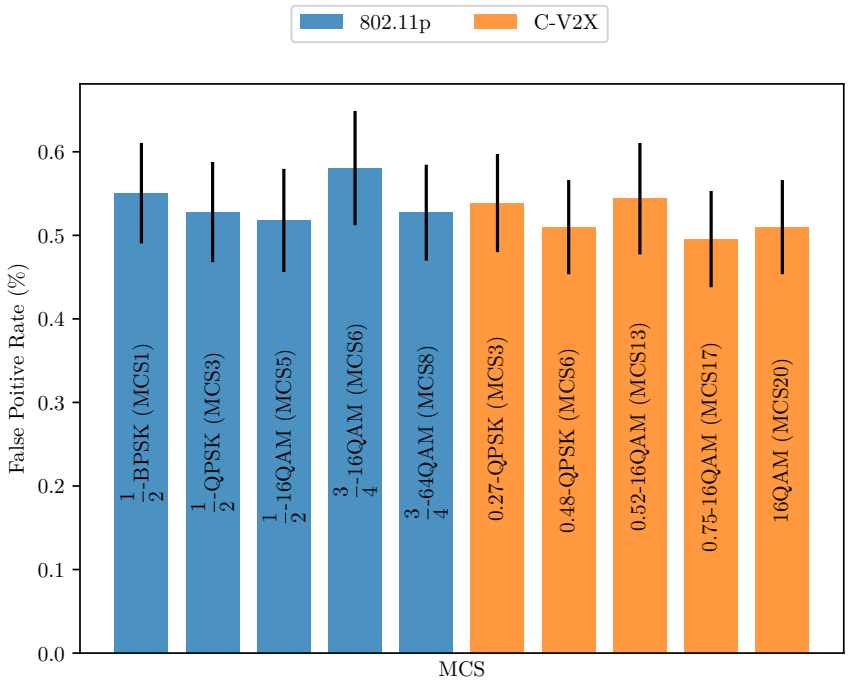

(a) False positive error rate.

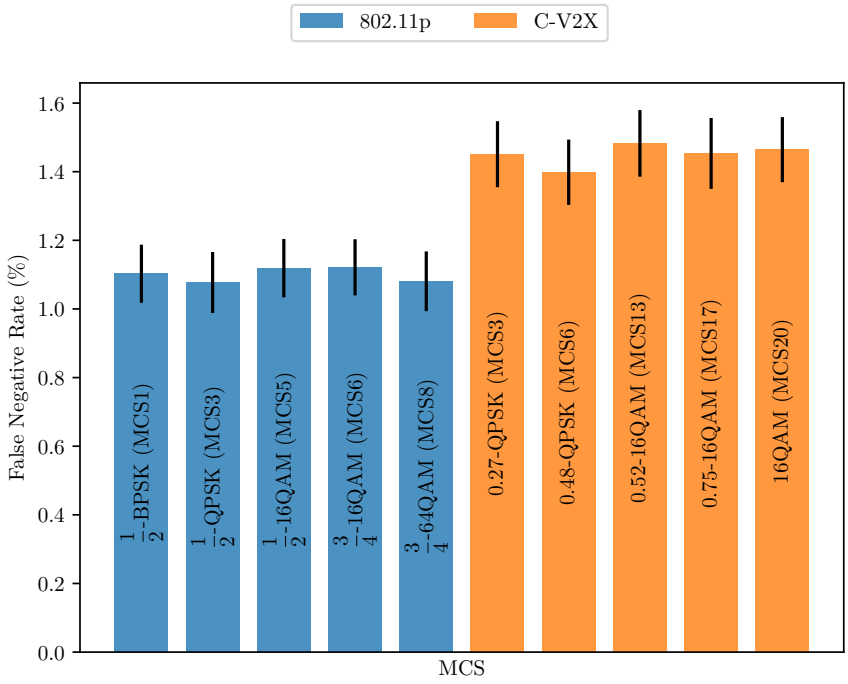

(b) False negative error rate.

Figure 7.7 The effect of MCS on the false positive error rate (a) and false negative error rate (b) for the 20 s AIP. The error bars show the 95% confidence intervals.

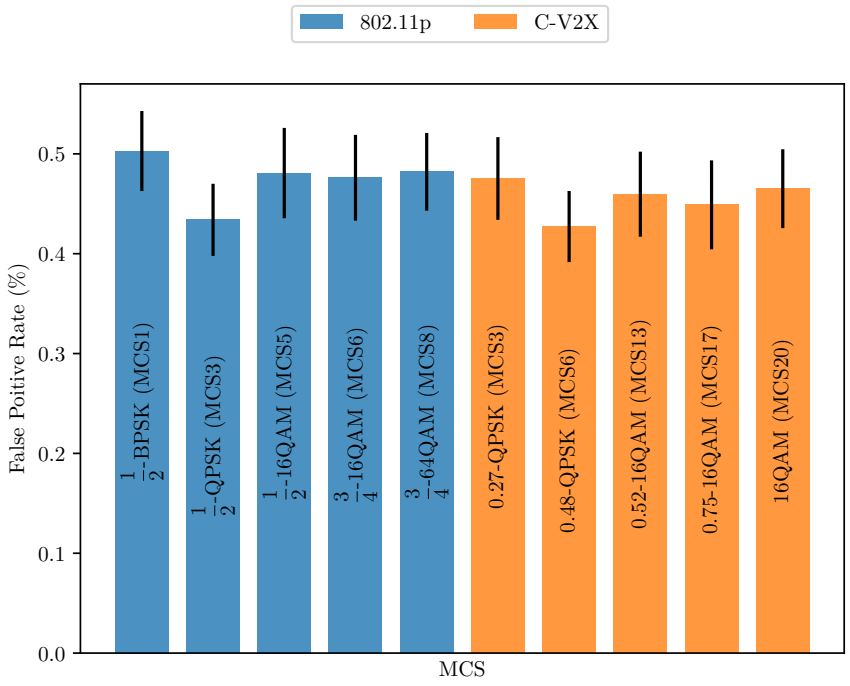

(a) False positive error rate.

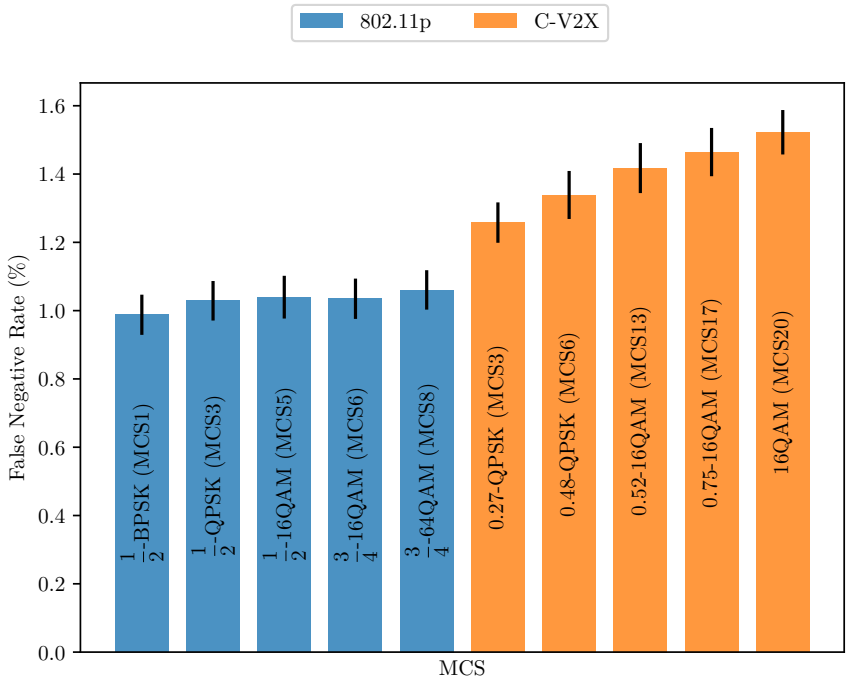

(b) False negative error rate.

Figure 7.8 The effect of MCS on the false positive error rate (a) and false negative error rate (b) for the 10 s AIP. The error bars show the 95% confidence intervals.

7.6 EFFECT OF TRANSMIT POWER

To discuss the effect of transmit power on the collision warning application error rate under C-V2X and 802.11p, the transmit power of all forklifts in the evaluation scenario will be varied. Based on the results in Section 7.3 and Section 7.5, only a single AIP is simulated as transmit power is expected to have the lowest impact on the performance of the algorithm. The 10 s AIP has selected as it is the largest AIP where differences in MCS become apparent. The parameter set used for these simulations is shown in Table 7.8. The results of these simulations are in Figures 7.9 and 7.10.

Figure 7.9 indicates there is no statistically significant effect of transmit power on the false positive rate for 802.11p. For the 0 dBm transmit power, the false positive error rate of C-V2X MCS20 is statistically significantly lower than the false positive error rates for the baseline, 802.11p, and the remaining transmit power values for C-V2X. However, this difference is small. These results agree with the factor impact analysis results presented in Table 7.4 (Section 7.3).

Unlike for the false positive error rate, Figure 7.10a shows that transmit power appears to have a massive effect on the false negative rate at the lowest transmit power for C-V2X (0 dBm). Figure 7.10b shows that for transmit powers above 0 dBm, there is no statistically significant difference or visible trend in the false negative rate as the transmit power increases, for either technology. The sharp increase in failure rate at 0 dBm is likely caused by an increase in data collisions. As part of the C-V2X resource allocation, the energy of a resource is compared to a threshold to determine whether it is likely to be unused (Section 2.4.1.1). For the 0 dBm transmit power, the threshold may not be low enough to detect the weak transmissions, meaning resources are more likely to be reserved multiple times, leading to increased collisions. The increased collision rate also explains the decrease in the false positive error rate for the 0 dBm transmit power in Figure 7.9: as collisions become more frequent, there are more successive collisions. More frequent successive collisions increase the likelihood that forklift information becomes stale and is forgotten, leading to fewer false positive errors which cannot be caused by missing forklift information, only by out of date information. The minimum transmit power behaviour was confirmed to exist by simulating the 3 dBm transmit power which produced a false negative error rate of $1.38 \pm 0.13\%$ for MCS3 and $1.60 \pm 0.14\%$ for MCS20, where the uncertainty on each value is the 95% confidence interval for 40 replications. Since these values are similar to the false negative rates for the 10–30 dBm cases, this indicates that this change is not gradual and there is some minimum transmit power threshold. However, future work could explore this more and confirm the resource allocation algorithm as the cause.

Table 7.8 The simulation parameters used to explore the effect of transmit power on the collision prediction algorithm error rate for the 10 s AIP.

Parameter	Value	
	802.11p	C-V2X
Run time (h)	2	
Transmit power (dBm)	0, 10, 15, 20, 30	
Thermal noise	-174 dB Hz^{-1}	
Noise figure	6 dB	
Receiver sensitivity	-100 dB	
Frequency	5.89 GHz	
Channel model	Warehouse channel (Chapter 6)	
Vehicle model	Model forklift (Section 4.2)	
MCS	$\frac{1}{2}$-BPSK (MCS1) $\frac{3}{4}$-64QAM (MCS8)	0.27-QPSK (MCS3) 16-QAM (MCS20)
Bandwidth	10 MHz	10.08 MHz
Number of resource blocks	—	56
Number of sub-channels	—	1
Resource reselection probability	—	0.2
Channel busy threshold	—	-92 dB
BLER data set	—	NIST [148]

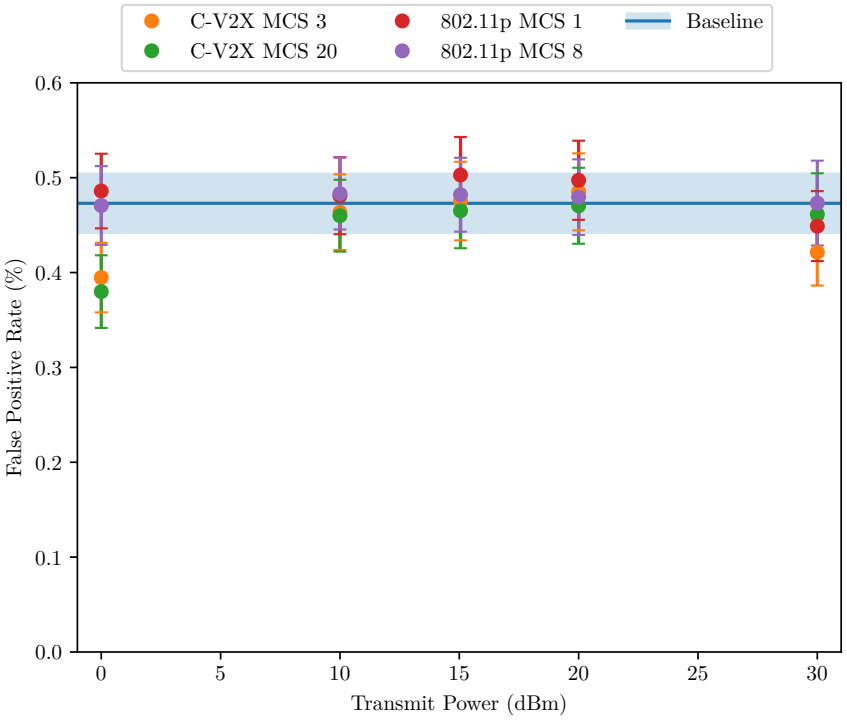

Figure 7.9 The false positive failure rate of the collision prediction algorithm as a function of transmit power. The error bars and the shaded blue band around the baseline error rate show the 95% confidence intervals.

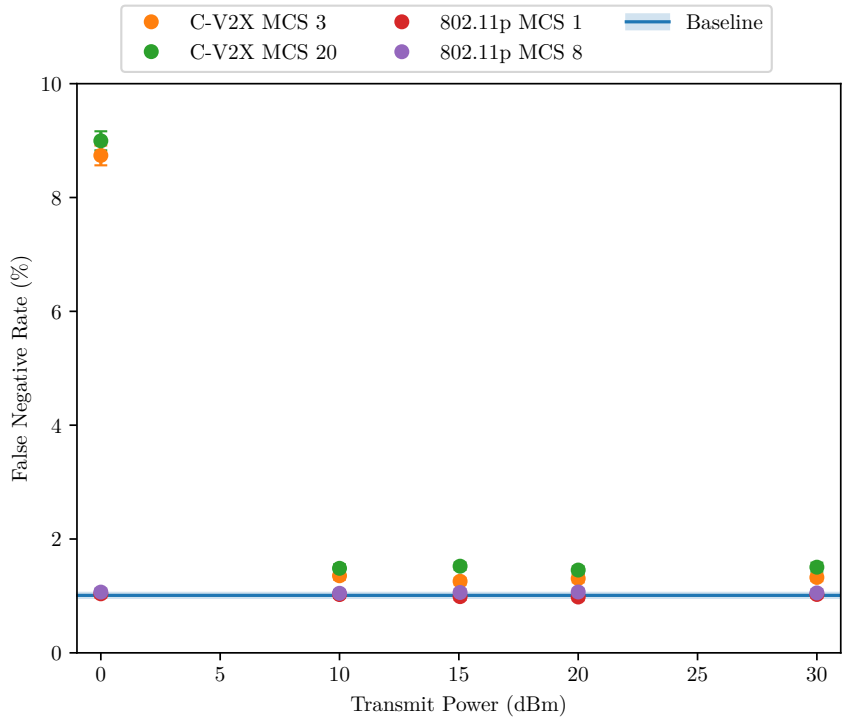

(a)

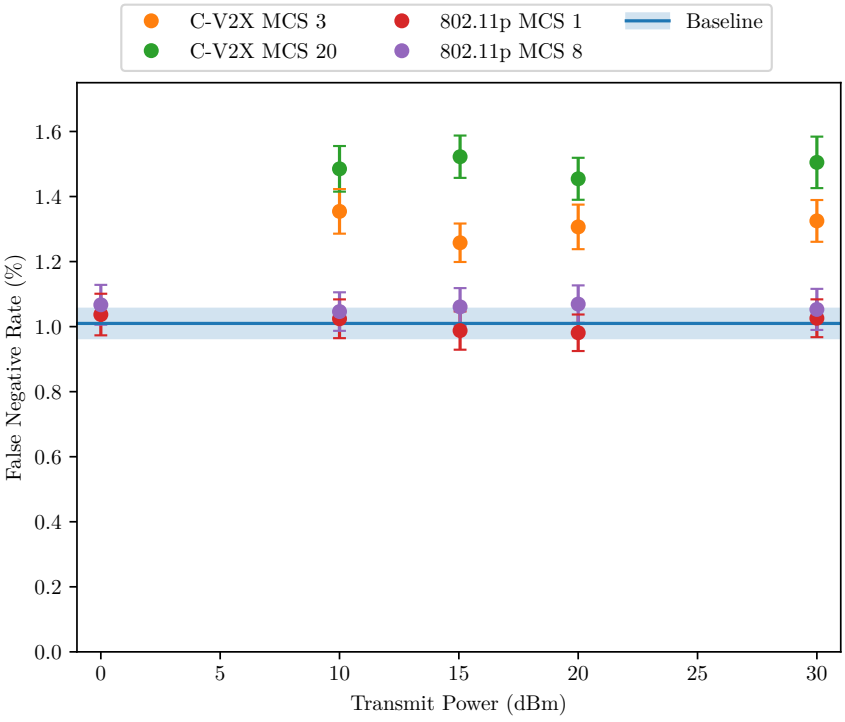

(b)

Figure 7.10 The false negative failure rate of the collision prediction algorithm as a function of transmit power. (b) is a plot of the same data as in (a), however the false negative rate axis is restricted to a maximum value of 1.75%. The error bars and the shaded blue band around the baseline error rate show the 95% confidence intervals.

7.7 DISCUSSION

Based on the results in Sections 7.3 and 7.4, the forklift AIP (density) has the largest impact on the error rate of a collision warning application under both technologies. For all the AIP simulated, 802.11p performs better than C-V2X. The conclusion that C-V2X is worse than 802.11p at higher densities (lower AIP) is well supported by the literature (Section 3.1). The difference in performance is likely to be primarily caused by the difference in MAC algorithms between technologies: 802.11p checks the channel is clear before transmitting, where C-V2X immediately transmits when its independent resource reservation begins. This is as all communication which affects the performance of the collision warning application occurs when the vehicles are close to the intersection, communicating over short distances. Thus, the primary driver of application errors above the baseline is likely to be packet collisions, as both technologies can reliably support short distance communication, even when in zone 3 of the warehouse channel model and using receivers with artificially high noise figures (Section 6.3.1). These packet collisions are primarily caused by each technologies channel access procedures. Throughout this simulation campaign a single sub-channel was used for C-V2X. Future studies should also consider the effect of multiple sub-channels which may alleviate some of the issues C-V2X experiences by allowing multiple transmissions to occur in parallel.

In Section 7.4 it was found that the AIP had no statistically significant effect on the false positive error rate across technologies ($p < 0.05$). This is expected, as the only way to create false positive error events is through out-of-date information from vehicles on the border of the forklift safe following distance. Thus, this type of failure is less likely to occur than false negative errors, meaning more trials are required to determine statistically significant differences between technologies. It is possible that more replications will reveal differences between the technologies.

For all densities explored in Section 7.4, the choice of MCS does not appear to matter when using 802.11p. This is as the two extremes of the MCS choice do not show any statistically significant difference ($p < 0.05$) for false negative error rates. This conclusion is supported by the exploration of MCS choice in Section 7.5, where there appears to be no statistically significant difference in the choice of MCS. However, this is not the case for C-V2X, where the performance of each MCS diverges at higher densities. For low AIP values, C-V2X's higher MCS (16-QAM) performed statistically significantly worse than its lower MCS (0.27-QPSK). This is also supported by Section 7.5, which shows that as MCS index increases, the false negative error rate increases as well. This change in performance as MCS index increases is likely due to interference from forklifts on the fringe of the simulation transmitting at the same time as others closer to the centre. These transmissions only result in interference, rather than making data completely irretrievable due to the relative separation between the transmitters and

receivers weakening the interfering signal. Higher index MCS are less noise-tolerant and thus will be more susceptible to dropping beacons with higher interference.

The results in Section 7.6 indicate that transmit power does not have a significant effect on the performance of the technologies once it is above a set level. Overall this fact is unsurprising as the critical distances in this scenario are significantly smaller than 50 m. At such short distances in such a weakly attenuating channel, even weak transmit powers can enable communication between devices (c.f. Figures 6.11 and 6.12). Additionally, all the simulations completed in this section have been free of shadowing and fading, so path loss is the only cause of signal attenuation. This is as the warehouse channel model, developed in Chapter 6, does not quantify these properties.

However, transmit power having little effect on the performance of the technology is contrary to the pilot study factor analysis in Section 7.3. The 2^k-factorial analysis indicated that for C-V2X the transmit power was the primary source of variation in the false negative error rate, explaining 60% of the variation in pilot study outcomes. This was anomalous to the remainder of the results for both false positive and false negative error rates of 802.11p and the false positive error rate of C-V2X, which indicated density was the primary explanation of the variance in the pilot study. The difference in impact is likely due to the selection of minimum transmit power value and the thresholding behaviour of the C-V2X resource allocation protocol when determining which resource blocks are likely to be already reserved (Section 7.6). This hypothesis could be tested by gradually reducing the channel busy threshold for the 0 dBm case and observing the collision algorithm error rate.

Research question Q2 (Section 1.1) focuses on the affect of AIP on the error rate of a collision warning system when using 802.11p and C-V2X. For 802.11p, at all the densities explored in this chapter, the false-negative error rate of the collision warning system is not significantly different from the established baseline error rate. At all densities, C-V2X performs statistically significantly worse than 802.11p and the baseline error rate. As the AIP decreases for C-V2X, the overall false negative error rate increases relative to the baseline false negative error rate. There is no corresponding statistically significant increase in the false positive error rate.

Research question Q3 addresses the effect of MCS and transmit power on the error rate of a collision avoidance application under each technology, as the AIP decreases. Based on the results in Sections 7.3, 7.5, and 7.6, the MCS and transmit power have very little influence on the performance of the algorithm when using either C-V2X or 802.11p. For the case of C-V2X, at higher densities, the more noise-tolerant MCS options perform better as they are more resistant to packet collisions from far away interferers. C-V2X also appears to have a minimum critical transmit power, above which the transmit power has little effect on the false negative rate. Below this critical transmit power, the performance of the algorithm is much worse.

Chapter 8

THE FUTURE OF V2X TECHNOLOGIES

This chapter discusses the future of V2X technologies. This discussion comes in two parts: the first answers research question Q4 (Section 1.1) by discussing what effect the next generation of V2X technologies (NR-V2X and 802.11bd) may have on the results presented in Chapter 7. The second is the final part of describing the differences between the two technologies (research question Q1), by discussing the current regulatory support for both technologies in different regions.

8.1 NEXT GENERATION V2X TECHNOLOGIES

This section discusses the possible impact the two next-generation V2X technologies may have on the results presented in Chapter 7. This is to answer research question Q4 which is interested in how the next generation V2X technologies might mitigate flaws in the current generation. Each technology will be treated separately below.

8.1.1 New Radio-V2X (NR-V2X)

The main flaw exposed in C-V2X by the results in Chapter 7 is likely caused by its scheduling algorithm causing increased packet collisions. However, there are no changes to NR-V2X which will mitigate this flaw, as it primarily uses the same scheduling algorithm. One change to NR-V2X which may help is the ability to schedule shorter transmissions (Section 2.4.2). This means it may be possible, for short messages, to reduce the increase in packet collisions as density increases through increasing the number of slots available for messages. This also may reduce the latency of messages, possibly to the benefit of any safety application using NR-V2X.

Another approach to reduce the overall application error rate may be to use the groupcast mechanism introduced by NR-V2X. This means that receiving vehicles can provide feedback. There are two possible configurations for the groupcast mode [50]: feedback based on distance to the transmitting forklift (option 1), or feedback from all forklifts (option 2). This would enable each vehicle to guarantee that vehicles in range have successfully received the information. However, how well the feedback mechanisms

would scale with density in the warehouse environment is unknown. To reduce overall data on the channel, the option 1 feedback mechanism should be used, where vehicles in range only send not-acknowledged messages if they could not correctly decode the data. For more information on both option 1 and option 2 feedback mechanisms, the reader is directed to [50].

8.1.2 IEEE 802.11bd

Similar to NR-V2X, there are very few changes to 802.11bd which are expected to have any significant effect on the performance of the collision warning application. This is as the majority of changes to 802.11bd are to the PHY, rather than the MAC. The main advantage for 802.11bd over 802.11p in the scenarios explored in Chapter 7 may be adaptive repetition. Adaptive repetition allows 802.11bd to transmit multiple copies of a packet depending on how busy the channel is (Section 2.4.4). This means that there are multiple chances for a message to be received correctly, even if one collides with another. However, this could also worsen the performance of 802.11bd compared to 802.11p when experiencing the hidden terminal problem. The hidden terminal problem is where a transmitter believes the channel is free, however in reality, there is another transmitter outside of radio range already transmitting. This can lead to collisions at receivers in range of both transmitters. When in this scenario, due to being out of range of other vehicles, an 802.11bd transmitter does not correctly calculate the channel-busy-ratio, which determines whether repetitions should be sent, it may send extra packets, increasing the likelihood of collisions. To determine the trade-off between the advantages of retransmissions versus the increased risk of packet collisions, further simulations or trials would need to be undertaken with a model of the 802.11bd adaptive repetition protocol.

8.2 REGULATORY SUPPORT AND SPECTRUM AVAILABILITY

For any V2X technology to be widely adopted in a region, some level of regulatory support is required. This is as all V2X technologies are wireless communication technologies and rely on access to particular segments of the radio spectrum to operate. One key requirement for mission-critical, wireless safety systems is often having dedicated, interferer-free spectrum, as interference decreases the maximum possible performance of the technology [180–182]. Interference causes performance degradation by: increasing the background noise, increasing the error or packet collision rate, or reducing opportunities to use the channel which can increase end-to-end delay or stop messages from being transmitted [182, 183]. Thus, the availability of dedicated, interferer-free spectrum, is a key factor in selecting a V2X technology. Additionally, since C-V2X and 802.11p radios cannot exchange information, a mixed deployment of technologies limits the maximum

gain possible from using V2X communications as there are two separate networks of vehicles unable to share possibly safety-critical information.

This section discusses the regulatory positions around spectrum availability for V2X technology around the world, influencing the selection of technologies in different regions. Specifically, the regulatory environment of three regions will be discussed in the following subsections: the United States of America, the European Union, and New Zealand. Finally, the impact of the different international positions on each technology and their use in the warehouse environment is discussed in Section 8.2.4.

8.2.1 United States of America (USA)

The USA was an early supporter of vehicular communication, allocating 75 MHz of spectrum (5.850–5.925 GHz) for Intelligent Transportation Systems (ITS) and V2X communication in October 1999 [184]. Additionally, the USA Department of Transportation was investigating ITS and helped define the Dedicated Short Range Communication (DSRC) set of protocols which use 802.11p (Section 2.4.3). The use of this 75 MHz band required technologies to comply with the American Society for Testing and Materials DSRC standard [185–187].[1]

In November 2020, the Federal Communication Commission (FCC), the federal regulatory body responsible for spectrum allocation, split the 75 MHz band in two: with the lower 45 MHz for unlicensed use and the upper 30 MHz for ITS [185]. The lower 45 MHz of unlicensed spectrum is intended to allow more wideband WiFi channels (i.e., 160 MHz channels for the IEEE 802.11ax and IEEE 802.11ac standards [189]), as part of the FCC's recognition of need for more WiFi spectrum. For the upper 30 MHz ITS band, the use of the entire band is dedicated to C-V2X. This cements C-V2X as the *de jure* V2X standard in the USA. 802.11p and 802.11bd may still operate in the now unlicensed 45 MHz band, however they will be subject to potential interference. At the time of writing, the additional 45 MHz of unlicensed band is only available for indoor use. After a one year transition period, ending in November 2021, outdoor use of this spectrum will be allowed [185].

8.2.2 European Union (EU)

Unlike the USA, which has selected a single technology to use within the ITS band, the EU has adopted a technology-neutral approach. In 2008, the EU allocated 5.875–5.905 GHz for ITS [190] and the use of the spectrum is based upon the application's purpose [185, 191]. However, some commenters ([192, 193]) have noted that the EU seems to favour C-V2X over 802.11p, which forms the basis of ITS-G5, an EU-based standard for V2X communication [91]. This is based on the European

[1] This was first standardised in 2002, before 802.11p was standardised in 2010, and references IEEE 802.11a as its base [188]. The current versions of the standard uses 802.11p [187].

Council rejecting the EU Commission's proposal to mandate ITS-G5 for any ITS deployment [194].

8.2.3 New Zealand (NZ)

In NZ, spectrum allocation is managed by Radio Spectrum Management (RSM) part of the Ministry of Business, Innovation, and Employment. RSM has reserved the 5.875–5.925 GHz band for possible allocation to ITS applications [195]. However, RSM is not currently actively working towards any specific goal for internal development of an ITS policy and is waiting on international standardisation and adoption efforts [196].

8.2.4 Discussion

The FCC has selected C-V2X as the V2X technology for use in the USA. This may be a mistake for the warehouse environment and scenario analysed in this research, as based on the conclusions of Chapter 7, C-V2X performs worse than 802.11p. This is as the main advantage of C-V2X is the better PHY performance. Based on the measurement performed in Chapter 6, where it was found that 802.11p, even at very low transmit powers, was able to successfully communicate down the length of the aisle, the improved PHY does not appear necessary for V2V warehouse communications. If anything, in a warehouse environment, the better PHY performance may be a drawback for C-V2X as it performs worse than 802.11p at higher densities (Section 7.4). With better PHY performance, the technology's communication range is longer and thus more forklifts are in range of each other, increasing the effective density.

Unlike the USA, which has possibly backed the wrong technology, neither the EU nor NZ have selected a V2X technology. However, this state of indecision cannot continue; advocates for both C-V2X and 802.11p agree that regardless of which standard is chosen, they cannot coexist [192]. This is backed up by the academic literature which finds that, without specific coexistence schemes, the performance of the technologies is degraded when they share spectrum [143,180–183,197]. This degradation in performance is compounded by the inability of C-V2X and 802.11p to exchange information, reducing the maximum possible gain in a mixed technology deployment.

The worst case scenario for 802.11p and 802.11bd is that the EU decides to standardise on C-V2X. This means two of the current largest markets for ITS will not support it, and as such will likely lead to the technology dying out. If this is the case, in light of the results presented in Chapter 7, a technologically worse option for warehouses will have to be accepted. It also means any devices deployed with 802.11p (such as those discussed in Section 3.2) will legally have to disable their functionality, operate in unlicensed spectrum and be potentially subject to interference, or be replaced with C-V2X devices. There is no technical solution to this problem as this is purely a function of the regulatory environment.

Chapter 9

CONCLUSIONS

This thesis investigated the use of V2X technologies in the warehouse environment. Specifically, it set out to find whether, when applied to aisle-end collision prevention, there were any differences between two key V2X technologies and if so, which is better. As part of this the following research questions were defined:

Q1 What are the key differences between the V2X technologies?

Q2 For two streams of forklifts arriving at the end of an aisle, what is the effect of average spacing between forklifts on the technologies' error rate of a collision warning application?

Q3 What is the effect of transmit power and modulation scheme on the error rate of a collision warning application?

Q4 What improvements do the evolved forms of the V2X standards offer that potentially mitigate any flaws in the current generation?

Firstly, Q1 was primarily investigated in Section 2.4 which introduced the V2X technologies currently available. Q1 was also explored in Section 3.1 which discussed some comparisons between the two main technologies (C-V2X and 802.11p) from the academic literature. Section 3.1 found that the main difference between the two technologies' performance was in the range and density each technology could support, with C-V2X having a longer range but poorer performance at high vehicle densities when compared to 802.11p. Research question Q1 was briefly also dealt with in Chapter 8 when discussing the current regulatory support for each technology. Currently, the USA supports C-V2X as the only possible V2X technology for the 5.9 GHz Intelligent Transportation System (ITS) band, the EU has adopted a technology neutral approach, and NZ is waiting on international standardisation efforts.

To address questions Q2 and Q3, an evaluation scenario and application was developed in Chapter 4 and implemented in a simulator discussed in Chapter 5. To support the simulator and more accurately represent the warehouse environment, a custom warehouse aisle-end channel model was designed and parameterised in Chapter 6.

A simulation campaign was then conducted using the evaluation scenario, simulator, and warehouse channel model to answer Q2 and Q3 by comparing the failure rate of the collision warning application (Chapter 7). The simulation campaign found that density, as measured by the Average Introduction Period (AIP) of forklifts, is the major factor which impacts both V2X technologies. For both technologies there was no increase from the baseline false positive error rate as the AIP was reduced (vehicle density increased). For 802.11p, the false negative error rate did not increase from baseline as the AIP was decreased. However, for C-V2X as the AIP was decreased, the false negative rate for MCS20 increased relative to the baseline. Comparatively, the choice of modulation scheme and transmit power had little effect on the failure rate of the collision warning application. For C-V2X, the false negative error rate is lower at high densities when a more noise tolerant MCS is used. Additionally, C-V2X appears to need a minimum transmit power for the channel to be considered busy when performing the resource allocation. Below this transmit power scheduling collisions are frequent and the false negative error rate is extremely high.

The final research question, Q4, was answered in Chapter 8. Based on the results of the simulation campaign, the next generation of V2X technologies will likely not mitigate the flaws of the current generation. This is as NR-V2X does not address the fundamental issues with C-V2X's resource allocation algorithm which led to worse performance at high densities when compared to 802.11p. Similarly, 802.11bd does not alter its channel access algorithm for backwards compatibility with 802.11p and instead focuses on improving the physical layer performance of 802.11p. These physical layer improvements are likely irrelevant to the warehouse environment as, based on the results in Chapter 7 for 802.11p, there appears to be no statistically significant relationship between the choice of MCS and transmit power (physical layer issues) and the collision warning application performance.

Based on the answers for research questions Q1–Q4, the overarching research question can finally be addressed. The first part: is there a difference between the two technologies, has a clear answer: yes. There are differences between the two technologies' performance. The second half, which asks which technology is better, does not have a definitive answer. In terms of technological performance in the scenario investigated, 802.11p has a statistically significant lower false negative error rate compared to C-V2X, making it better for this application. However, when considering the regulatory environment discussed in Section 8.2, C-V2X is better suited for use in the USA as it can legally operate in the 5.9 GHz ITS band, away from potential interference.

9.1 FUTURE WORK

To further explore the use of V2X technologies in the warehouse environment, the following future research directions are suggested:

- **Validation of the C-V2X simulator using real-world hardware.** In Chapter 5, the C-V2X simulator was verified against the theoretical model in [156] to ensure it represented the model correctly. Neither the C-V2X simulator used here, nor the theoretical model in [156] have been validated against real-world implementations of C-V2X. To ensure that the models represent an approximation of reality, at least basic testing with real C-V2X hardware should be performed and the simulation model compared against this data.

- **Consider the effect of multiple sub-channels on C-V2X.** Throughout the simulation campaign in Chapter 7, a single sub-channel was used. Future research should consider the effect using multiple sub-channels has on the performance of C-V2X, where multiple transmissions can occur in parallel without colliding.

- **Investigate the minimum transmit power behaviour exhibited by C-V2X.** In Chapter 7, it was found that C-V2X had a critical transmit power, below which the collision warning application performed much worse. This was hypothesised to be the result of the received power frequently being below the threshold for the C-V2X resource allocation algorithm to detect the channel as busy, leading to frequent packet collisions. This hypothesis should be tested by gradually decreasing the channel-busy threshold and observing the effect on the collision warning application error rate.

- **Develop a more general and representative warehouse channel model.** In Chapter 6, a simple, application specific warehouse aisle-end channel model was developed. Further research should continue to characterise the warehouse channel environment at V2X frequencies, expanding the focus of the model to the whole warehouse and includes inter-aisle signal propagation. This could take the form of a series of path loss curves for different warehouse elements (e.g. single racking, empty bay, free space) which can then be used to form a piecewise propagation loss based on the distance the signal propagates through each environmental element. This approach is explored for traditional roads in [177], and can be easily expanded to the warehouse environment through further warehouse measurements.

- **Introduce jitter into the beacon period of the collision warning application.** The application described in Chapter 4 has perfect clocks, and thus generates messages exactly every beacon period (after the initial random offset). It would be interesting to see the effect of jitter in the beacon period on the performance of the technologies. This is as real-world radios typically cannot guarantee the exact period between beacons will be met. Including jitter may increase the false negative rate for C-V2X as the messages may appear aperiodic, causing frequent resource reservations, leading to more collisions.

- **Evaluate performance of 802.11bd and NR-V2X in the scenario.** Section 8.1 discussed the next generation of V2X technologies in a qualitative way. Quantitatively evaluating the next generation will allow the predictions in Section 8.1 to be verified. This would require development of appropriate simulators for NR-V2X and 802.11bd.

Appendix A

PACKET ERROR RATE IS THE COMPLEMENT OF PACKET RECEPTION RATE

Theorem 1. *Packet error rate (PER) is the complement of Packet Reception Rate (PRR). That is PER* $= 1 - PRR$.

Proof. PER is defined as,

$$\text{PER} = \frac{T_e}{T}, \tag{A.1}$$

where T_e is the number of packets received that have one or more errors in it, and T is the total number of packets. PRR is defined as,

$$\text{PRR} = \frac{T_c}{T}, \tag{A.2}$$

where T_c is the number of packets received with no errors.

Given that a packet is received correctly or received with errors, the total number of packets received can be stated as,

$$T = T_c + T_e, \tag{A.3}$$

thus,

$$T_e = T - T_c, \tag{A.4}$$

Substituting Equation A.4 into the definition of PER, we get:

$$\begin{aligned} \text{PER} &= \frac{T_e}{T} \\ &= \frac{T - T_c}{T} \\ &= 1 - \frac{T_c}{T} \\ &= 1 - \text{PRR}. \end{aligned}$$

□

Appendix B

POSIBILITY OF SAFE FOLLOWING DISTANCE VIOLATIONS

This appendix proves that violations of safe following distances after the simulation ground truth check (which occurs the instant the computing vehicle enters the intersection) are only possible when the violating vehicle is behind the turning vehicle. Note, this only holds for the scenario constructed in Chapter 4. Specifically, this proof concerns safety distance violations where two vehicles enter the unsafe range of each other whilst turning, but when the ground truth check was performed they obeyed the safe following distance rules. From this definition it follows that, safe following distance errors after the ground truth check are only possible when the two vehicles can move closer together than the instant the ground truth check was performed.

In the scenario in question, all vehicles travel with a constant speed and only one vehicle has a changing velocity, the turning vehicle. Thus, the only opportunity for safe following distance violations after the ground truth check is when the vehicle is turning, as following distance can only change when velocity changes. There are two possible cases of safe following distance violations: violations with a vehicle in front of the turning vehicle, and violations with a vehicle behind the turning vehicle.

Case 1: Vehicle Behind the Turning Vehicle. The first case is where the vehicle is behind (on the left hand side of the intersection) of the turning vehicle (Figure B.1).

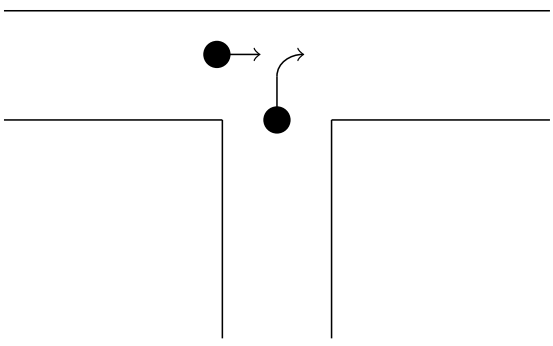

Figure B.1 Case 1, where the vehicle is behind the turning vehicle.

In this case, we only look at the lateral component, the one running along the top of the T-intersection, as defined in Figure 4.3. From the point of view of the turning vehicle, where approaching velocities are negative, the relative velocity ($v_{\text{rel}}(t)$) of the approaching vehicle is,

$$v_{\text{rel}}(t) = \int_0^t a(\tau)\, d\tau - v_{\max}, \quad t \in [0, \infty), \tag{B.1}$$

where $v_{\max}$ is the velocity of the vehicle B (Figure B.1), $a(\cdot)$ is the acceleration of the turning vehicle. Since the vehicle accelerates from zero to $v_{\max}$ over a finite period of time,

$$0 \leq \int_0^t a(\tau)\, d\tau \leq v_{\max}, \quad t \in [0, \infty), \tag{B.2}$$

then $v_{\text{rel}}(t)$ can be bounded as,

$$-v_{\max} \leq v_{\text{rel}}(t) \leq 0, \quad t \in [0, \infty). \tag{B.3}$$

Thus, since the relative velocity is always negative or zero, the distance between the two vehicles is always constant or decreasing, and safe following distance violations after the ground truth check are possible.

Case 2: Vehicle Ahead of the Turning Vehicle. The second possible case is where the vehicle is ahead of (to the right of the intersection) the turning vehicle (Figure B.2). Similarly to case 1, we only look at the lateral component running along the top of the intersection. The relative velocity between the two vehicles, from the point of view of the turning vehicle, where approaching velocities are negative, is,

$$v_{\text{rel}}(t) = v_{\max} - \int_0^t a(\tau)\, d\tau, \quad t \in [0, \infty), \tag{B.4}$$

where $v_{\max}$ is the velocity of vehicle A in Figure B.2. Since Equation (B.2) still holds, the relative velocity is bounded as,

$$0 \leq v_{\text{rel}}(t) \leq v_{\max}, \quad t \in [0, \infty). \tag{B.5}$$

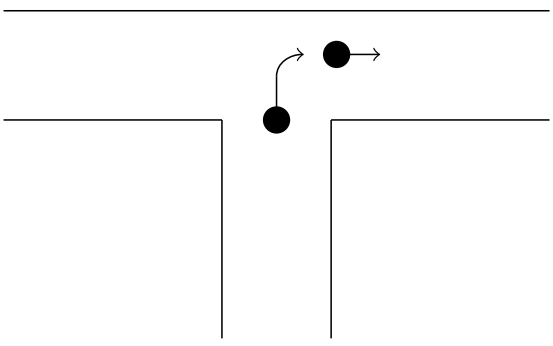

Figure B.2 Case 2, where the vehicle is ahead of the turning vehicle.

Therefore, the relative separation between the two vehicles is either constant or increasing, and safe following distance violations after the ground truth check are not possible.

Appendix C

C-V2X BLOCK ERROR RATE DATA SETS

The data sets presented here are not the complete data sets and only include the values needed for the analytical calculations performed through this thesis. Linear interpolation was used to generate Block Error Rate (BLER) values for intermediate signal-to-interference-and-noise-ratio (SINR) values.

C.1 HUAWEI DATA SET

Table C.1 include the BLER tables used in analytical calculations using the Huawei data set. These data sets were extracted from the simulator used in [156] and available online [157]. Note that these values are originally from a Huawei report on DMRS [149].

C.2 NIST DATA SET

Table C.2 includes the BLER tables used for analytical calculations involving the NIST data set. These data sets were produced as part of the NIST investigation into the block error rate performance of mode 1 and mode 2 device-to-device communication in LTE which was documented in [148]. These specific tables are from the NS-3 simulator developed alongside that project documented in [161] and released online [199].

Table C.1 The Huawei BLER data set extracted from [157] which is licensed under GNU GPLv3 [198]. Note this is only for the payload part of a C-V2X transmissions. The control information (SCI) uses MCS 0 which is not provided by the Huawei data set.

MCS 9	
SINR	BLER
<0	1
0	1
2	0.9
4	0.7
6	0.4
8	0.13
10	0.045
12	0.017
14	0.007
16	0.001
18	0.001
20	0.001
$20+10^{-6}$	0.0001
$>20+10^{-6}$	0.0001

Table C.2 The two BLER tables for analytical calculation using the NIST BLER data set. Extracted from [199] which is licensed under the GNU GPLv2 license [200].

MCS 0		MCS 9	
SINR	BLER	SINR	BLER
<-6.2	1	<0.6	1
-6.2	1	0.6	1
-6	0.9883	0.8	0.9992
-5.8	0.9784	1	0.9972
-5.6	0.9721	1.2	0.9832
-5.4	0.9631	1.4	0.9368
-5.2	0.9517	1.6	0.822
-5	0.9325	1.8	0.6452
-4.8	0.9133	2	0.416
-4.6	0.8783	2.2	0.2032
-4.4	0.849	2.4	0.0748
-4.2	0.8048	2.6	0.0204
-4	0.7565	2.8	0.0048
-3.8	0.6958	>2.8	0
-3.6	0.6325		
-3.4	0.5703		
-3.2	0.5049		
-3	0.4273		
-2.8	0.3733		
-2.6	0.2989		
-2.4	0.2437		
-2.2	0.1932		
-2	0.1467		
-1.8	0.1126		
-1.6	0.0785		
-1.4	0.0592		
-1.2	0.0423		
-1	0.0265		
-0.8	0.0186		
-0.6	0.011		
-0.4	0.0072		
-0.2	0.0031		
0	0.0026		
0.2	0.0011		
0.4	0.0008		
0.6	0.0003		
0.8	0.0002		
1	0.0001		
1.2	0		
>1.2	0		

Appendix D

WAREHOUSE MEASUREMENT SCHEMATICS

D.1 LOCATION 1 — TESTING WAREHOUSE

Location 1 is a testing warehouse for warehouse equipment based in South Auckland. It consists of a large open area, with a limited area of racking along one side. The roof of Location 1 is made of corrugated metal panels with periodic transparent corrugated plastic sections to allow natural light in. Figure D.1 is a replicated copy of the floor plan provided in Figure 6.6. The following sections detail the racking setup and position of transmitter and receiver for each measurement scenario.

At Location 1 only the bottom most level of the racking was filled. In all measurements the transmit and receive antennas were 1.0 m from the floor.

D.1.1 Scenario S1 — Clear Space

The zone highlighted in orange in Figure D.1 is the area in which the clear space measurement scenario was performed. Figure D.2 provides an abridged floor plan for the scenario. Figure D.3 shows the raw measurement results and path loss model fitting for the scenario.

D.1.2 Scenario S2 — Empty Racking

Figure D.4 shows the setup for Scenario S2. The raw measurements and path loss model fitting are provided in Figure D.5.

D.1.3 Scenario S3 — Highly Absorbent

To create a highly absorbent scenario the racking had water-filled Intermediate Bulk Containers (IBCs) placed on the racking. Each IBC was filled to approximately 1 tonne weight with tap water. This weight includes the IBC which weighs approximately 40 kg. The level of contaminants in the tap-water is unknown.

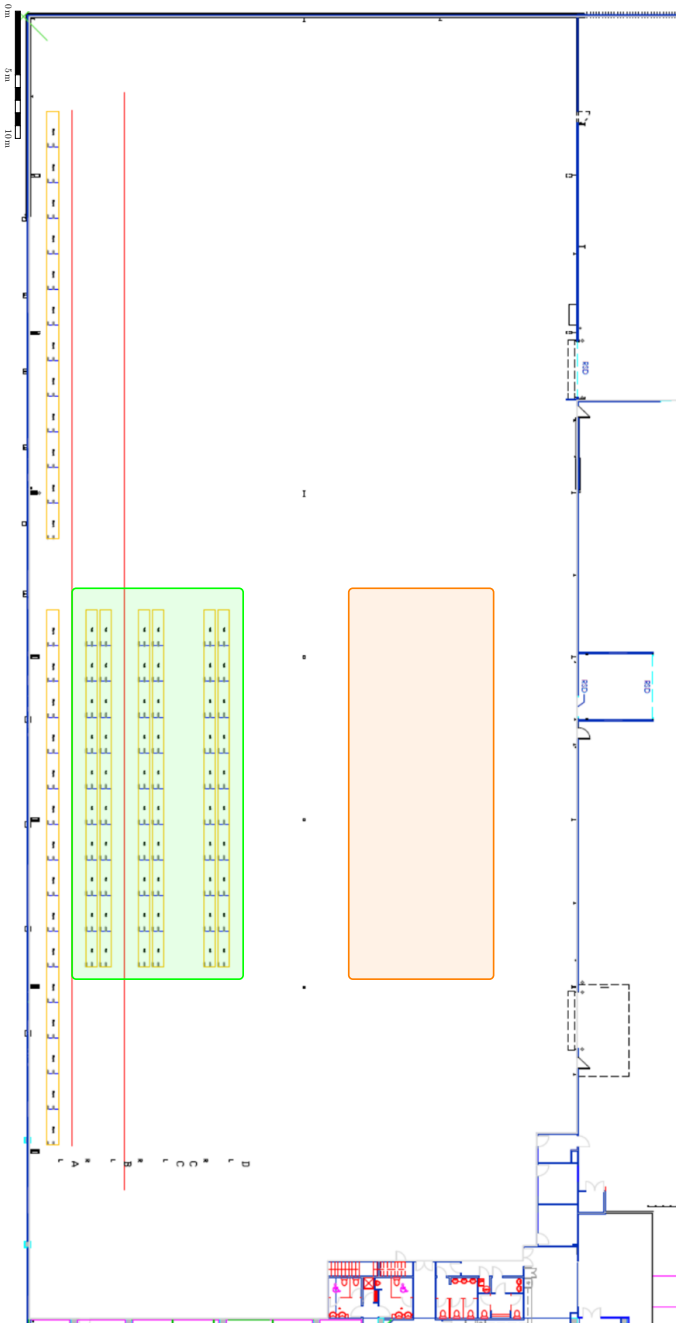

Figure D.1 The floor plan of Location 1 with the area for the clear space experiment (S1) highlighted in orange and the racked area (S2–S5) highlighted in green.

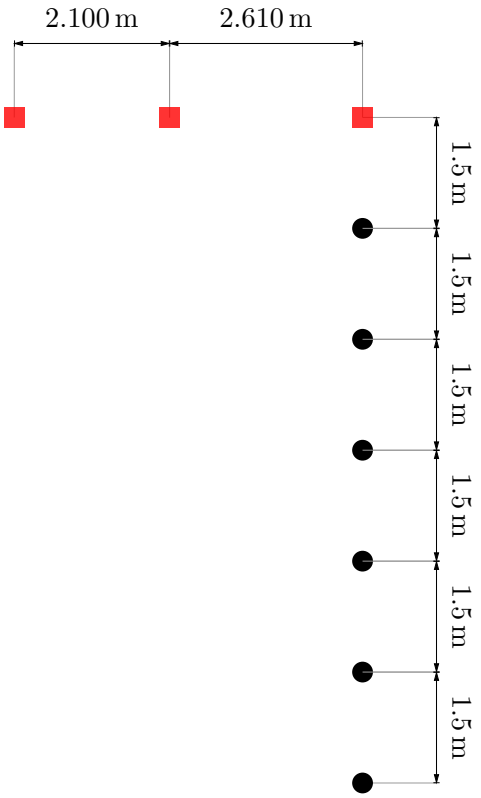

Figure D.2 The abridged measurement schematic for Scenario S1. Not shown is the remaining 12 measurements points, all spaced 1.5 m apart. For path loss measurements, the transmitter was placed on the red squares and the receiver on the black circles. For packet reception rate testing the opposite setup was used.

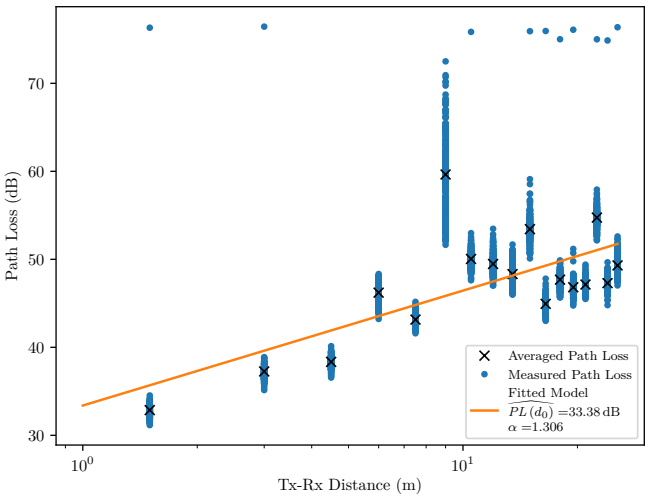

(a) Zone 1

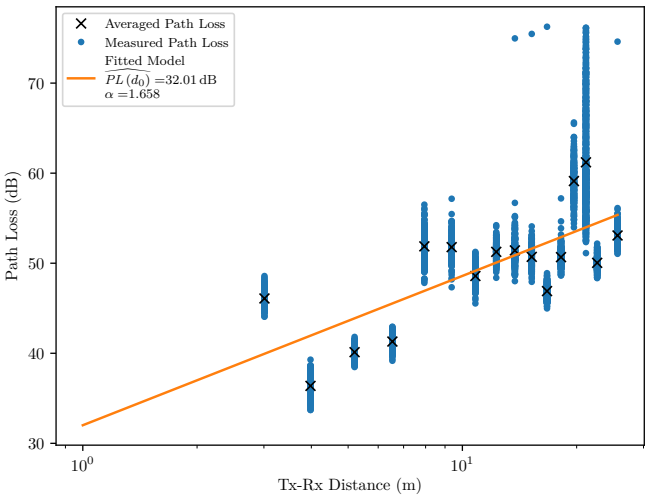

(b) Zone 2

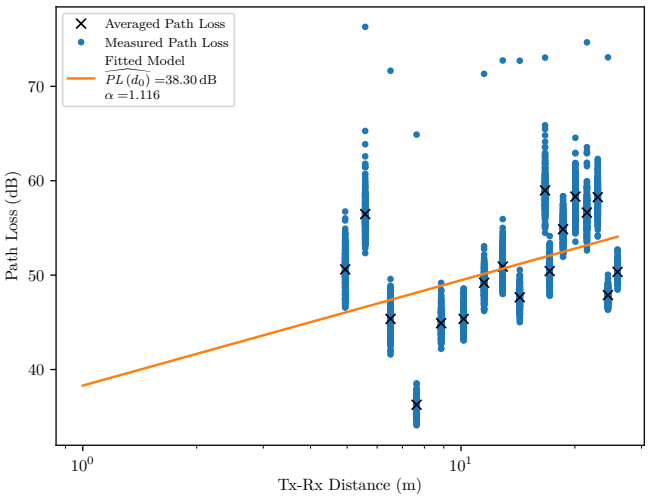

(c) Zone 3

Figure D.3 The raw measurement data and path loss model fit for Scenario S1.

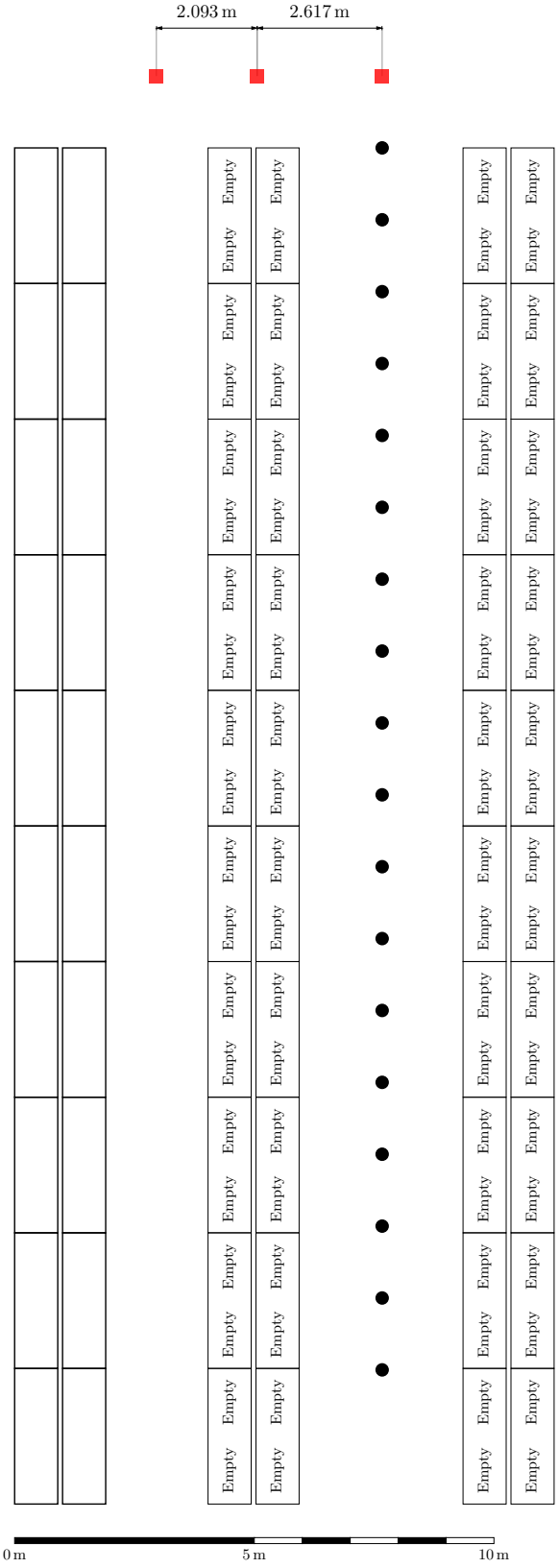

Figure D.4 The setup for Scenario S2. For path loss measurements, the transmitter was placed on the red squares and the receiver on the black circles. For packet reception rate testing the opposite setup was used. Bays without text indicate that the contents of the racking was not noted.

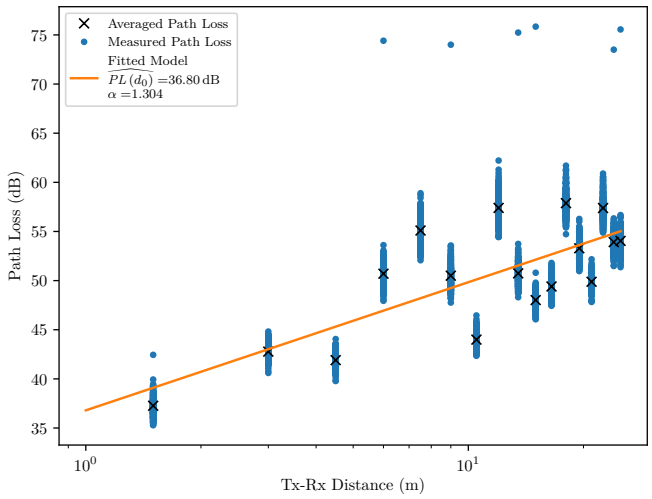

(a) Zone 1

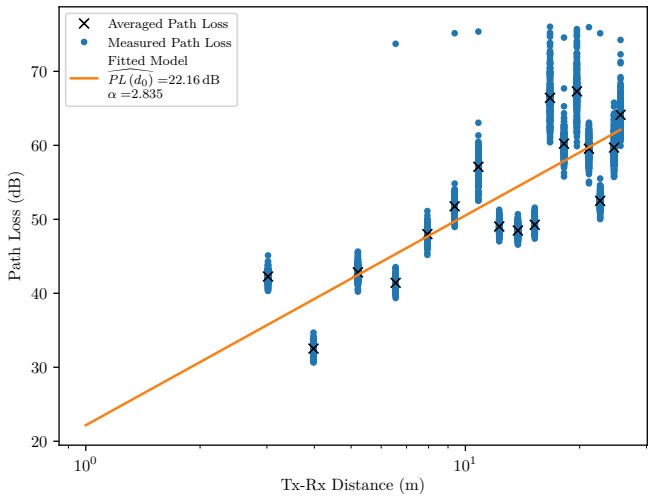

(b) Zone 2

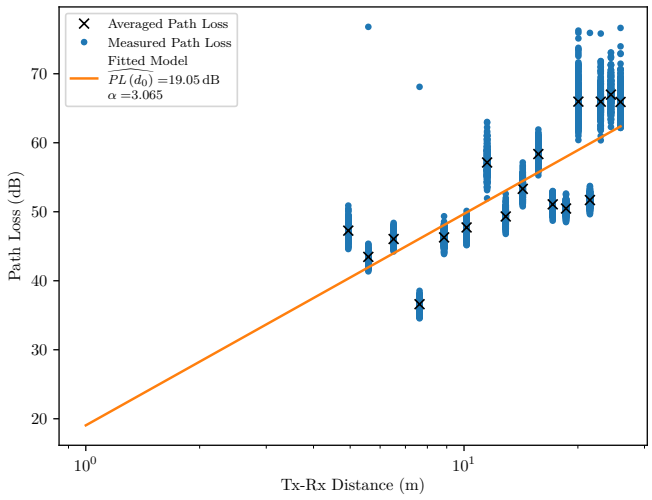

(c) Zone 3

Figure D.5 The raw measurement data and path loss model path loss model fit for Scenario S2.

There were a limited number of IBCs available so only half the racking was filled with IBCs. An overall schematic of where the IBCs were placed in the racking is shown in Figure D.6 with the location of the measurement points for Scenario S3. A picture of the IBCs setup in the racking is provided in Figure D.7. The raw measurements and path loss model fitting are included in Figure D.8.

D.1.4 Scenario S4 — Highly Reflective

To create a highly reflective scenario, the racks had 2 mm thick Aluminium Composite Material (ACM) sheets hung centred in the racks, as in Figure D.9. ACM consists of two thin sheets of aluminium with a polyethylene core sandwiched between them (Figure D.10). The ACM had custom-fabricated sheet metal hooks riveted to them to allow them to hang off the front of the racking.

Like the IBCs, there were a limited number of ACM sheets available so only half the bays were filled. The placement of the ACM is shown in Figure D.11. Figure D.12 shows a view looking down the aisle of the ACM sheets in the racking. It also shows the ACM end cap placed on the end of one of the aisle to make the aisle appear as it had a metal volume inside it, rather than just metal sheets. The raw measurements and path loss model fitting results are included in Figure D.13.

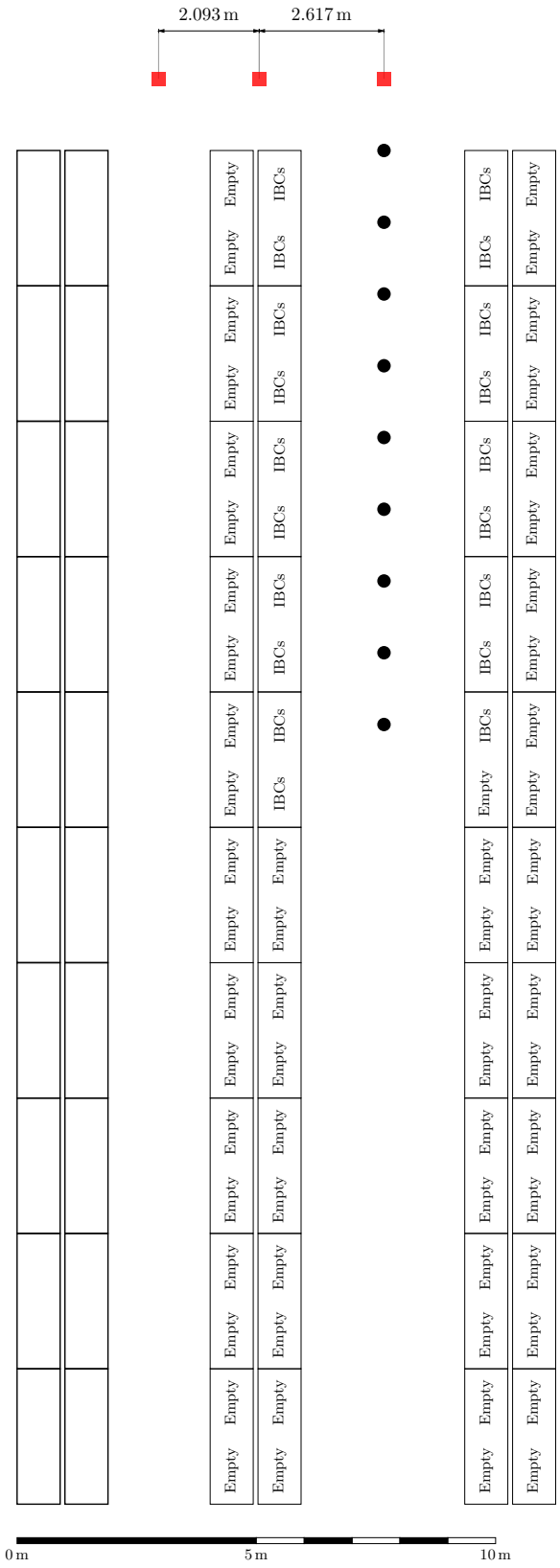

Figure D.6 The setup for Scenario S3. For path loss measurements, the transmitter was placed on the red squares and the receiver on the black circles. For packet reception rate testing the opposite setup was used. Bays without text indicate that the contents of the racking was not noted.

Figure D.7 The IBCs setup in the racking whilst zone 1 packet reception rate measurements were being taken for Scenario S3. All racking content is artificially staged.

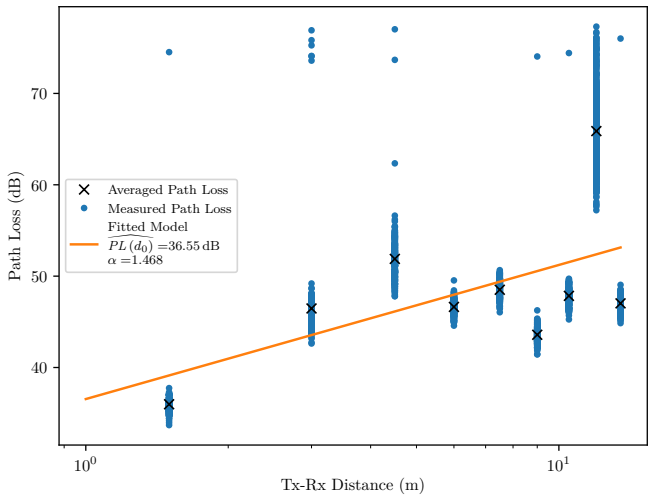

(a) Zone 1

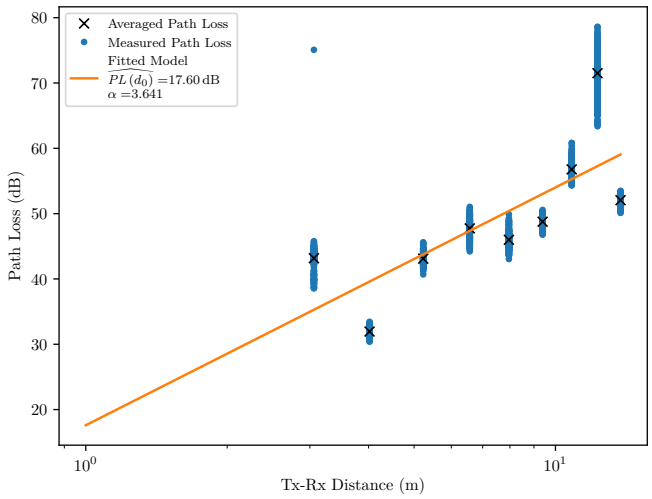

(b) Zone 2

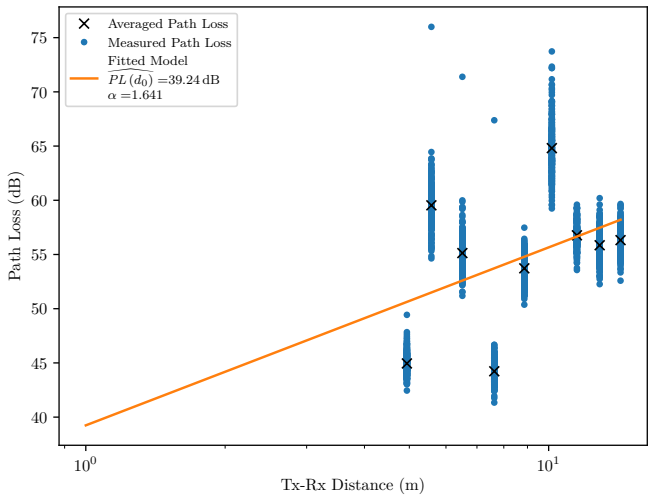

(c) Zone 3

Figure D.8 The raw measurement data and path loss model fit for Scenario S3.

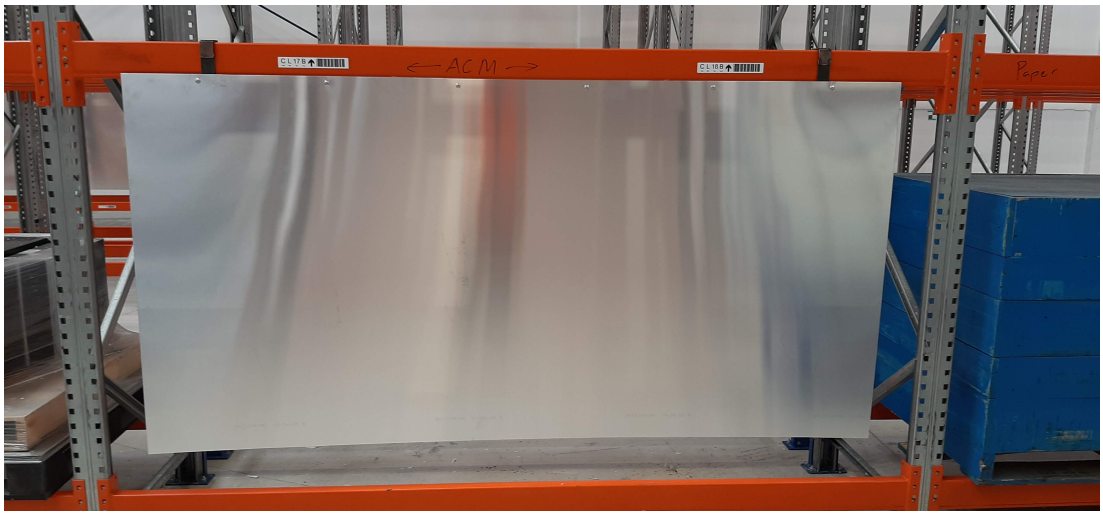

Figure D.9 An ACM panel hanging in a single bay. All racking content is artificially staged.

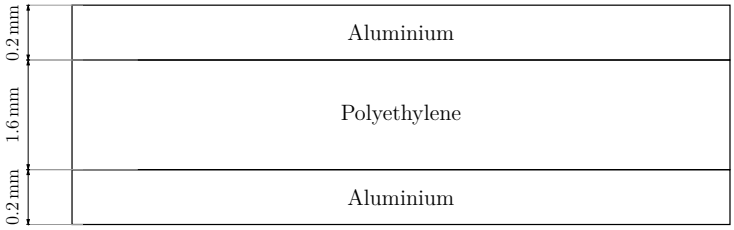

Figure D.10 The layers of an ACM panel.

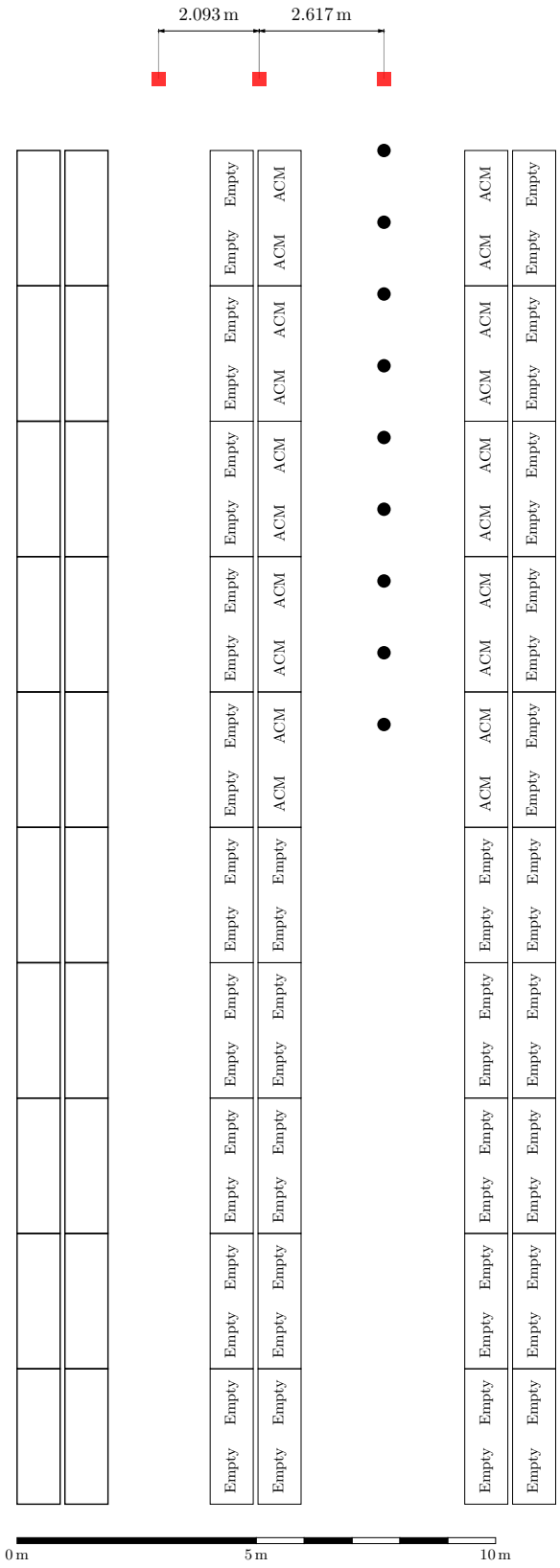

Figure D.11 The setup for Scenario S4. For path loss measurements, the transmitter was placed on the red squares and the receiver on the black circles. For packet reception rate testing the opposite setup was used. Bays without text indicate that the contents of the racking was not noted.

Figure D.12 The view looking down the aisle from behind the transmitter which is in the zone 3 measurement position (not visible). Note the ACM end cap on the right hand side of the aisle. The end cap is in place to make the racking appear more full when in zone 2, where the transmitter is placed in between the two aisles. All racking content is artificially staged.

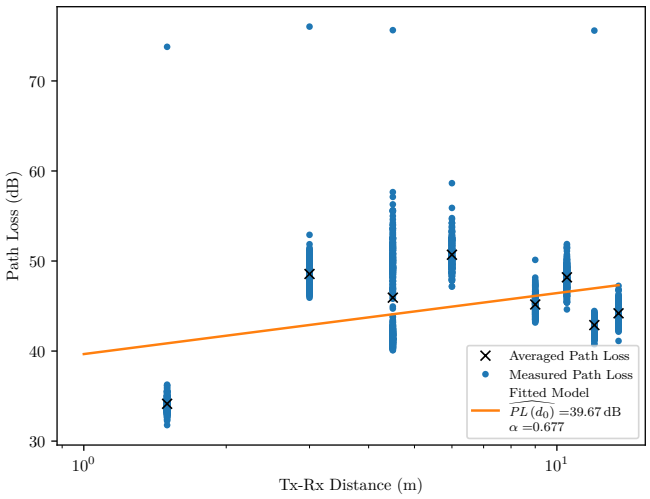

(a) Zone 1

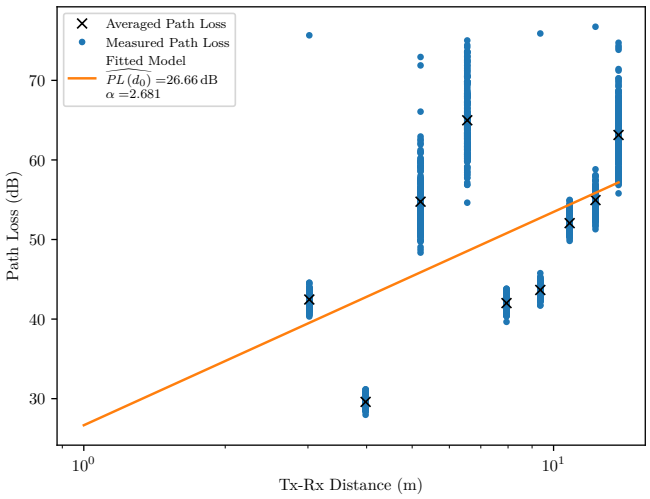

(b) Zone 2

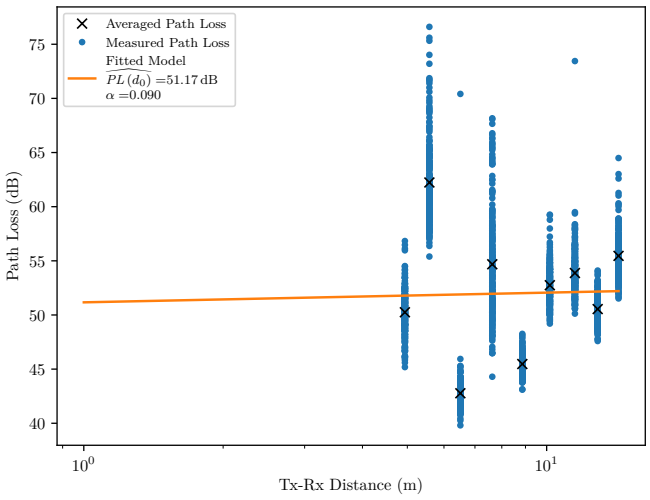

(c) Zone 3

Figure D.13 The raw measurement data and path loss model fit for Scenario S4.

D.1.5 Scenario S5 — Mixed

In this scenario the racks were filled with the following contents:

1. Water filled IBC — See Section D.1.3 for a description of the IBCs.
2. ACM — See Section D.1.4 for a description of ACM.
3. Paper — Wooden crates of densely packed paper in file boxes.
4. Powdered Soup — Pallets of dried cup-a-soup packets in cardboard outer boxes The outer boxes are wrapped in plastic to keep them on the wooden pallet.
5. Soap — Twin packs of soap bars in cardboard outer boxes. The outer boxes are wrapped in plastic to keep them on the wooden pallet.
6. Wooden crate parts — Disassembled wooden crate sides stacked on top of each other.
7. Stacked pallets — Multiple wooden pallets stacked on top of each other.
8. Tug hood — Metal hood for tug trucks on wooden pallet.
9. Mechanical parts — Boxed metal and plastic mechanical parts wrapped in bubble wrap. The parts are in cardboard outer boxes which are loose on a wooden pallet.
10. Computers — Desktop computer towers stacked on a wooden pallet and wrapped with plastic wrap
11. Iced Tea — Boxes of 500 mL plastic bottles containing iced tea, wrapped with plastic wrap to keep the boxes on the wooden pallet.
12. Béarnaise sauce — Boxes of 1 L packets of béarnaise sauce in cardboard outer boxes. The cardboard outer boxes are secured to the wooden pallet with plastic wrap.
13. Laundry liquid — Boxes of 1.4 L plastic bottles containing laundry liquid, wrapped with plastic wrap to keep the boxes on their wooden pallet.

The numbering is used as key for the scenario schematic provided in Figure D.14. A view of the aisle during the packet reception rate measurements in included in Figure D.15. The raw measurement results and path loss model fitting are provided in Figure D.16.

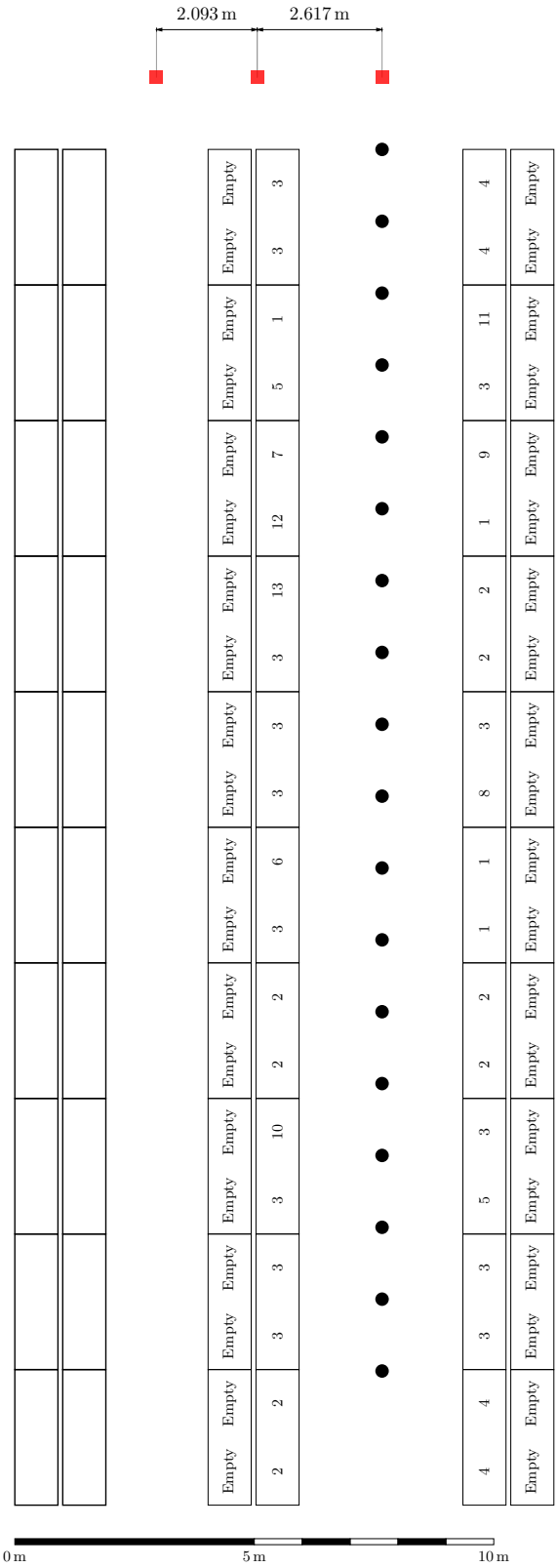

Figure D.14 The setup for Scenario S5. The numbers in each bay indicate what the bay was filled with and the key in numbered list in Section D.1.5. Bays without text indicate the contents of the racking was not noted. For path loss measurements, the transmitter was placed on the red squares and the receiver on the black circles. For packet reception rate testing the opposite setup was used.

(a) The view from the transmitter end of the mixed scenario during path loss measurements. The transmitter is sitting on wooden pallets in the zone 3 measurement position.

(b) A reverse view, looking towards the transmitter, partway down the aisle during the packet reception rate testing for the mixed scenario.

Figure D.15 Views of the aisle during the mixed scenario testing. All racking content is artificially staged.

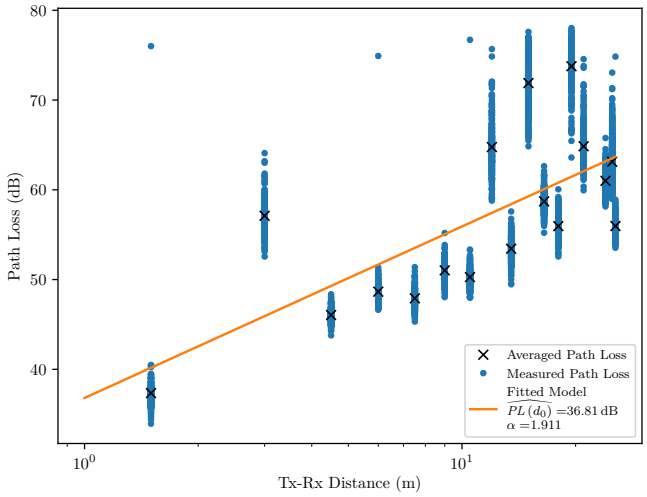

(a) Zone 1

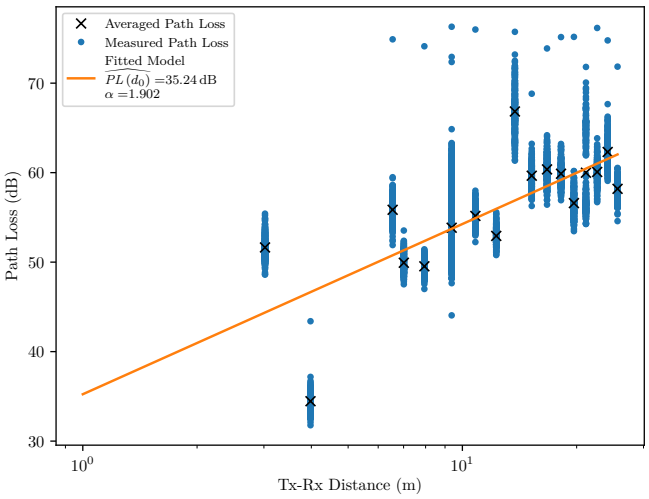

(b) Zone 2

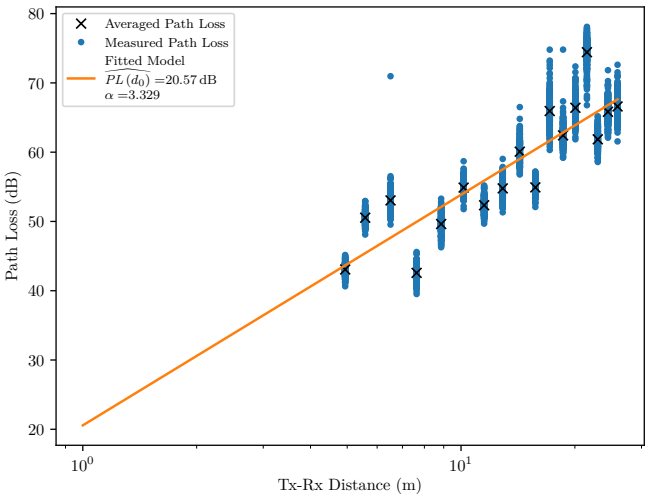

(c) Zone 3

Figure D.16 The raw measurement data and path loss model fit for Scenario S5.

D.2 LOCATION 2 — LOGISTICS WAREHOUSE

Location 2 is a commercial logistics centre based in Rolleston, a town south of Christchurch, New Zealand. The company which owns and operates the warehouse offers complete supply chain solutions and uses the warehouse as a centre for their general logistics operations. As such Location 2 contains a wide variety of materials, primarily retail food goods and plastic pellets for manufacturing.

Location 2 has a drop ceiling with fluorescent lighting and sprinkler system. Sections of the drop ceiling are made of transparent plastic panels, which allow sunlight from clear panels in the roof through, helping light the warehouse. The roof of the warehouse is made of metal corrugated roofing panels with clear plastic panels matching the clear panels in the drop ceiling (Figure D.17).

Figure D.18 is replicated copy of the floor plan provided in Figure 6.7. It also highlights what the different areas are used for, in addition to the areas of interest. Not shown in the floor plan are two large, covered incoming goods areas on either side of the building (Figure D.19). Also not indicated in Figure D.18 is the position of automated pallet wrapping machines and pedestrian safety barriers (Figure D.20).

In all measurements the transmit and receive antennas were 1.0 m from the floor.

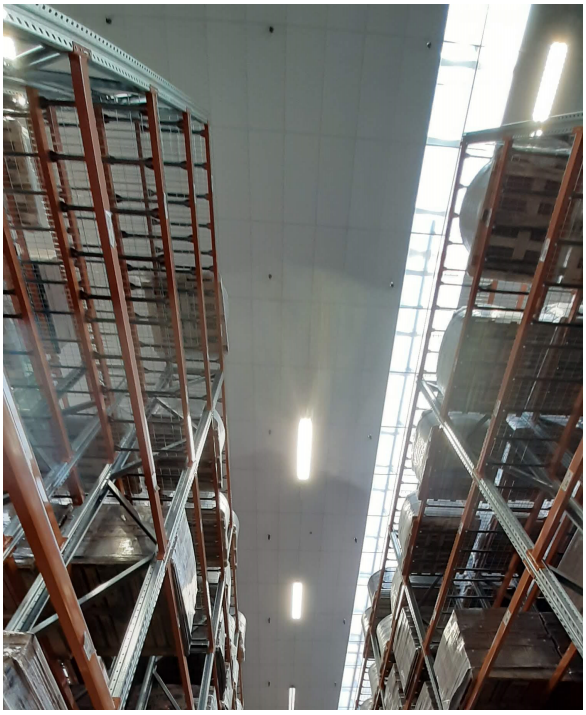

Figure D.17 The ceiling of Location 2 in Scenario S6.

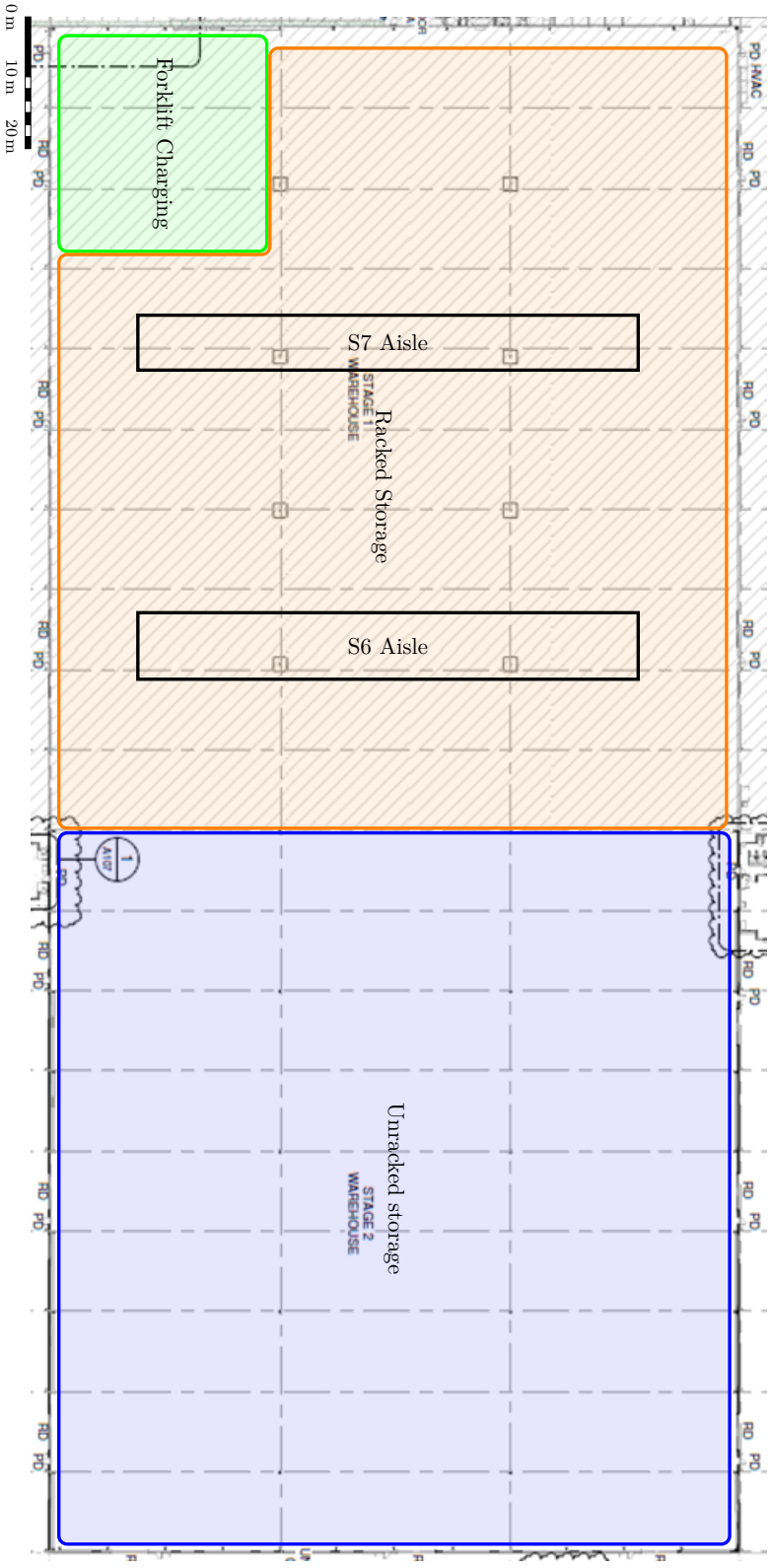

Figure D.18 The floor plan of Location 2 with the different areas of the warehouse labelled. The scale is accurate for the building floor plan, however, the indicated areas are not exact. RD and PD stand for roller-door and pedestrian-door, respectively.

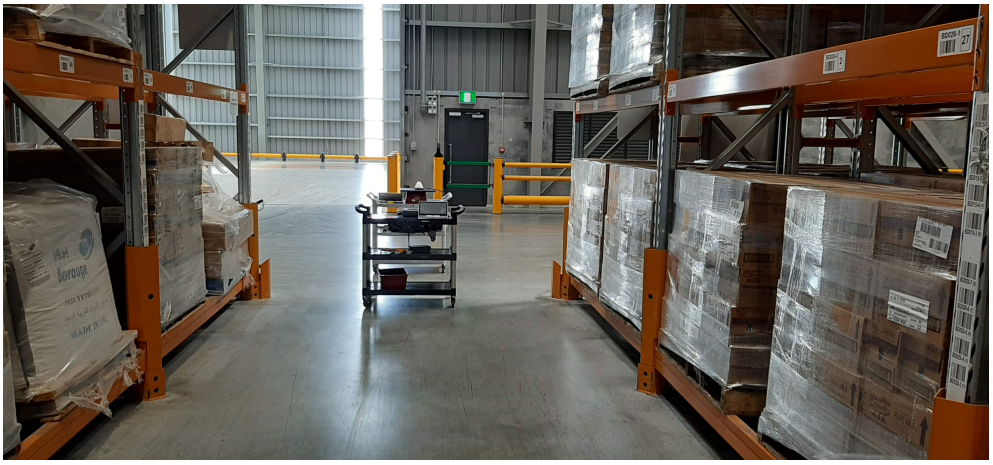

Figure D.19 The view at the start of the aisle in Scenario S6 looking towards the transmitter. This shows the roller- and pedestrian-doors into the covered incoming/outgoing goods area.

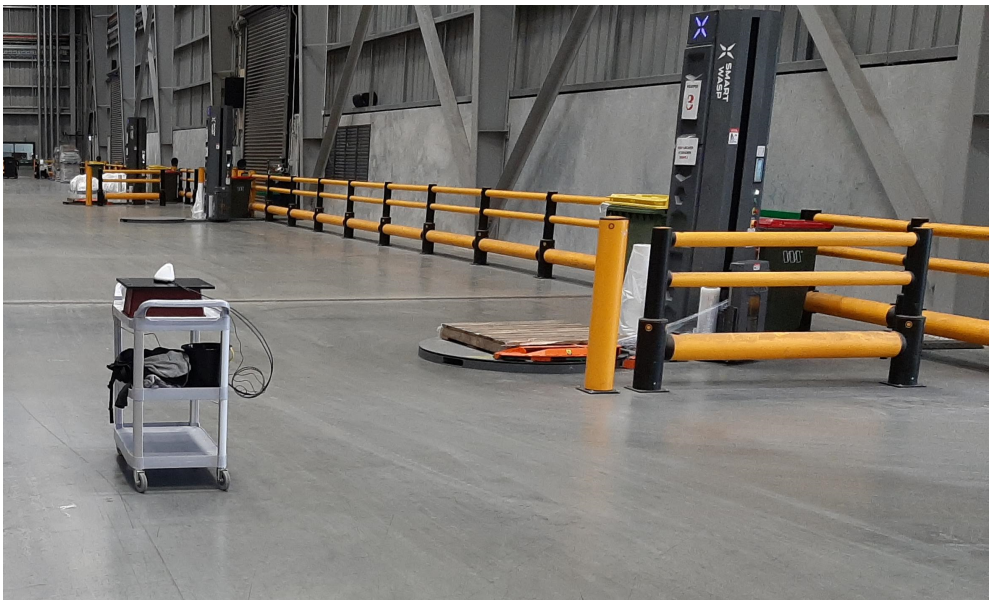

Figure D.20 The automated pallet wrapping machines and pedestrian safety barriers. The pedestrian safety barriers run the length of the warehouse and are made of steel tubing.

D.2.1 Scenario S6

The aisle used for Scenario S6 primarily stored cartons of Ultra High Temperature (UHT) milk in in boxes and bags of polyethylene pellets on pallets. The aisles either side were of a similar composition. The layout of the racking, the location of two structural columns, and the location of data points is in Figure D.21. All the racking units were seven bays high and the aisle was 27 bays long, with each bay being 2.87 m wide.

Figure D.22 includes the raw path loss results and path loss model fitting for this scenario.

D.2.2 Scenario S7

The aisle in Scenario S7 was used to primarily store chips/crisps in boxes on pallets. The aisles either side were largely the same, but also had UHT milk in some bays. Partway through the path loss testing some of the aisle contents were shifted for safety reasons. However, this was limited to the contents of a single bay. In Figure D.23 the view down the aisle is presented. Figure D.24 provides a diagram of the racking layout and measurement locations. Similar to Scenario S6, two bays along the aisle were missing to accommodate structural columns. The raw measurements and path loss model fitting results are include in Figure D.25. All the racking units were seven bays high and the aisle was 27 bays long, with each bay being 2.87 m wide.

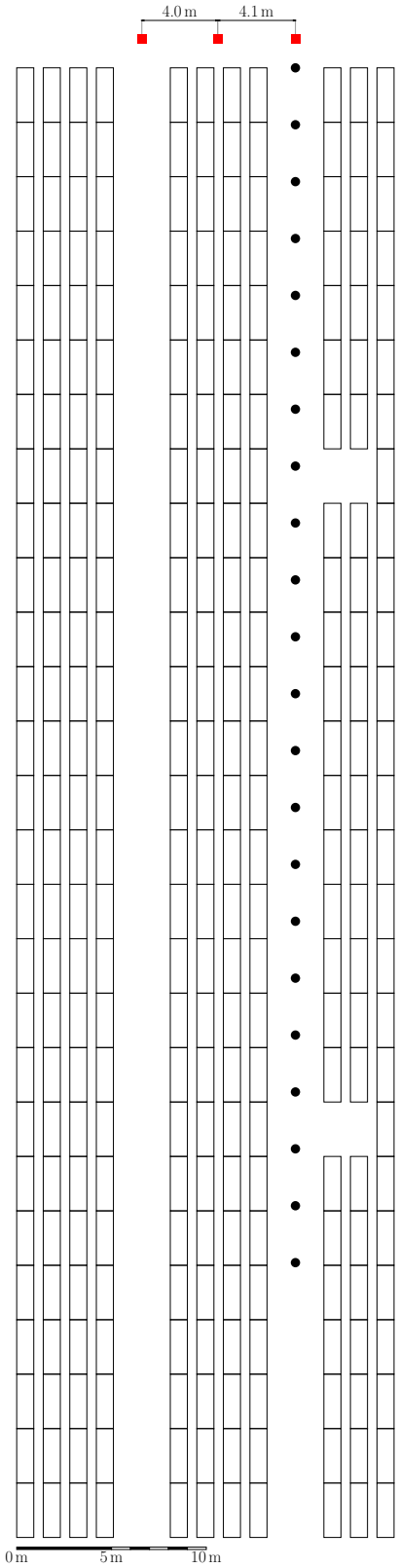

Figure D.21 The layout of the racking and a schematics of the measurements taken for Scenario S6. The bays missing in the rightmost grouping of racking are removed for roof support columns. For path loss measurements, the transmitter was placed on the red squares and the receiver on the black circles. For packet reception rate testing the opposite setup was used.

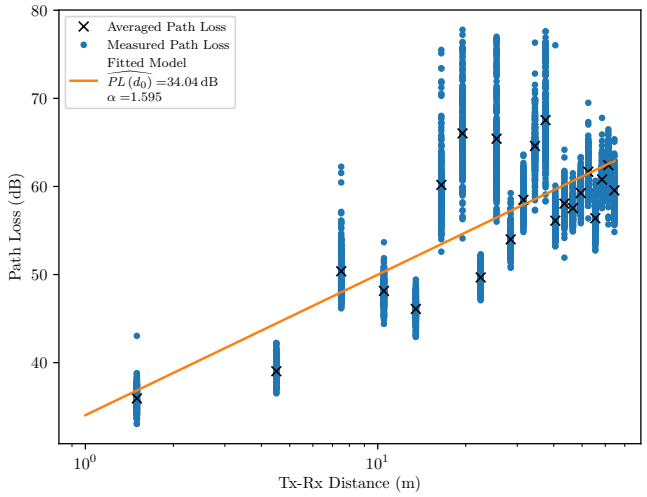

(a) Zone 1

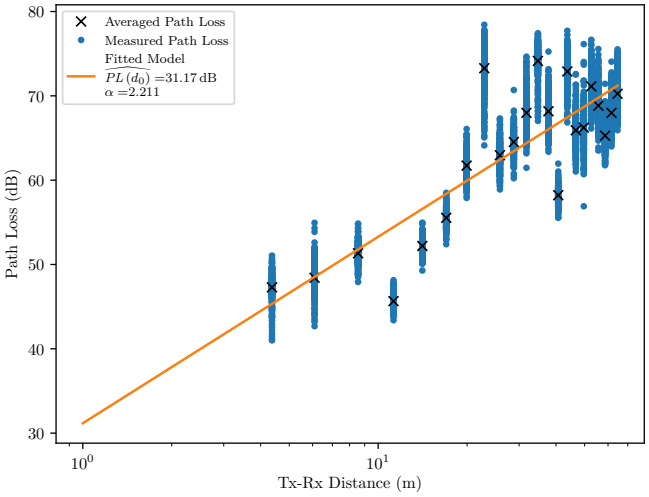

(b) Zone 2

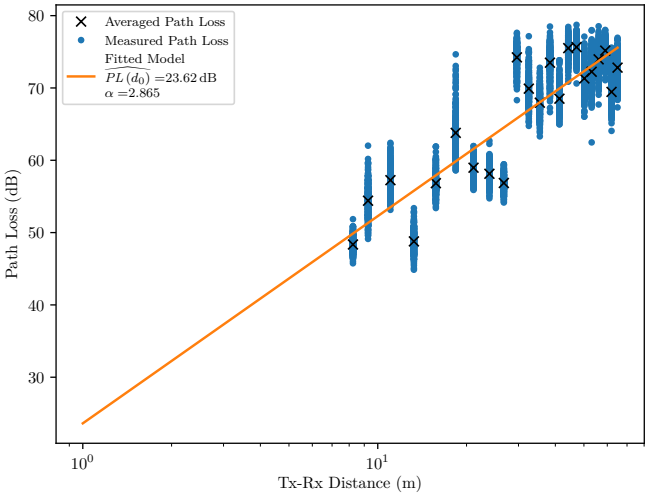

(c) Zone 3

Figure D.22 The raw measurement data and path loss model fit for Scenario S6.

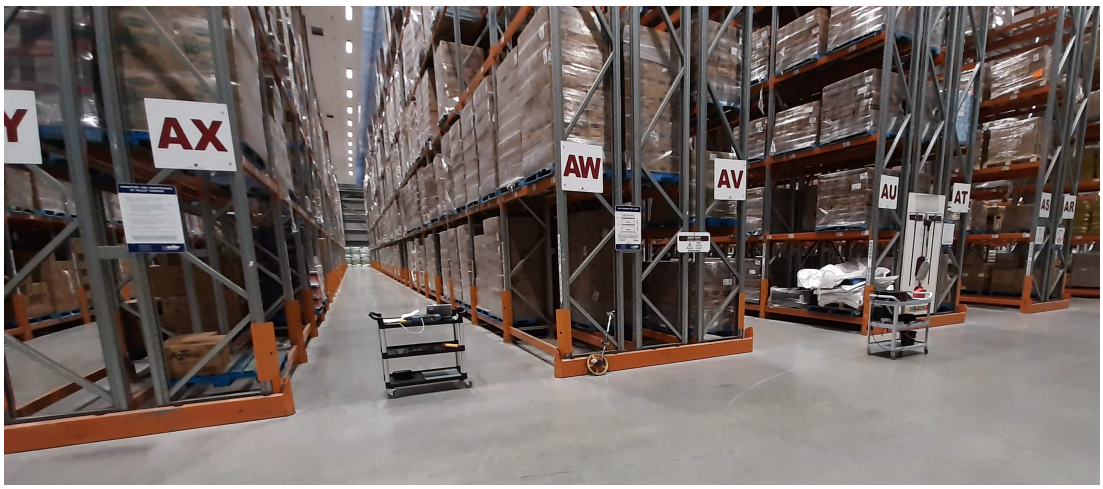

Figure D.23 The view down the aisle measured in Scenario S7.

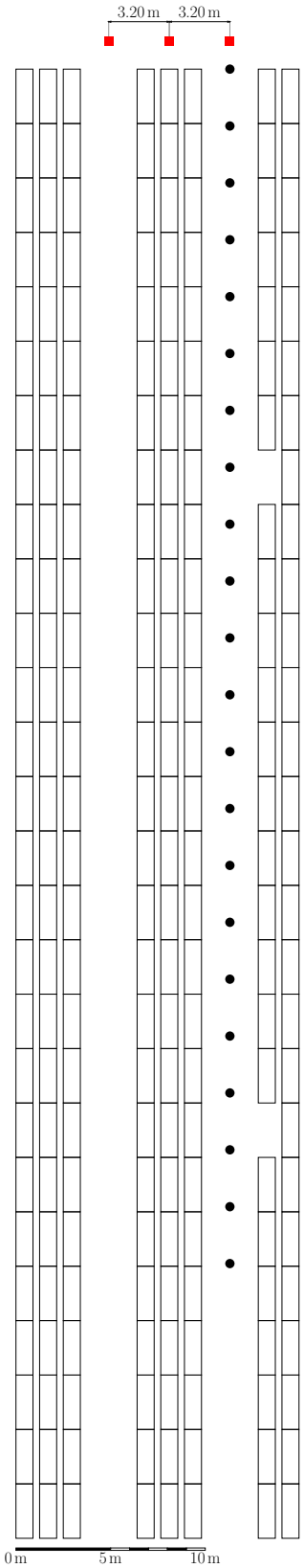

Figure D.24 The layout of the racking and a schematics of the measurements taken for Scenario S7. The bays missing in the rightmost grouping of racking are removed for roof support columns. For path loss measurements, the transmitter was placed on the red squares and the receiver on the black circles.

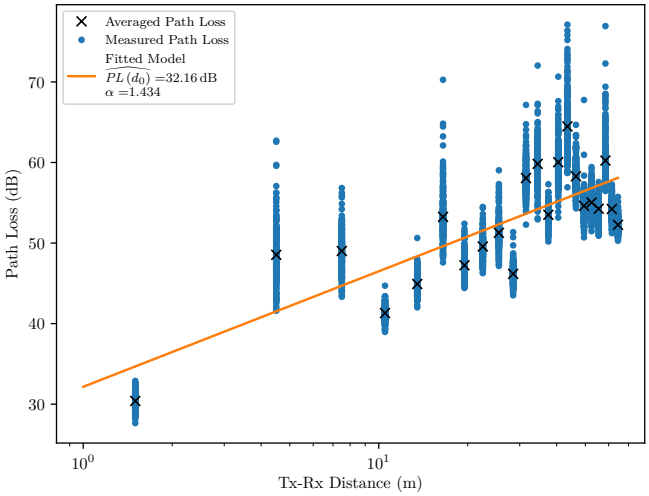

(a) Zone 1

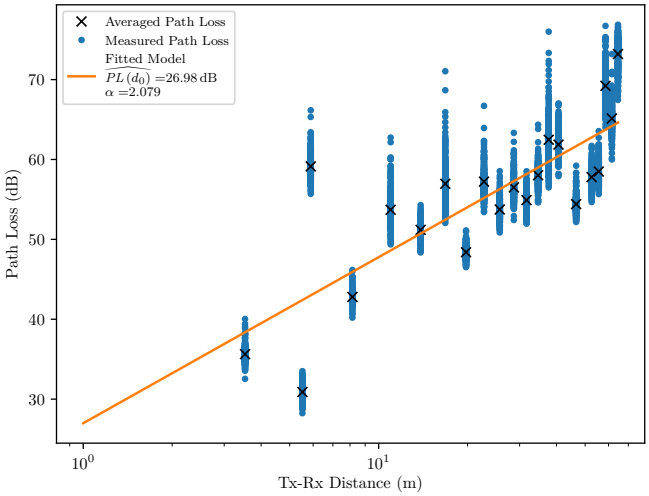

(b) Zone 2

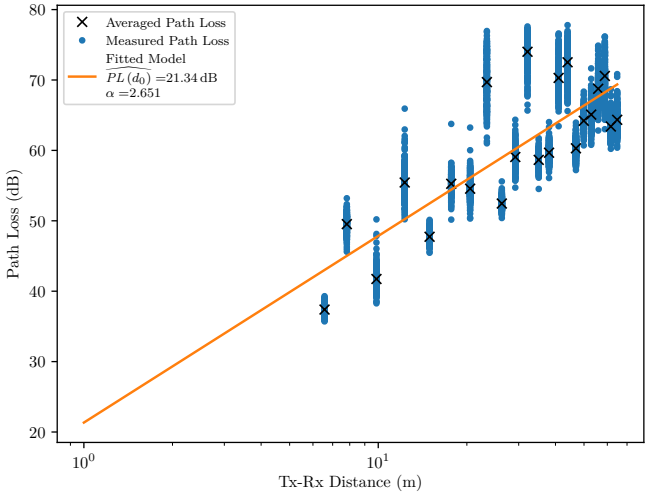

(c) Zone 3

Figure D.25 The raw measurement data and path loss model fit for Scenario S7.

REFERENCES

[1] P. Sewalkar and J. Seitz, "Vehicle-to-pedestrian communication for vulnerable road users: Survey, design considerations, and challenges," *Sensors*, vol. 19, 01 2019.

[2] S. Wang, S. Djahel, Z. Zhang, and J. McManis, "Next road rerouting: A multiagent system for mitigating unexpected urban traffic congestion," *IEEE Transactions on Intelligent Transportation Systems*, vol. 17, no. 10, pp. 2888–2899, 2016.

[3] G. Li, B. He, and A. Du, "A traffic congestion aware vehicle-to-vehicle communication framework based on voronoi diagram and information granularity," *Peer-to-Peer Networking and Applications*, vol. 11, no. 1, pp. 124–138, 2018.

[4] L. Chen and C. Englund, "Cooperative intersection management: A survey," *IEEE Transactions on Intelligent Transportation Systems*, vol. 17, no. 2, pp. 570–586, 2016.

[5] S. Saxena, I. K. Isukapati, S. F. Smith, and J. M. Dolan, "Multiagent sensor fusion for connected & autonomous vehicles to enhance navigation safety," in *2019 IEEE Intelligent Transportation Systems Conference (ITSC)*, 2019, pp. 2490–2495.

[6] Radio New Zealand, "Worksafe promises to crack down on 'hidden' deaths." [Online]. Available: https://www.rnz.co.nz/national/programmes/morningreport/audio/2018734438/worksafe-promises-to-crack-down-on-hidden-deaths

[7] B. T. Railsback and R. M. Ziernicki, "Hazard analysis and risk assessment for the operators of stand-up forklifts," in *ASME International Mechanical Engineering Congress and Exposition*, vol. Volume 16: Safety Engineering, Risk Analysis and Reliability Methods, 10 2008, pp. 237–242. [Online]. Available: https://doi.org/10.1115/IMECE2008-66427

[8] D. Flore. (2016, September) V2X. 3GPP. [Online]. Available: https://www.3gpp.org/v2x

[9] *IEEE Standard for Information technology— Local and metropolitan area networks— Specific requirements— Part 11: Wireless LAN Medium Access Control (MAC) and Physical Layer (PHY) Specifications Amendment 6: Wireless Access in Vehicular Environments*, IEEE Std. IEEE Std 802.11p-2010 (Amendment to IEEE Std 802.11-2007 as amended by IEEE Std 802.11k-2008, IEEE Std 802.11r-2008, IEEE Std 802.11y-2008, IEEE Std 802.11n-2009, and IEEE Std 802.11w-2009), July 2010.

[10] G. Naik, B. Choudhury, and J. Park, "IEEE 802.11bd & 5G NR V2X: Evolution of radio access technologies for V2X communications," *IEEE Access*, vol. 7, pp. 70 169–70 184, 2019.

[11] 5G Automotive Association, "An assessment of LTE-V2X (PC5) and 802.11p direct communications technologies for improved road safety in the EU," 5G Automotive Association, Tech. Rep., December 2017. [Online]. Available: http://5gaa.org/wp-content/uploads/2017/12/5GAA-Road-safety-FINAL2017-12-05.pdf

[12] A. Turley, K. Moerman, A. Filippi, and V. Martinez, "C-ITS: Three observations on LTE-V2X and ETSI ITS-G5 — a comparison," NXP Semiconductors, Tech. Rep. CITSCOMPWP rev0, February 2018. [Online]. Available: https://www.nxp.com/docs/en/white-paper/CITSCOMPWP.pdf

[13] M. Chowdhury, M. Rahman, A. Rayamajhi, S. M. Khan, M. Islam, Z. Khan, and J. Martin, "Lessons learned from the real-world deployment of a connected vehicle testbed," *Transportation Research Record*, vol. 2672, no. 22, pp. 10–23, 2018. [Online]. Available: https://doi.org/10.1177/0361198118799034

[14] K. Gay and V. Kniss, "Safety pilot model deployment: Lessons learned and recommendations for future connected vehicle activities," US Department of Transporation, Tech. Rep. FHWA-JPO-16-363, September 2015.

[15] J. Oouchi, "DSRC car-mounted equipment including sensitivity-increasing means for communication in an electronic toll collection system," US Patent US6 959 177B1, March, 2005.

[16] C. Priemer and B. Friedrich, "A decentralized adaptive traffic signal control using V2I communication data," in *2009 12th International IEEE Conference on Intelligent Transportation Systems*, 2009, pp. 1–6.

[17] X. Wu, R. Miucic, S. Yang, S. Al-Stouhi, J. Misener, S. Bai, and W. Chan, "Cars talk to phones: A DSRC based vehicle-pedestrian safety system," in *2014 IEEE 80th Vehicular Technology Conference (VTC2014-Fall)*, 2014, pp. 1–7.

[18] Caterpillar Global Mining, "Cat MineStar solutions for underground," August 2019. [Online]. Available: https://www.youtube.com/watch?v=FfntMuhp1bA

[19] F. Riaz and M. A. Niazi, "Road collisions avoidance using vehicular cyber-physical systems: a taxonomy and review," *Complex Adaptive Systems Modeling*, vol. 4, no. 1, pp. 1–34, 2016.

[20] E. D. Kaplan, "Introduction," in *Understanding GPS: Principles and Applications*, 2nd ed., E. D. Kaplan and C. J. Hegarty, Eds. Artech House, 2006.

[21] R. Conley, R. Cosentino, C. J. Hegarty, E. D. Kaplan, J. L. Leva, M. U. de Haag, and K. Van Dyke, "Performance of stand-alone GPS," in *Understanding GPS: Principles and Applications*, 2nd ed., E. D. Kaplan and C. J. Hegarty, Eds. Artech House, 2006.

[22] "Satellite-based augmentation system," Land Information New Zealand, December 2020. [Online]. Available: https://web.archive.org/web/20210315212229/https://www.linz.govt.nz/data/geodetic-services/satellite-based-augmentation-system

[23] K. Ozsoy, A. Bozkurt, and I. Tekin, "Indoor positioning based on global positioning system signals," *Microwave and Optical Technology Letters*, vol. 55, no. 5, pp. 1091–1097, 2013. [Online]. Available: https://onlinelibrary.wiley.com/doi/abs/10.1002/mop.27520

[24] A. Mustovic, "Wireless information transfer in an indoor factory or warehouse environment," Master's thesis, Linköping University, Linköping, Sweden, May 2016.

[25] R. M. Estep, "Development of a real-time pedestrian localisation system for a warehouse environment," Master's thesis, University of Canterbury, Christchurch, New Zealand, Feb 2016. [Online]. Available: http://dx.doi.org/10.26021/3138

[26] V. Barral, P. Suárez-Casal, C. J. Escudero, and J. A. García-Naya, "Multi-sensor accurate forklift location and tracking simulation in industrial indoor environments," *Electronics*, vol. 8, no. 10, 2019. [Online]. Available: https://www.mdpi.com/2079-9292/8/10/1152

[27] D. Khan, S. Ullah, and S. Nabi, "A generic approach toward indoor navigation and pathfinding with robust marker tracking," *Remote Sensing*, vol. 11, no. 24, 2019. [Online]. Available: https://www.mdpi.com/2072-4292/11/24/3052

[28] G. Écorchard, K. Košnar, and L. Přeučil, "Wearable camera-based human absolute localization in large warehouses," in *Twelfth International Conference on Machine Vision (ICMV 2019)*, W. Osten and D. P. Nikolaev, Eds., vol. 11433, International Society for Optics and Photonics. SPIE, 2020, pp. 754 – 761. [Online]. Available: https://doi.org/10.1117/12.2559424

[29] W. Kwon, J. H. Park, M. Lee, J. Her, S. H. Kim, and J. W. Seo, "Robust autonomous navigation of unmanned aerial vehicles (UAVs) for warehouses inventory application," *IEEE Robotics and Automation Letters*, vol. 5, no. 1, pp. 243–249, 2020.

[30] R. Baird, "An autonomous forklift research platform for warehouse operations," Master's thesis, Massachusetts Institute of Technology, Massachusetts, USA, September 2018. [Online]. Available: https://hdl.handle.net/1721.1/121621

[31] G. Vasiljević, D. Miklić, I. Draganjac, Z. Kovači´, and P. Lista, "High-accuracy vehicle localization for autonomous warehousing," *Robotics and Computer-Integrated Manufacturing*, vol. 42, pp. 1–16, 2016. [Online]. Available: https://doi.org/10.1016/j.rcim.2016.05.001

[32] 3GPP, "Partners." [Online]. Available: https://www.3gpp.org/about-3gpp/partners

[33] ——, "About 3GPP home." [Online]. Available: https://www.3gpp.org/about-3gpp/about-3gpp

[34] Official IEEE 802.11 working group project timelines - 2021-03-16. IEEE 802.11 Working Group. [Online]. Available: https://grouper.ieee.org/groups/802/11/Reports/802.11_Timelines.htm

[35] D. Jiang and L. Delgrossi, "IEEE 802.11p: Towards an international standard for wireless access in vehicular environments," in *VTC Spring 2008 - IEEE Vehicular Technology Conference*, May 2008, pp. 2036–2040.

[36] B. Sun and H. Zhang, "802.11 NGV proposed PAR," IEEE P802.11-TASK GROUP BD (NGV), Tech. Rep., November 2018.

[37] *IEEE Guide for Wireless Access in Vehicular Environments (WAVE) Architecture*, IEEE Std. IEEE Std 1609.0-2019 (Revision of IEEE Std 1609.0-2013), Apr 2019.

[38] 3GPP, "Evolved universal terrestrial radio access (E-UTRA) physical access procedures," 3GPP, Tech. Rep. TS36.213v14, September 2016.

[39] A. Bazzi, G. Cecchini, M. Menarini, B. M. Masini, and A. Zanella, "Survey and perspectives of vehicular wi-fi versus sidelink cellular-V2X in the 5G era," *Future Internet*, vol. 11, no. 6, p. 122, May 2019. [Online]. Available: http://dx.doi.org/10.3390/fi11060122

[40] R. Molina-Masegosa and J. Gozalvez, "LTE-V for Sidelink 5G V2X Vehicular Communications: A New 5G Technology for Short-Range Vehicle-to-Everything Communications," *IEEE Vehicular Technology Magazine*, vol. 12, no. 4, pp. 30–39, 2017.

[41] H. G. Myung, J. Lim, and D. J. Goodman, "Single carrier FDMA for uplink wireless transmission," *IEEE Vehicular Technology Magazine*, vol. 1, no. 3, pp. 30–38, 2006.

[42] B. Toghi, M. Saifuddin, H. N. Mahjoub, M. O. Mughal, Y. P. Fallah, J. Rao, and S. Das, "Multiple access in cellular V2X: Performance analysis in highly congested vehicular networks," in *2018 IEEE Vehicular Networking Conference (VNC)*, Dec 2018, pp. 1–8.

[43] A. Mukherjee, *5G New Radio: Beyond Mobile Broadband*. US: Artech House, 2019.

[44] J. Hu, S. Chen, L. Zhao, Y. Li, J. Fang, B. Li, and Y. Shi, "Link level performance comparison between LTE V2X and DSRC," *Journal of Communications and Information Networks*, vol. 2, no. 2, pp. 101–112, 2017.

[45] P. Srivastava, "Tutorial on functionality and performance of Uu link (air interface) of LTE system," Master's thesis, University of Texas at Arlington, Texas, USA, January 2010.

[46] 3GPP, "Release 14 description; summary of rel-14 work items," 3GPP Technical Specification Group Services and System Aspects, Tech. Rep. TR 21.914 V14.0.0, May 2018.

[47] ——, "Evolved universal terrestrial radio access (E-UTRA) physical access proceedures," 3GPP, Tech. Rep. TS36.213v16, January 2020.

[48] ——, "Study on enhancements of 3GPP support for 5G V2X services," 3GPP, Tech. Rep. TR22.886, August 2016.

[49] Vodafone, "New SID: Study on NR V2X," 3GPP TSG RAN, Tech. Rep. RP-181429, July 2018.

[50] M. H. Castañeda Garcia, A. Molina-Galan, M. Boban, J. Gozalvez, B. Coll-Perales, T. Şahin, and A. Kousaridas, "A tutorial on 5G NR V2X communications," *IEEE Communications Surveys Tutorials*, 2021.

[51] M. Drago, T. Zugno, M. Polese, M. Giordani, and M. Zorzi, "MilliCar — an ns-3 module for mmWave NR V2X networks," *ArXiv*, vol. abs/2002.10347, 2020.

[52] Y. Niu, Y. Li, D. Jin, L. Su, and A. V. Vasilakos, "A survey of millimeter wave communications (mmWave) for 5G: opportunities and challenges," *Wireless Networks*, vol. 21, no. 8, pp. 2657–2676, 2015. [Online]. Available: https://doi.org/10.1007/s11276-015-0942-z

[53] J. B. Kenney, "Dedicated short-range communications (DSRC) standards in the united states," *Proceedings of the IEEE*, vol. 99, no. 7, pp. 1162–1182, July 2011.

[54] Y. Zang, L. Stibor, G. Orfanos, S. Guo, and H.-J. Reumerman, "An error model for inter-vehicle communications in highway scenarios at 5.9 GHz," in *Proceedings of the 2nd ACM International Workshop on Performance Evaluation of Wireless Ad Hoc, Sensor, and Ubiquitous Networks*, ser. PE-WASUN 05. New York, NY, USA: Association for Computing Machinery, 2005, pp. 49–56. [Online]. Available: https://doi.org/10.1145/1089803.1089966

[55] V. Rai, F. Bai, J. Kenney, and K. Laberteaux, "Cross-channel interference test results: A report from the VSC-A project," IEEE 802.11 Task Group p, Tech. Rep. IEEE 802.11 11-07-2133-00-000p, July 2007.

[56] M. Gast, *802.11 wireless networks: the definitive guide*, 1st ed. Sebastopol, Calif: O'Reilly, 2002.

[57] C. Han, M. Dianati, R. Tafazolli, R. Kernchen, and X. Shen, "Analytical study of the IEEE 802.11p MAC sublayer in vehicular networks," *IEEE Transactions on Intelligent Transportation Systems*, vol. 13, no. 2, pp. 873–886, June 2012.

[58] M. I. Hassan, H. L. Vu, and T. Sakurai, "Performance analysis of the IEEE 802.11 MAC protocol for DSRC with and without retransmissions," in *2010 IEEE International Symposium on "A World of Wireless, Mobile and Multimedia Networks" (WoWMoM)*, June 2010, pp. 1–8.

[59] *IEEE Standard for Information technology—Telecommunications and information exchange between systems Local and metropolitan area networksSpecific requirements — Part 11: Wireless LAN Medium Access Control (MAC) and Physical Layer (PHY) Specifications*, IEEE Std. IEEE Std 802.11-2016 (Revision of IEEE Std 802.11-2012), Dec 2016.

[60] B. Sun, H. Zhang, B. Sadeghi, J. Lepp, P. Ecclesine, J. Kenney, and M. Fischer, "TGbd agreed terminonlogy and requirements," IEEE P802.11-TASK GROUP BD (NGV), Tech. Rep. IEEE 802.11-19-0202/r1, January 2019. [Online]. Available: https://mentor.ieee.org/802.11/dcn/19/11-19-0202-01-00bd-tgbd-definitions-and-requirements.pptx

[61] B. Sadeghi, "802.11bd specification framework document," IEEE 802.11 Task Group bd, Tech. Rep. IEEE 802.11-20-0497r07, September 2020. [Online]. Available: https://mentor.ieee.org/802.11/dcn/19/11-19-0497-07-00bd-802-11bd-specification-framework-document.docx

[62] *IEEE Standard for Information technology— Telecommunications and information exchange between systems Local and metropolitan area networks— Specific requirements—Part 11: Wireless LAN Medium Access Control (MAC) and Physical Layer (PHY) Specifications—Amendment 4: Enhancements for Very High Throughput for Operation in Bands below 6 GHz.*, IEEE Std. IEEE Std 802.11ac-2013 (Amendment to IEEE Std 802.11-2012, as amended by IEEE Std 802.11ae-2012, IEEE Std 802.11aa-2012, and IEEE Std 802.11ad-2012), Dec 2013.

[63] Hyun-Seok Ryu, Jun-Seok Lee, and C. G. Kang, "BER analysis of dual-carrier modulation (DCM) over Rayleigh fading channel," in *International Congress on Ultra Modern Telecommunications and Control Systems*, 2010, pp. 717–721.

[64] M. Fischer, A. Filippi, and V. Martinez, "Interoperable NGV PHY improvements," IEEE NGV Study Group, Tech. Rep. IEEE 802.11-18-1186r0, July 2018. [Online]. Available: https://mentor.ieee.org/802.11/dcn/18/11-18-1186-00-0ngv-interoperable-ngv-phy-improvements.pptx

[65] M. López and L. Wilhelmsson, "Midamble design," IEEE P802.11-TASK GROUP BD (NGV), Tech. Rep. IEEE 802.11-20/0682r3, April 2020.

[66] D. Lim, E. Park, I. Jang, S. Kim, J. Kim, and J. Choi, "Performance evaluation of mid-amble," IEEE P802.11-TASK GROUP BD (NGV), Tech. Rep. IEEE 802.11-19/740r2, May 2019.

[67] I. Sarris, "Considerations on NGV PHY design," IEEE P802.11-TASK GROUP BD (NGV), Tech. Rep. IEEE 80.211-19/0310r0, March 2019.

[68] D. Lim, E. Park, I. Jang, S. Kim, J. Kim, and J. Choi, "Further investigation on mid-amble performance," IEEE P802.11-TASK GROUP BD (NGV), Tech. Rep. IEEE 802.11-19/1109r1, September 2019.

[69] H. Motozuka, T. Sakamoto, G. Wee, M. Irie, K. Takahashi, B. Sadeghi, T. Shimizu, S. Sand, and P. Unterhuber, "OCB for 60 GHz V2X," IEEE P802.11-TASK GROUP BD (NGV), Tech. Rep. IEEE 802.11-19/1162r2, September 2019.

[70] H. Motozuka, T. Sakamoto, K. Nakano, A. Egami, G. Wee, M. Irie, and K. Takahashi, "Preliminary test results of 11ad-based 60GHz mmW for V2I use cases," IEEE P802.11-TASK GROUP BD (NGV), Tech. Rep. IEEE 802.11-19-0100r0, November 2019.

[71] H. Motozuka, T. Sakamoto, M. Irie, K. Takahashi, G. Wee, M. Sim, and T. Shimizu, "NGV 60GHz beamforming," IEEE P802.11-TASK GROUP BD (NGV), Tech. Rep. IEEE 802.11-20/1302r3, September 2020.

[72] S. Sand, P. Unterhuber, B. Siebler, M. Schmidhammer, F. de Ponte Müller, A. Lehner, F. Beren, S. Schiessl, I. Sarris, B. Sadeghi, J. Segev, and Q. Li, "802.11bd NGV ranging status and types," IEEE P802.11-TASK GROUP BD (NGV), Tech. Rep. IEEE 802.11-20/1728r3, November 2020.

[73] M. Fischer, A. Filippi, and V. Martinez, "Considerations for backwards compatibility," IEEE 802.11 Task Group bd, Tech. Rep. IEEE 802.11-19-0079r0, November 2019. [Online]. Available: https://mentor.ieee.org/802.11/dcn/19/11-19-0079-00-00bd-considerations-for-backward-compatibility.pptx

[74] M. C. Jeruchim, P. Balaban, and K. S. Shanmugan, *Simulation of communication systems: modeling, methodology, and techniques*, 2nd ed. New York: Kluwer Academic/Plenum Publishers, 2000.

[75] A. Schmitz, M. Schinnenburg, J. Gross, and A. Aguiar, "Channel modeling," in *Modeling and tools for network simulation*, K. Wehrle, M. Güneş, and J. Gross, Eds. Heidelberg; New York: Springer, 2010, ch. 11.

[76] S. Pratschner, B. Tahir, L. Marijanovic, M. Mussbah, K. Kirev, R. Nissel, S. Schwarz, and M. Rupp, "Versatile mobile communications simulation: the Vienna 5G Link Level Simulator," *Eurasip Journal on Wireless Communications and Networking*, vol. 2018, no. 1, pp. 1–15, 2018.

[77] P. V. Pinheiro and F. Boavida, "Cluster-oriented emulation tool for performance evaluation of very large-scale networking scenarios," in *Simulation technologies in networking and communications: selecting the best tool for the test*, A.-S. K. Pathan, M. M. Monowar, S. Khan, and K. Ahmed, Eds. Boca Raton, Florida: CRC Press, 2015.

[78] S. S. Haykin, *Communication systems*, 4th ed. New York: Wiley, 2001.

[79] M. Pätzold, *Mobile radio channels*, 2nd ed. Chichester, West Sussex, U.K; Hoboken, N.J: Wiley, 2012.

[80] D. Gómez-Barquero, D. Gozálvez, P. F. Gómez, and N. Cardona, "Fading margin reduction due to interburst upper layer FEC in terrestrial mobile broadcast systems," *IEEE Transactions on Vehicular Technology*, vol. 60, no. 7, pp. 3110–3117, 2011.

[81] A. Aguiar and J. Gross, "Wireless channel models," Telecommunications Networks Group, Technical University Berlin, Berlin, Germany, Tech. Rep. TKN-03-007, April 2003.

[82] T. S. Rappaport, R. W. Heath, R. C. Daniels, and J. N. Murdock, *Millimeter wave wireless communications*. Upper Saddle River, NJ: Prentice Hall, 2015.

[83] N. C. Beaulieu and C. Cheng, "Efficient Nakagami-m fading channel simulation," *IEEE Transactions on Vehicular Technology*, vol. 54, no. 2, pp. 413–424, 2005.

[84] T.-M. Wu, "Generation of Nakagami-m fading channels," in *2006 IEEE 63rd Vehicular Technology Conference*, vol. 6, 2006, pp. 2787–2792.

[85] P. Kyösti, J. Meinilä, L. Hentila, X. Zhao, T. Jämsä, C. Schneider, M. Narandzić, M. Milojević, A. Hong, J. Ylitalo, V.-M. Holappa, M. Alatossava, R. Bultitude, Y. Jong, and T. Rautiainen, "WINNER II channel models; part I channel models," WINNER, Tech. Rep. IST-4-027756 WINNER II D1.1.2, September 2007.

[86] ——, "WINNER II channel models; part II radio channel measurement and analysis results," WINNER, Tech. Rep. IST-4-027756 WINNER II D1.1.2, September 2007.

[87] 3GPP, "Study on channel model for frequencies from 0.5 to 100 GHz," 3GPP Technical Specification Group Radio Access Network, Tech. Rep. TR 38.901 V16.0.1, December 2019.

[88] ITU-R, "Guidelines for evaluation of radio interfrace technologies for IMT-advanced," International Telecommunications Union, Tech. Rep. ITU-R M.2135-1, December 2009. [Online]. Available: https://www.itu.int/dms_pub/itu-r/opb/rep/R-REP-M.2135-1-2009-PDF-E.pdf

[89] M. Peter, K. Sakaguchi, S. Jaeckel, S. Wu, M. Nekovee, J. Medbo, K. Haneda, S. L. H. Nguyen, R. Naderpour, J. Vehmas, F. Mani, A. Bamba, R. DErrico, M. Rybakowski, J.-M. Conrat, A. Goulianos, P. Cain, M. Rumney, M. Dieudonne, H. Wang, and M. Kottkamp, "Measurement campaigns and initial channel models for preferred suitable frequency ranges," mmMAGIC, Tech. Rep. H2020-ICT-671650-mmMAGIC/D2.1, March 2016.

[90] W. Anwar, N. Franchi, and G. Fettweis, "Physical Layer Evaluation of V2X Communications Technologies: 5G NR-V2X, LTE-V2X, IEEE 802.11bd, and IEEE 802.11p," in *2019 IEEE 90th Vehicular Technology Conference (VTC2019-Fall)*. IEEE, sep 2019, pp. 1–7. [Online]. Available: https://ieeexplore.ieee.org/document/8891313/

[91] V. Mannoni, V. Berg, S. Sesia, and E. Perraud, "A comparison of the V2X communication systems: ITS-G5 and C-V2X," *IEEE Vehicular Technology Conference*, vol. 2019-April, 2019.

[92] ETSI, "Intelligent transport systems (ITS); access layer specification for intelligent transport systems operating in the 5 GHz frequency band," ETSI, Tech. Rep. Draft ETSI EN 302 663 v1.2.0, November 2012. [Online]. Available: https://www.etsi.org/deliver/etsi_en/302600_302699/302663/01.02.00_20/en_302663v010200a.pdf

[93] R. Molina-Masegosa, J. Gozalvez, and M. Sepulcre, "Comparison of IEEE 802.11p and LTE-V2X: An evaluation with periodic and aperiodic messages of constant and variable size," *IEEE Access*, vol. 8, pp. 121 526–121 548, July 2020.

[94] 3GPP, "Study on LTE-based V2X services (release 14)," 3GPP Technical Specification Group Radio Access Network, Tech. Rep. TR 36.885 V14.0.0, June 2016.

[95] Qualcomm, "Accelerating C-V2X commercialization," Qualcomm, Tech. Rep., September 2017. [Online]. Available: https://www.qualcomm.com/media/documents/files/accelerating-c-v2x-commercialization.pdf

[96] P. Alexander, D. Haley, and A. Grant, "Cooperative intelligent transport systems: 5.9-GHz field trials," *Proceedings of the IEEE*, vol. 99, no. 7, pp. 1213–1235, 2011.

[97] A. Tomasi, "Reliable communication in mine environments for autonomous vehicles," Master's thesis, KTH Royal Institute of Technology, Stockholm, Sweden, 2016.

[98] L. Manara, "Investigating antenna placement on autonomous mining vehicle," Master's thesis, KTH Royal Institute of Technology, Stockholm, Sweden, 2016.

[99] A. Chehri, H. Chehri, N. Hakim, and R. Saadane, "Realistic 5.9 GHz DSRC vehicle-to-vehicle wireless communication protocols for cooperative collision warning in underground mining," in *Smart Transportation Systems 2020*, X. Qu, L. Zhen, R. J. Howlett, and L. C. Jain, Eds. Singapore: Springer Singapore, 2020, pp. 133–141.

[100] Y. Jin, "Feasibility study of vehicular teleoperation over cellular network in urban scenario," Master's thesis, KTH Royal Institute of Technology, Stockholm, Sweden, December 2017.

[101] Modular Mining, "Mine safety awareness." [Online]. Available: https://www.modularmining.com/our-solutions/safety/

[102] Wenco, "The Next Step for V2X: High Precision GNSS and Further Options for Enhanced Mine Safety," November 2019. [Online]. Available: http://www.wencomine.com/wp-content/uploads/2019/11/The-Next-Step-for-V2X-1.pdf

[103] R. Croonenbroeck, L. Underberg, A. Wulf, and R. Kays, "Measurements for the development of an enhanced model for wireless channels in industrial environments," *International Conference on Wireless and Mobile Computing, Networking and Communications*, vol. 2017-Octob, 2017.

[104] E. Tanghe, W. Joseph, L. Verloock, L. Martens, H. Capoen, K. Van Herwegen, and W. Vantomme, "The industrial indoor channel: large-scale and temporal fading at 900, 2400, and 5200 MHz," *IEEE Transactions on Wireless Communications*, vol. 7, no. 7, pp. 2740–2751, 2008.

[105] P. Bosselmann, "Planning and analysis of UHF RFID systems for consumer goods logistics using ray tracing predictions," in *2007 1st Annual RFID Eurasia*, 2007.

[106] S. Sangodoyin, V. Kristem, A. F. Molisch, R. He, F. Tufvesson, and H. M. Behairy, "Statistical Modeling of Ultrawideband MIMO Propagation Channel in a Warehouse Environment," *IEEE Transactions on Antennas and Propagation*, vol. 64, no. 9, pp. 4049–4063, 2016.

[107] S. Sangodoyin, R. He, A. F. Molisch, V. Kristem, and F. Tufvesson, "Ultrawideband MIMO channel measurements and modeling in a warehouse environment," in *2015 IEEE International Conference on Communications (ICC)*, 2015, pp. 2277–2282.

[108] A. Karaagac, J. Haxhibeqiri, W. Joseph, I. Moerman, and J. Hoebeke, "Wireless industrial communication for connected shuttle systems in warehouses," *IEEE International Workshop on Factory Communication Systems - Proceedings, WFCS*, pp. 1–4, 2017.

[109] L. Wang, B. Ai, D. He, G. Li, K. Guan, R. He, and Z. Zhong, "Channel characteristics analysis in smart warehouse scenario," in *2017 IEEE International Symposium on Antennas and Propagation USNC/URSI National Radio Science Meeting*, 2017, pp. 1417–1418.

[110] M. Malinverno, G. Avino, C. Casetti, C. F. Chiasserini, F. Malandrino, and S. Scarpina, "Performance analysis of C-V2I-based automotive collision avoidance," in *2018 IEEE 19th International Symposium on "A World of Wireless, Mobile and Multimedia Networks" (WoWMoM)*, 2018, pp. 1–9.

[111] X. Xu, K. Liu, K. Xiao, L. Feng, Z. Wu, and S. Guo, "Vehicular fog computing enabled real-time collision warning via trajectory calibration," *Mobile Networks and Applications*, vol. 25, no. 6, pp. 2482–2494, 2020.

[112] B. Qian, H. Zhou, F. Lyu, J. Li, T. Ma, and F. Hou, "Toward collision-free and efficient coordination for automated vehicles at unsignalized intersection," *IEEE Internet of Things Journal*, vol. 6, no. 6, pp. 10 408–10 420, 2019.

[113] M. R. Hafner, D. Cunningham, L. Caminiti, and D. Del Vecchio, "Cooperative collision avoidance at intersections: Algorithms and experiments," *IEEE Transactions on Intelligent Transportation Systems*, vol. 14, no. 3, pp. 1162–1175, 2013.

[114] M. Ferreira, R. Fernandes, H. Conceição, W. Viriyasitavat, and O. K. Tonguz, "Self-organized traffic control," in *Proceedings of the Seventh ACM International Workshop on VehiculAr InterNETworking*, ser. VANET 10. New York, NY, USA: Association for Computing Machinery, 2010, pp. 85–90. [Online]. Available: https://doi.org/10.1145/1860058.1860077

[115] L. Guo, D. Wang, P. Li, L. Zhang, M. Ren, H. Liu, and A. Wang, "A novel virtual traffic light algorithm based on V2V for single intersection in vehicular networks," in *International Conference on Combinatorial Optimization and Applications*. Springer, 2019, pp. 235–251.

[116] P. Wang and C.-Y. Chan, "Vehicle collision prediction at intersections based on comparison of minimal distance between vehicles and dynamic thresholds," *IET Intelligent Transport Systems*, vol. 11, no. 10, pp. 676–684, 2017.

[117] S. Joerer, M. Segata, B. Bloessl, R. Lo Cigno, C. Sommer, and F. Dressler, "A vehicular networking perspective on estimating vehicle collision probability at intersections," *IEEE Transactions on Vehicular Technology*, vol. 63, no. 4, pp. 1802–1812, 2014.

[118] P. Droździel, S. Tarkowski, I. Rybicka, and R. Wrona, "Drivers reaction time research in the conditions in the real traffic," *Open Engineering*, vol. 10, no. 1, pp. 35–47, 2020. [Online]. Available: https://doi.org/10.1515/eng-2020-0004

[119] NZ Transport Agency Staff, *The Official New Zealand Road Code 2019/2020*. NZ Transport Agency, 2019.

[120] *Occupational Safety and Health Standards; Materials Handling and Storage; Powered industrial trucks*, §1910.178(n)(1), Occupational Safety and Health

Administration Std. 1910.178. [Online]. Available: https://www.osha.gov/laws-regs/regulations/standardnumber/1910/1910.178

[121] H. Feng, C. Liu, Y. Shu, and O. W. Yang, "Location prediction of vehicles in VANETs using a Kalman filter," *Wireless personal communications*, vol. 80, no. 2, pp. 543–559, 2015.

[122] R. K. Jaiswal and C. Jaidhar, "Location prediction algorithm for a nonlinear vehicular movement in VANET using extended Kalman filter," *Wireless Networks*, vol. 23, no. 7, pp. 2021–2036, 2017.

[123] L. N. Balico, A. A. F. Loureiro, E. F. Nakamura, R. S. Barreto, R. W. Pazzi, and H. A. B. F. Oliveira, "Localization prediction in vehicular ad hoc networks," *IEEE Communications Surveys & Tutorials*, vol. 20, no. 4, pp. 2784–2803, 2018.

[124] OpenSim Ltd. What is OMNeT++. [Online]. Available: https://omnetpp.org/intro/

[125] A. Varga, "OMNeT++," in *Modeling and tools for network simulation*, K. Wehrle, M. Güneş, and J. Gross, Eds. Heidelberg;New York;: Springer, 2010, ch. 3.

[126] OpenSim Ltd. What is INET framework? [Online]. Available: https://inet.omnetpp.org/Introduction.html

[127] C. Sommer, R. German, and F. Dressler, "Bidirectionally Coupled Network and Road Traffic Simulation for Improved IVC Analysis," *IEEE Transactions on Mobile Computing (TMC)*, vol. 10, no. 1, pp. 3–15, January 2011.

[128] C. Sommer. Veins. [Online]. Available: https://veins.car2x.org/

[129] D. Krajzewicz, J. Erdmann, M. Behrisch, and L. Bieker, "Recent development and applications of SUMO - Simulation of Urban MObility," *International Journal On Advances in Systems and Measurements*, vol. 5, no. 3&4, pp. 128–138, December 2012. [Online]. Available: http://elib.dlr.de/80483/

[130] A. Virdis, G. Stea, and G. Nardini, "SimuLTE - a modular system-level simulator for LTE/LTE-A networks based on OMNeT++," in *2014 4th International Conference On Simulation And Modeling Methodologies, Technologies And Applications (SIMULTECH)*, Aug 2014, pp. 59–70.

[131] A. Virdis, G. Nardini, and G. Stea, "Modeling unicast device-to-device communications with simuLTE," in *2016 1st International Workshop on Link- and System Level Simulations (IWSLS)*, July 2016, pp. 1–6.

[132] B. McCarthy and A. O'Driscoll, "OpenCV2X mode 4: A simulation extension for cellular vehicular communication networks," *IEEE International Workshop on Computer Aided Modeling and Design of Communication Links and Networks, CAMAD*, vol. 2019-Septe, 2019.

[133] A. Hegde and A. Festag, *Artery-C: An OMNeT++ Based Discrete Event Simulation Framework for Cellular V2X*. New York, NY, USA: Association for Computing Machinery, 2020, pp. 47–51. [Online]. Available: https://doi.org/10.1145/3416010.3423240

[134] G. F. Riley and T. R. Henderson, "The ns-3 network simulator," in *Modeling and tools for network simulation*, K. Wehrle, M. Güneş, and J. Gross, Eds. Heidelberg;New York;: Springer, 2010, ch. 2.

[135] J. Bu, G. Tan, N. Ding, M. Liu, and C. Son, "Implementation and evaluation of WAVE 1609.4/802.11p in ns-3," in *Proceedings of the 2014 Workshop on Ns-3*, ser. WNS3 14. New York, NY, USA: Association for Computing Machinery, 2014. [Online]. Available: https://doi.org/10.1145/2630777.2630778

[136] B. Sliwa, J. Pillmann, F. Eckermann, L. Habel, M. Schreckenberg, and C. Wietfeld, "Lightweight joint simulation of vehicular mobility and communication with LIM0Sim," in *2017 IEEE Vehicular Networking Conference (VNC)*, Nov 2017, pp. 81–88.

[137] F. Eckermann, M. Kahlert, and C. Wietfeld, "Performance analysis of C-V2X mode 4 communication introducing an open-source C-V2X simulator," in *2019 IEEE 90th Vehicular Technology Conference (VTC-Fall)*, Honolulu, Hawaii, USA, September 2019.

[138] *The LENA ns-3 LTE Module Documentation*. [Online]. Available: http://networks.cttc.es/wp-content/uploads/sites/2/2014/01/lena-lte-module-doc.pdf

[139] N. Patriciello, S. Lagen, B. Bojovic, and L. Giupponi, "An E2E simulator for 5G NR networks," *Simulation Modelling Practice and Theory*, vol. 96, p. 101933, 2019.

[140] Modeling, simulation and performance evaluation of NR V2X. Centre Tecnològic de Telecomunicacions de Catalunya (CTTC). [Online]. Available: http://www.cttc.es/project/modeling-simulation-and-performance-evaluation-of-nr-v2x/

[141] G. Cecchini, A. Bazzi, B. M. Masini, and A. Zanella, "LTEV2Vsim: An LTE-V2V simulator for the investigation of resource allocation for cooperative awareness," in *2017 5th IEEE International Conference on Models and Technologies for Intelligent Transportation Systems (MT-ITS)*, 2017, pp. 80–85.

[142] B. Kang, J. Yang, J. Paek, and S. Bahk, "ATOMIC: Adaptive transmission power and message interval control for C-V2X mode 4," *IEEE Access*, vol. 9, pp. 12 309–12 321, 2021.

[143] A. Bazzi, A. Zanella, I. Sarris, and V. Martinez, "Co-channel coexistence: Let ITS-G5 and sidelink C-V2X make peace," in *2020 IEEE MTT-S International Conference on Microwaves for Intelligent Mobility (ICMIM)*, 2020, pp. 1–4.

[144] 3GPP, "Evolved universal terrestrial radio access (E-UTRA); radio resource control (RRC); protocol specification," 3GPP, Tech. Rep. TS36.331v16.1, July 2020.

[145] ——, "Evolved universal terrestrial radio access (E-UTRA); packet data convergence protocol (PDCP) specification," 3GPP, Tech. Rep. TS36.323v16, April 2020.

[146] ——, "Evolved universal terrestrial radio access (E-UTRA); radio link control (RLC) protocol specification," 3GPP, Tech. Rep. TS36.322v16, July 2020.

[147] S. Yi, S. Chun, Y. Lee, S. Park, and S. Jung, *Radio Protocols for LTE and LTE-Advanced*, 1st ed. Chichester, UK: Wiley, 2012.

[148] J. Wang and R. A. Rouil, "BLER performance evaluation of LTE device-to-device communications," National Institute of Standards and Technology, Tech. Rep. 8157, Nov 2016. [Online]. Available: https://doi.org/10.6028/NIST.IR.8157

[149] Huawei and HiSilicon, "DMRS enhancement of V2V," 3GPP TSG RAN WG1, Tech. Rep. R1-160284, February 2016.

[150] C. Sommer, D. Eckhoff, A. Brummer, D. S. Buse, F. Hagenauer, S. Joerer, and M. Segata, "Veins: The open source vehicular network simulation framework," in *Recent Advances in Network Simulation: The OMNeT++ Environment and its Ecosystem*, 2019, ch. 6.

[151] G. Evropeytsev, S. E. Pomares Hernández, J. R. Pérez Cruz, L. M. Rodríguez Henríquez, and E. López Domínguez, "A scalable indirect position-based causal diffusion protocol for vehicular networks," *IEEE Access*, vol. 7, pp. 14 767–14 778, 2019.

[152] G. Sun, Y. Zhang, H. Yu, X. Du, and M. Guizani, "Intersection fog-based distributed routing for V2V communication in urban vehicular ad hoc networks," *IEEE Transactions on Intelligent Transportation Systems*, vol. 21, no. 6, pp. 2409–2426, 2020.

[153] C. Sommer, S. Joerer, M. Segata, O. K. Tonguz, R. L. Cigno, and F. Dressler, "How shadowing hurts vehicular communications and how dynamic beaconing can help," *IEEE Transactions on Mobile Computing*, vol. 14, no. 7, pp. 1411–1421, 2015.

[154] X. M. Zhang, L. Yan, H. Zhang, and D. K. Sung, "A concurrent transmission based broadcast scheme for urban VANETs," *IEEE Transactions on Mobile Computing*, vol. 18, no. 1, pp. 1–12, 2019.

[155] I. Soto, O. Amador, M. Urueña, and M. Calderon, "Strengths and weaknesses of the ETSI adaptive DCC algorithm: A proposal for improvement," *IEEE Communications Letters*, vol. 23, no. 5, pp. 802–805, 2019.

[156] M. Gonzalez-Martín, M. Sepulcre, R. Molina-Masegosa, and J. Gozalvez, "Analytical Models of the Performance of C-V2X Mode 4 Vehicular Communications," *IEEE Transactions on Vehicular Technology*, vol. 68, no. 2, pp. 1155–1166, Feb 2019. [Online]. Available: https://ieeexplore.ieee.org/document/8581518/

[157] M. Sepulcre. C-V2X. [Online]. Available: https://github.com/msepulcre/C-V2X

[158] R. Molina-Masegosa and J. Gozalvez, "System level evaluation of LTE-V2V mode 4 communications and its distributed scheduling," in *2017 IEEE 85th Vehicular Technology Conference (VTC Spring)*, 2017, pp. 1–5.

[159] 3GPP, "Evolved universal terrestrial radio access (E-UTRA) physical channels and modulation," 3GPP, Tech. Rep. TS36.211v13.2, July 2016.

[160] ——, "Evolved universal terrestrial radio access (E-UTRA) physical channels and modulation," 3GPP, Tech. Rep. TS36.211v16.2, July 2020.

[161] R. Rouil, F. J. Cintrón, A. Ben Mosbah, and S. Gamboa, "Implementation and validation of an LTE D2D model for ns-3," in *Proceedings of the Workshop on ns-3*, 2017, pp. 55–62.

[162] T. Abbas, K. Sjöberg, J. Karedal, and F. Tufvesson, "A measurement based shadow fading model for vehicle-to-vehicle network simulations," *International Journal of Antennas and Propagation*, vol. 2015, 2015.

[163] *N9342C Handheld Spectrum Analyzer (HSA); 7 GHz; Data Sheet*, Keysight, December 2017. [Online]. Available: https://www.keysight.com/us/en/assets/7018-02496/data-sheets/5990-5587.pdf

[164] *MK5 OBU*, Cohda Wireless. [Online]. Available: https://www.cohdawireless.com/wp-content/uploads/2018/08/CW_Product-Brief-sheet-MK5-OBU.pdf

[165] *SMW-303 multiband, 3-cable DSRC or WiFi MIMO & GPS*, MobileMark, September 2018.

[166] *NexWaveRF; 5.8 GHz SpiroNET omnidirectional antenna*, ImmersionRC Limited, July 2014. [Online]. Available: https://www.immersionrc.com/?download=2741

[167] *User's Guide; HP 8590 E-Series and L-Series Spectrum Analyzers*, Hewlett Packard, July 1998. [Online]. Available: https://literature.cdn.keysight.com/litweb/pdf/08590-90301.pdf

[168] *MGW303 Series at 5.9 GHz radiation Pattern*, MobileMark, June 2017. [Online]. Available: https://www.mobilemark.com/wpfd_file/mgw303-series-at-5-9-ghz-radiation-pattern/

[169] P. Coronel, J. Simunovic, K. Sandeep, and P. Kumar, "Dielectric properties of pumpable food materials at 915 MHz," *International Journal of Food Properties*, vol. 11, no. 3, pp. 508–518, 2008. [Online]. Available: https://www.tandfonline.com/doi/abs/10.1080/10942910701472755

[170] S. N. Abdullah, K. Y. You, N. Hisham Khamis, and C. Y. Chong, "Modelling the dielectric properties of cow's raw milk under vat pasteurization," *Progress In Electromagnetics Research*, vol. 84, pp. 157–166, 2019.

[171] H. Saghlatoon, L. Sydänheimo, L. Ukkonen, and M. Tentzeris, "Optimization of inkjet printing of patch antennas on low-cost fibrous substrates," *IEEE Antennas and wireless propagation letters*, vol. 13, pp. 915–918, 2014.

[172] I. Kharrat, P. Xavier, T.-P. Vuong, J.-M. Duchamp, P. Benech, and G. E. P. Tourtollet, "Low-loss paper substrate for printed high efficiency antennas at 2.45 GHz," *IEEE Antennas and Wireless Propagation Letters*, vol. 14, pp. 1400–1403, 2015.

[173] M. E. d. Cos Gómez, F. L. Las Heras Andrés *et al.*, "Polypropylene-based dual-band CPW-fed monopole antenna," *IEEE Antennas and Propagation Magazine*, 2013.

[174] W. C. van Etten, *Introduction to Random Signals and Noise.* Wiley, 2005.

[175] J. G. Proakis, *Digitial Communications*, 1st ed. McGraw-Hill, 1983.

[176] J. Conan, "The weight spectra of some short low-rate convolutional codes," *IEEE Transactions on Communications*, vol. 32, no. 9, pp. 1050–1053, 1984.

[177] C. Sommer, D. Eckhoff, R. German, and F. Dressler, "A computationally inexpensive empirical model of IEEE 802.11p radio shadowing in urban environments," in *2011 Eighth International Conference on Wireless On-Demand Network Systems and Services*, 2011, pp. 84–90.

[178] J. D. Little, "Little's law as viewed on its 50th anniversary," *Operations research*, vol. 59, no. 3, pp. 536–549, 2011.

[179] R. Jain, *The Art of Computer Systems Performance Analysis: Techniques for Experimental Design, Measurement, Simulation, and Modeling.* Wiley, 1991.

[180] G. Naik and J. Jerry Park, "Impact of Wi-Fi transmissions on C-V2X performance," in *2019 IEEE International Symposium on Dynamic Spectrum Access Networks (DySPAN)*, 2019, pp. 1–10.

[181] K. Lan, C. Chou, and D. Jin, "The effect of 802.11a on DSRC for ETC communication," in *2012 IEEE Wireless Communications and Networking Conference (WCNC)*, 2012, pp. 2483–2487.

[182] B. Cheng, H. Lu, A. Rostami, M. Gruteser, and J. B. Kenney, "Impact of 5.9 GHz spectrum sharing on DSRC performance," in *2017 IEEE Vehicular Networking Conference (VNC)*, 2017, pp. 215–222.

[183] S. Kim and M. Bennis, "Spatiotemporal analysis on broadcast performance of DSRC with external interference in 5.9 GHz band," 2019.

[184] FCC, "In the matter of amendment of parts 2 and 90 of the Commission's rules to allocate the 5.850–5.925 GHz band to the mobile service for dedicated short range communications of intelligent transportation services," Federal Communications Commission, Tech. Rep. ET Docket No. 98-95; RM-9096, October 1999. [Online]. Available: https://docs.fcc.gov/public/attachments/FCC-99-305A1.pdf

[185] ——, "FIRST REPORT AND ORDER, FURTHER NOTICE OF PROPOSED RULEMAKING, AND ORDER OF PROPOSED MODIFICATION," Federal Communications Commission, Tech. Rep. FCC-20-164A1, 2020. [Online]. Available: https://docs.fcc.gov/public/attachments/FCC-20-164A1.pdf

[186] ——, "In the matter of: Amendment of the commissions rules regarding dedicated short-range communication services in the 5.850–5.925 GHz band (5.9 GHz band); amendment of parts 2 and 90 of the commissions rules to allocate the 5.850–5.925 GHz band to the mobile service for dedicated short range communications of intelligent transportation services," Federal Communications Commission, Tech. Rep. 71 FR 52747 (09/07/2006); WT Docket No. 01-90; ET Docket No. 98-95 RM-9096, July 2006. [Online]. Available: https://docs.fcc.gov/public/attachments/FCC-06-110A1.pdf

[187] *Standard Specification for Telecommunications and Information Exchange Between Roadside and Vehicle Systems — 5-GHz Band Dedicated Short Range Communications (DSRC) Medium Access Control (MAC) and Physical Layer (PHY) Specifications*, American Society for Testing and Materials Std. ASTM E2213 – 03(2018). [Online]. Available: https://www.astm.org/Standards/E2213.htm

[188] *Standard Specification for Telecommunications and Information Exchange Between Roadside and Vehicle Systems — 5 GHz Band Dedicated Short Range Communications (DSRC) Medium Access Control (MAC) and Physical Layer (PHY) Specifications*, American Society for Testing and Materials Std. ASTM E2213 – 02. [Online]. Available: https://www.astm.org/DATABASE.CART/HISTORICAL/E2213-02.htm

[189] E. Khorov, A. Kiryanov, A. Lyakhov, and G. Bianchi, "A tutorial on IEEE 802.11ax high efficiency WLANs," *IEEE Communications Surveys Tutorials*, vol. 21, no. 1, pp. 197–216, 2019.

[190] "2008/671/EC: Commission decision of 5 August 2008 on the harmonised use of radio spectrum in the 5875 – 5905 MHz frequency band for safety-related applications of intelligent transport systems (ITS) (notified under document number c(2008) 4145) (text with EEA relevance)," European Commission, August 2008. [Online]. Available: http://data.europa.eu/eli/dec/2008/671/oj

[191] *Intelligent Transport Systems (ITS); Radiocommunications equipment operating in the 5 855 MHz to 5 925 MHz frequency band; Harmonised Standard covering the essential requirements of article 3.2 of Directive 2014/53/EU*, ETSI Std. ETSI EN 302 571 V2.1.1, February 2017.

[192] S. T. Conway, K. A. Donohue, and M. A. Settle, "Comments of the 5G automotive association," 5GAA, March 2020. [Online]. Available: https://ecfsapi.fcc.gov/file/10309096401111/5GAA%20Comments%20(3-9-2020).pdf

[193] J. Choi, V. Marojevic, C. B. Dietrich, J. H. Reed, and S. Ahn, "Survey of spectrum regulation for intelligent transportation systems," *IEEE Access*, vol. 8, pp. 140 145–140 160, 2020.

[194] D. Riquet, "MOTION FOR A RESOLUTION pursuant to rule 105(3) of the rules of procedure on the Commission delegated regulation of 13 March 2019 supplementing directive 2010/40/EU of the European Parliament and of the Council with regard to the deployment and operational use of cooperative intelligent transport systems (2019/2651(DEA))," European Parliament, April 2019. [Online]. Available: https://www.europarl.europa.eu/doceo/document/B-8-2019-0239_EN.pdf

[195] Radio Spectrum Managment; Ministry of Business, Innovation & Employment, "Important information for users of WiFi devices in the 5GHz band." [Online]. Available: https://www.rsm.govt.nz/assets/Uploads/documents/b8c1468d8e/5-ghz-info-leaflet-2019-update.pdf

[196] ——, "Intelligent transport systems." [Online]. Available: https://web.archive.org/web/20210206114748/https://www.rsm.govt.nz/

business-individuals/buying-electrical-and-electronic-products-in-new-zealand/intelligent-transport-systems/

[197] K. Ansari, "Joint use of DSRC and C-V2X for V2X communications in the 5.9 GHz ITS band," *IET Intelligent Transport Systems*, vol. 15, no. 2, pp. 213–224, 2021. [Online]. Available: https://doi.org/10.1049/itr2.12015

[198] "GNU general public licsense (v3)," Free Software Foundation, June 2007. [Online]. Available: https://www.gnu.org/licenses/gpl-3.0.html

[199] "psc-ns3," NIST, June 2020. [Online]. Available: https://github.com/usnistgov/psc-ns3

[200] "GNU general public licsense (v3)," Free Software Foundation, June 1991. [Online]. Available: https://www.gnu.org/licenses/old-licenses/gpl-2.0.en.html